Architecture, Design, and Tradeoffs in Biomolecular Feedback Systems

Thesis by
Noah Andrew Olsman

In Partial Fulfillment of the Requirements for the
Degree of
Doctor of Philosophy

CALIFORNIA INSTITUTE OF TECHNOLOGY
Pasadena, California

2019
Defended November 16, 2018

Noah Andrew Olsman
ORCID: 0000-0002-4351-3880

ACKNOWLEDGEMENTS

Well you're in your little room, and you're working on something good.
But if it's really good, you're gonna need a bigger room.
And when you're in the bigger room, you might not know what to do.
You might have to think of,
How you got started,
Sitting in your little room.
— Jack White, *Little Room*

I have been incredibly fortunate to be surrounded by supportive and stimulating people throughout my life. My family has always encouraged with my natural tendency to pursue a wide variety of different interests, even when they (and, frankly, I) did not know where these pursuits would take me. I am fairly confident that most parents would not have put up with a 16-year-old spending most school nights playing online poker. That freedom throughout my life allowed me the opportunity to find what truly interests me and follow it through, and has been an important aspect of the way I think about science. I would also like to thank my brother Matthew for providing guidance over the years and being a source of support and perspective.

I will forever be indebted to the Caltech community. Despite living the majority of my life in Los Angeles, I had little understanding until I came here what Caltech is as an institution. Unlike any other place I have spent time, Caltech provides a small world in which it is possible to interact with people from every field in the scientific landscape. Where most universities seek to expand and encompass as many disciplines as possible, Caltech is a little room that encourages its students to be creative in a way that is unrestrained by limitations and bureaucracy. For the rest of my life I will make an active effort to keep in mind what it was like sitting in this little room.

That community is, of course, a product of the people that constitute it. I am endlessly appreciative of my advisers Lea Goentoro and John Doyle, who have given me an unreasonable amount of personal liberty in deciding how my graduate school experience played out. Rather than pushing me to pick a narrow topic, they each were incredibly generous in allowing me to spend time on a variety of side projects that contributed immensely to my personal and intellectual development

over the last five years. This could not have happened without the other faculty such as Omer Tamuz, Kai Zinn, Justin Bois, and Richard Murray at Caltech who helped me explore a broad range of interesting topics.

Beyond the academic aspects of Caltech, the friends I have made here are as much a part of my experience as the research I have done. Chris Frick, Harry Nunns, Kibeom Kim, Mike Abrams, Ty Basinger, Mengsha Gong, and David Gold made Lea's lab so much more than a work environment. Our camping trips and weekly barbecues/political debates will likely remain in my memory a long time after I have forgotten about the projects I worked on.

There is no way I can do justice to the array of friends I made while at Caltech, but I am certain that I will keep in contact with many of them long after we all graduate. In particular, Donal O'Sullivan, Juba Ziani, Mason McGill, Cat Alvarez, Paul Plucinsky, Sam Squires, Janis Hesse, Juri Minxha, Gabi Tavares, Paul Mazur, Tal Einav, Fangzhou Xiao, and Dan Naftalovich have made Caltech a great personal experience and provided a community that will likely be hard to replicate.

As much as I love the environment of Caltech, I am equally grateful for the community I have found outside of academia. Ajay Bawa, Christian Johnson, and the innumerable other friends I made as a part of Seed Consulting Group have convinced me to be optimistic about the capacity of people to change the world around them. Julia Aks and Mike Gan have provided an endlessly rewarding friendship that has given me a deep appreciation for how intense and deep passion can come packaged with kind and generous people.

I could not have asked for a better experience in graduate school. While I hope the rest of my academic career will be just as fulfilling, I have a feeling that my time at Caltech will stand out as one of the best periods of my life.

ABSTRACT

A core pursuit in systems and synthetic biology is the analysis of the connection between the low-level structure and parameters of a biomolecular network and its high-level function and performance. Elucidating this mapping has become increasingly feasible as precise measurements of both input parameters and output dynamics become abundant. At the same time, cross-pollination between biology and engineering has led to the realization that many of the mathematical tools from control theory are well-suited to analyze biological processes.

The goal of this thesis is to use tools from control theory to analyze a variety of biomolecular systems from both natural and synthetic settings, and subsequently yield insight into the architecture, tradeoffs, and limitations of biological network. In Chapter 2, I demonstrate how allosteric proteins can be used to respond logarithmically to changes in signal. In Chapter 3, I show how control theoretic techniques can be used to inform the design of synthetic integral feedback networks that implement feedback with a sequestration mechanism. Finally, in Chapter 4 I present a novel simplified model of the *E. coli* heat shock response system and show how the the mapping of circuit parameters to function depends on the network's architecture.

The unifying theme of this research is that the conceptual framework used to study engineered systems is remarkably well-suited to biology. That being said, it is important to apply these tools in a way that is informed by the molecular details of biological processes. By combining structural and biochemical data with the functional perspective of engineering, it is possible to understand the architectural principles that underlie living systems.

PUBLISHED CONTENT AND CONTRIBUTIONS

[1] Noah Olsman, Carmen Amo Alonso, and John C Doyle. "Architecture and Trade-Offs in the Heat Shock Response System". In: *Decision and Control (CDC), 2018 IEEE 57th Annual Conference on*. **I am the primary author, and developed the main results and figures in the paper. Carmen Amo Alonso performed analysis of advanced warning from feedforward response**. IEEE. 2018.

[2] Noah Olsman and Lea Goentoro. "There's (still) plenty of room at the bottom". In: *Current opinion in biotechnology* 54 (2018). **I am the primary author, and developed all results and figures in the paper.**, pp. 72–79.

[3] Noah Olsman, Fangzhou Xiao, and John Doyle. "Evaluation of Hansen et al.: Nuance Is Crucial in Comparisons of Noise". In: *Cell Systems* 7.4 (2018). **I am the primary author, and wrote the main text and performed review with Fangzhou Xiao.**, pp. 352–355.

[4] Noah Olsman et al. "Hard limits and performance tradeoffs in a class of sequestration feedback systems". In: *bioRxiv* (2018). **I am the primary author, and developed most results and all figures in the paper. Yoke Peng Leong proved results pertaining to the stability margin of the system with controller degradation.**, p. 222042.

[5] Bader Al-Anzi et al. "Modeling and analysis of modular structure in diverse biological networks". In: *Journal of theoretical biology* 422 (2017). **I am a co-author, and developed some figures and contributed to primary results.**, pp. 18–30.

[6] Elchanan Mossel, Noah Olsman, and Omer Tamuz. "Efficient Bayesian Learning in Social Networks with Gaussian Estimators". In: *Communication, Control, and Computing (Allerton), 2016 54th Annual Allerton Conference on*. **I proved results about privacy and optimal network topologies for Bayesian learning**. IEEE. 2016, pp. 425–432.

[7] Noah Olsman and Lea Goentoro. "Allosteric proteins as logarithmic sensors". In: *Proceedings of the National Academy of Sciences* 113.30 (2016). **I was the primary author, and developed all results and figures in the paper**, E4423–E4430.

[8] Bader Al-Anzi et al. "Experimental and computational analysis of a large protein network that controls fat storage reveals the design principles of a signaling network". In: *PLoS computational biology* 11.5 (2015). **I helped perform statistical analysis of Gene Ontology categories.**, e1004264.

CONTENTS

Acknowledgements . . . iii
Abstract . . . v
Published Content and Contributions . . . vi
Contents . . . vii
List of Figures . . . viii
Chapter I: Philosophical Context and Motivation for Systems Thinking in Biology . . . 1
1.1 Telos: A Story . . . 2
1.2 Putting Descartes Before the Horse . . . 4
1.3 The Times They Are a-Changin' . . . 6
1.4 Plenty of Room at the Bottom . . . 8
1.5 Chance and Necessity . . . 9
1.6 Aliens, Demons, and Chemical Machines . . . 10
1.7 The Ship of Modernity . . . 15
Chapter II: Allosteric Proteins as Logarithmic Sensors . . . 19
2.1 Introduction . . . 19
2.2 Results . . . 21
2.3 Discussion . . . 32
2.4 Supplemental Material . . . 34
Chapter III: Hard Limits and Performance Tradeoffs in a Class of Sequestration Feedback Systems . . . 50
3.1 Introduction . . . 50
3.2 Results . . . 52
3.3 Discussion . . . 72
3.4 Supplemental Information . . . 73
Chapter IV: Architecture and Tradeoffs in the Heat Shock Response System . . . 97
4.1 Introduction . . . 97
4.2 Reduced-Order Model . . . 98
4.3 Architecture . . . 101
4.4 Tradeoff Analysis . . . 107
4.5 Discussion . . . 109
4.6 Supplemental Information . . . 111
Chapter V: Conclusion . . . 114
Bibliography . . . 118

LIST OF FIGURES

Number *Page*

2.1 Sensory Systems Have Conflicting Goals. 20
2.2 An MWC Protein Can Act as a Logarithmic Sensor. 24
2.3 The Regulatory Circuit of the G Protein-Coupled Receptors Can Act as a Logarithmic Sensor. 27
2.4 Logarithmic-Feedback Circuit. 28
2.5 Biophysical Measurements Show That Allosteric Proteins are Logarithmically Tunable. 31
2.6 Allostery and Feedback in Glycolysis and Oxygen Regulation. 33
2.7 Effects of ε_0 on the Sensitivity Function. 37
2.8 Saturation Effects in the Sensitivity Function. 39
2.9 Logarithmic Tuning in the KNF Model. 41
2.10 Fold-Change Detection with an MWC Tar/Tsr Sensor. 44
2.11 Fold-Change Detection with a GPCR Sensor. 45
3.1 The Sequestration Feedback Network. 53
3.2 The Sensitivity Function. 57
3.3 Hard Limits and Performance Tradeoffs in Sequestration Feedback Circuits. 61
3.4 A Synthetic Growth Control Circuit. 65
3.5 Using Sequestration to Control an Unstable Network. 70
4.1 Block Diagram of the Full HSR System. 98
4.2 The Dynamics of HSR Architectures. 102
4.3 Block Diagram of the Sequestration and Degradation Feedback Architecture. 104
4.4 Block Diagram of the Sequestration Feedback Architecture. 105
4.5 Tradeoffs Across HSR Architectures. 108

Chapter 1

PHILOSOPHICAL CONTEXT AND MOTIVATION FOR SYSTEMS THINKING IN BIOLOGY

> *Science is built up with facts, as a house is with stones. But a collection of facts is no more a science than a heap of stones is a house.*
> — Henri Poincaré

The primary goal of this thesis is to develop a theoretical approach to studying the functional and computational capacity of biological molecules. The core research builds on an intellectual trajectory that has largely coalesced in the last two decades into the fields of systems and synthetic biology, but which has roots that pervade the history of science. The core thread running through each of these fields is the idea that living organisms are made up of cells, and these cells use networks of molecular interactions to do everything from the most basic biological processes of synthesizing new proteins and duplicating DNA for cell division to the complex task of processing sensory information and incorporating it into the cognitive behavior of intelligent life. Consequently, it has become clear that the only way to truly understand what differentiates life from non-life is to understand the evolution, function, and architecture of these biomolecular networks.

This insight was captured almost 60 years ago, when Richard Feynman gave a now-famous lecture titled "There's Plenty of Room at the Bottom" [1], in which he argued that we had only just begun to understand the extent to which the physical world can be manipulated at the molecular scale. He expressed wonderment at processes like photosynthesis and the translation of proteins. At the time, relatively little was known about the structure, function, and organization of the molecules that underlie these phenomena, but it was clear from their design that evolution is a resourceful engineer.

Feynman's vision has largely become a reality. We now understand, in a much deeper way than previously imaginable, that single cells have an astonishing capacity to sense and make decisions about their environment. From quorum sensing in bacteria to embryonic development in animals, a great deal of information must be processed using only DNA, RNA, and proteins. When studying information processing in

biology, we often focus on the computational capacity of circuits and motifs of a few components [2] and networks of tens to hundreds of elements [3, 4, 5]. While there is certainly still much to be explored at the level of circuits and networks, this perspective often coarse-grains the finer molecular details of these systems. The viewpoint taken here will zoom in on these molecular details, and highlight several cases where molecules perform an impressive range of computation.

Since the research I will present in each chapter draws from a broad array of biological processes, it is difficult to assemble a coherent history that provides sufficient context. Instead, I will focus more on the *philosophical* context of this work. While philosophy is not often discussed explicitly in modern scientific writing, I believe that to ignore it is to ignore the intellectual foundation on which fields like systems and synthetic biology were built.

I will break this analysis into three time periods: ancient, Enlightenment, and modern. The first three subsections draw heavily on a variety of entries from the *Stanford Encyclopedia of Philosophy*, which has proven to be a rich source not only for philosophical literature, but also historical context [6]. Unless otherwise noted, this is the source for all historical information and quotes in these sections. My goal is to elucidate one of the foundational questions in biology: Life appears to exhibit purpose-driven behavior that separates it from non-life, yet is made up of the same type of material as the rest of the physical world. What process underlies the apparent purposefulness of life? This question dates back at least to Aristotle, and my discussion here will attempt to trace its scientific trajectory to the modern era of molecular biology. The core focus of the final subsections will be an analysis of Jacques Monod's work in the mid-20th century with an emphasis on his book *Chance and Necessity*, which lays out a coherent integration of molecular biology into the broader philosophical scope of the preceding sections [7].

1.1 Telos: A Story

> *Tiger got to hunt, bird got to fly;*
> *Man got to sit and wonder 'why, why, why?'*
> *Tiger got to sleep, bird got to land;*
> *Man got to tell himself he understand.*
> — Kurt Vonnegut, *Cat's Cradle*

One of the oldest scientific debates for which we have a written history is that of

whether or not material objects can be said to have purpose. This discussion dates back at least to ancient Greece, when Aristotle in the 4th century BCE considered the notion of *telos*, a Greek word meaning 'purpose', 'goal', or 'end'. While Aristotle considered telos in a broad context — ranging from politics to physics — we will focus primarily on on its application to biology and the living world. He realized early on that there were two core component of telos: the purpose of an object (e.g., a knife's purpose is to cut things) and the agent which imbues that object with purpose (e.g., a person made the knife with the intent that it be used to cut things). Regarding the latter, Aristotle wrote in his *Physics* [8], implicitly casting aside Plato's premise of an intelligent designer creating the universe:

> "It is absurd to suppose that ends are not present [in nature] because we do not see an agent deliberating."

That being said, Aristotle also rejected the application of the reductionism of Democritus to the context of biology. In his *Generation of Animals*, he writes:

> "Democritus, however, neglecting the final cause, reduces to necessity all the operations of nature. Now, they are necessary, it is true, but yet they are for a final cause and for the sake of what is best in each case."

Clearly, Aristotle had a nuanced view of life in the context of natural philosophy. Variations on this debate continued for centuries, until the Western world underwent a dramatic intellectual upheaval in the 17th century known as the Enlightenment. In particular, the Scientific Revolution, spurred by the likes of Galileo Galilei and Isaac Newton, drove a wedge between the worlds of materialism and idealism. This left biology in a precarious position, straddling the two realms.

Around this time a new philosophical term was coined, *teleology*, the study of intrinsic purpose in the natural world [9]. The emergence of a term for a fundamentally Aristotelian idea may signify that thinkers of the time were being forced to grapple with the dissonance between the reductionism of the physical sciences and the idealism of moral and political philosophy. How is it that humans can be both physical objects devoid of purpose, but also metaphysical beings with moral, political, and social obligations? René Descartes is credited with an attempt at resolving this issue by means of the notion of *dualism*, that the mind and body are two separate entities, one physical and one non-physical. This helped prop up the idea that humankind

holds a special place in the universe and was an important steppingstone towards a scientific view of humanism, but for our purposes mostly dodged the actual issue of resolving the philosophical tensions between the living and non-living worlds.

1.2 Putting Descartes Before the Horse

> *If you try and take a cat apart to see how it works, the first thing you have on your hands is a non-working cat.*
> — Douglas Adams, *The Salmon of Doubt*

It is important to note that post-Enlightenment scientific theory was dominated by the physical sciences. While Newton's *Principia* was published in 1687 and laid the theoretical groundwork for physics as we know it, such a cohesive synthesis of ideas about biology took almost two more centuries. In light of this, it makes sense that work in the interim amounted to an attempt to shoehorn the study of life into the framework of existing physical theories. The result of this was an extensive physical characterization of organisms, captured by the foundational work of Carl Linnaeus in the 18th century which culminated in the modern notion of taxonomy. Though this descriptive work laid the foundation for the scientific study of biology, its capacity to explain *why* each organism has its particular sets of traits and features was limited.

Linnaeus did notice in his taxonomy as early as 1744 that there was an inescapable similarity between many species, when he published *Oratio de telluris habitabilis incremento (Oration on the Increase of the Habitated World)*. His theory of origins boiled down to all modern life having descended from a few original, divinely-created forms. Linnaeus proposed the proto-Mendelian mechanism of diversity via hybridization of species, but this served more to connect the dots between observations than it did to propose a coherent theory of evolution.

The movement towards a more foundational theory of life can be attributed to Georges-louis Leclerc, Comte de Buffon, an 18th century French natural philosopher whose foundational insight was that organisms do not exist in a vacuum. Buffon's 36 volume *Natural History* presented a sprawling investigation of the natural world. Importantly, this work "presented a secular and realist account of the origins of the earth and its life forms." Specifically, Buffon considered that geography and environment should have an influence on the species that inhabit a given region.

A consequence of this perspective was that, to understand the living world, scientists must go out into nature and study biology in its natural environment. Further, Buffon put forward a contrast between 'inert' and 'vital' matter, which ran contrary to post-Newtonian ideas that all forms of matter are essentially uniform and equivalent. While not literally correct, Buffon's thinking marked an important shift towards acknowledging that a purely context-independent theory of biology may be insufficient to completely explain life. What he lacked was a coherent framework for thinking about this sort of vitalism: what is it that living matter is 'trying' to do?

The crucial next step was taken by Buffon's student Jean Baptiste Lamarck (born 1744), who put forth the idea of *transformism*, which was a first attempt to scientifically study the transformation of species. While the ancient Greeks had at times discussed the idea of transformation, Lamarck was the first to attempt an empirical scientific exploration of this type of relatedness between species. Importantly, this required him to both examine data and to put forth a causal mechanistic theory of change over time.

While Lamarckian evolution is often presented solely as the theory of inheritance of acquired characteristics, his actual views, fittingly, transformed quite dramatically over the course of his life. His real innovation was not so much the correctness (or lack thereof) of his theory, but that he made the conceptual leap of realizing what a mechanistic theory of biological origins should look like. Early in his career, Lamarck put forward a theory of linear descent or degeneracy, starting from the most complex organisms and ending with the simplest (in this work he focused on invertebrates). By 1800 he reversed this ordering, but still believed in a linear arrangement of species transformation. In this framework, species did not originate from a common ancestor but rather descended directly from a wide range of primitive organisms.

This later developed into a more coherent theory of evolution, where Lamarck hypothesized that the mechanism of evolution was the interaction of a species with its local environment. In this theory, animals would acquire traits throughout their life and pass them on to their young. While the mechanism of change turns out to be largely wrong, the idea that interactions between the environment and an organism's fitness drives evolution was of fundamental importance. Lamarck seems to have stuck with his linear idea of evolution, though there appears to be some evidence that, later in his life, he considered the idea of species branching out from common ancestors.

1.3 The Times They Are a-Changin'

The line it is drawn, the curse it is cast
The slow one now, will later be fast
As the present now will later be past
The order is rapidly fadin'.
And the first one now will later be last
For the times they are a-changin'.
— Bob Dylan

With the roots of evolutionary theory now in place, the early 19th century saw the rapid development of many competing theories of life. A key point is that, along with theoretical inquiry, as the field of evolutionary biology matured there emerged a core set of facts that any viable theory needed to explain. For example, it was known at this point that there existed both *homology* between species, anatomically similar parts across widely varied species (such as the heart and liver), and *analogy*, anatomically distinct features that served a common functional adaptation (e.g. wings evolving in both birds and bats). This intellectual trajectory, of course, culminated in the publication in 1859 of Charles Darwin's *On the Origin of Species*. As with all great human achievements, it is impossible to succinctly describe Darwin's work on evolution without vastly oversimplifying the context and historical precedent. For the purpose of the discussion here, I will focus primarily on the aspects of his theory that relate to the overarching issue we hope to address: to what extent is it correct to think of biology as a purpose-driven (i.e. teleological) phenomenon?

Darwin became concerned with this problem long before the final publication of *Origin*, writing in 1842:

> "Nature lets [an] animal live, till on actual proof it is found less able to do the required work to serve the desired end, man judges solely by his eye, and knows not whether nerves, muscles, arteries, are developed in proportion to the change of external form."

We see that he must have had some sense of agency in how natural forms emerge. He at this point had at least begun to formulate the idea of evolution by natural selection, but his comparison of Nature's agency to that of a human's has a distinctly teleological tone. From the context of his other contemporary writing, he had not yet conceptualized to what end Nature would perform such a selection, just that

some apparent agency superior to that of humankind was exerting selective pressure on life. Importantly, it is not clear that Darwin had a clear picture of what could drive evolution. His theory at his point appears mostly consistent with a Lamarckian view of acquired traits.

It is worth emphasizing this point, as most of the evolutionary work preceding Darwin had been limited to particular branches of life, for example the invertebrates or the plants. While post-Lamarckian scientists were aware of anatomical similarities between organisms, it seems that their views of evolution focused on the incremental improvements that species made in adapting to their environment, consistent with a linear history that was perhaps selecting for some optimally fit descendent. What these theories all lacked was a model of diversification; what mechanism would cause lineages to branch out from a common ancestor if each lineage was being optimized by some Natural force? While these theories formalized the idea of natural selection, they had little they could scientifically explain about what drives the changes to fitness upon which selection acts. There is implicit in each of these ideas some notion of vitalism, that organisms have some inexplicable drive to adapt.

The idea that Darwin (and independently, Alfred Russell Wallace) formalized was that natural selection does not need to be driven by some intrinsic desire to adapt within each organism, but that random variability provided an entirely mechanistic force that could facilitate fitness-based selective pressure. This was more than a clever scientific observation: this idea presented a fundamental philosophical break with the teleological theory of life. If the diversity and evolution of life is driven by random variations, there is no need for any sort of agency — intrinsic or extrinsic — to explain the origin of species.

Take, for example, the Linnaean categorization of species. In a Lamarckian world, these species might represent the different lineages of descent that exist in the modern world. This classification is scientifically meaningful, because each species may well have descended from a separate ancestral origin that was acted upon by different adaptive and selective pressures. Darwin went as far as to observe that the Linnaen classification of species was scientifically meaningless under a theory of common descent, in that each organism has a shared ancestry and is simply the end result of the same general selective pressure coupled with natural variations. The categorization of organisms into species was more a useful conceptual tool to help humans think about life than it was a deep fact of nature. There is an irony in the fact that *On the Origin of Species* was, in a sense, just as much about the demise of

species as it was about their origin.

A strictly non-teleological view of biology may not have come easily to Darwin, as evidenced by changes in language between the first edition of *Origin* in 1959 and subsequent ones where he altered the language to downplay the idea of Nature exerting direct agency over life. As the theory evolved, natural variation took an increasingly central mechanistic role. Later editions also favored the term 'survival of the fittest' over 'natural selection', with similar teleological implications. An important counter-point to this interpretation is explicit reference in some editions of the book to a 'Creator' responsible for the origin of life. It is unclear to what extent this reflected Darwin's own beliefs and to what extent it was the product of theological pressures of the time.

1.4 Plenty of Room at the Bottom

> *Teleology is like a mistress to a biologist: he cannot live without her but he's unwilling to be seen with her in public.*
> — J.B.S. Haldane

A key idea that began to take shape in 19th century biology was the notion of 'traits', and how those traits related to fitness. The general framing of these traits were in terms of physiology and anatomy, with some generic notion of inheritance that lacked a concrete physical manifestation. Though cell theory (the idea that all organisms are made up of microscopic cells) was formulated by 1839, little was known about the inner workings of these cells. By the early 20th century the term 'gene' had emerged, however it was mostly a placeholder for whatever material mediated the transfer of heritable traits [10].

Over the next 50 years, this qualitative theory of inheritance crystallized into a physical theory that laid the groundwork for the field of molecular biology. Somewhat ironically, the shift in perspective towards viewing life as a fundamentally molecular process did less to advance reductionism than it did to imbue simple physical components with purpose-driven behavior. DNA, which was originally thought to simply be a structural component of the nucleus, suddenly became an information-carrying vessel [11]. Enzymes orchestrated a vast sea of biochemical reactions. RNA served as a messenger between the instructions of genes and the functions of proteins. As with any good paradigm shift in science, these discoveries raised more philosophical questions than they answered.

For our purposes, the most interesting of these questions is this: when does an assembly of decidedly dead molecules suddenly become a living cell? The storage of information alone cannot be what underlies life, and on the other hand humans routinely create complex chemical reactors, which are not equivalent to living organisms. Life consists of microscopic interactions forming macroscopic structure, yet the same could be said of the crystallization of sodium chloride into a block of salt.

The perspective I will present on this question will focused on the work of Jacques Monod, the 20th-century biologist who shared the 1965 Nobel Prize in Physiology and Medicine for the discovery of gene regulation. Monod was also involved in creating the first models of allosteric regulation. The goal of this section will be to both provide modern historical context for the work in my thesis, and to relate my research direction to the philosophical and scientific ideas set out by Monod.

1.5 Chance and Necessity

> *Everything existing in the Universe is the fruit of chance and of necessity.*
> — Democritus

Throughout Monod's scientific life, he expressed a broad philosophical perspective on the nature of biology. He famously said, "What is true for *E. coli* is true for the elephant" [11], expressing a unified view of life that stood in stark contrast to the specialized study of species that dominated 19th-century biology. Later in his life, he became close friends with the philosopher Albert Camus, even going as far as to co-author a critique of Lysenkoism [12], a politically motivated branch of soviet pseudoscience that (unsuccessfully) challenged the Darwinian theory of genetics.

Shortly before Monod's death in 1976, he published a synthesis of his philosophical perspective titled *Chance and Necessity* [7], a book targeted at a non-technical audience but with an in-depth exploration of the important discoveries of the time. In particular, Monod sought to coalesce the classical teleological perspective that we have discussed at length in the previous section with the new frontier of molecular biology that emerged in the mid-20th century. What I find most fascinating about Monod's philosophy is that it was not isolated from his science; his perspective permeates the research he did and represents a paradigm shift in biological thought that we are still seeing unfold today.

1.6 Aliens, Demons, and Chemical Machines

> *We live on an island surrounded by a sea of ignorance. As our island of knowledge grows, so does the shore of our ignorance.*
> – John Archibald Wheeler

Artifacts and fictions

Monod starts *Chance and Necessity* with a chapter titled *Of Strange Objects*, where he proposes a thought experiment: What if an alien space agency were to land a probe on Earth, whose goals was to classify the objects it found as either artificial or natural? This question is first posed to seem trivial; of course a mountain and a cloud are qualitatively different from a knife or an airplane. A key constraint is that, because of the aliens' ignorance, any method they have of distinguishing the natural from the artificial must be *objective* rather than *projective*. The latter implies that the intent of the object's creator can be inferred (should it exist), whereas the former relies only on observable properties intrinsic to the object.

The problem comes when we try to define *a priori* criteria that separate the two categories. As a naive approach, Monod proposes two simple properties the aliens could measure to gauge artificiality: regularity and repetition. Objects shaped by nature tend to have macroscopic structure that is geometrically complex and generally lacks properties like smoothness, right angles, and a high degree of symmetry which are commonly found in human-made artifacts. Nominally, these criteria would let the aliens group rocks and trees as natural and houses and trains as artificial. This algorithm might, however, fail to recognize a quartz crystal or a diamond as being of natural origin. These objects are highly symmetrical, often contain sharp boundaries and smooth surfaces. What the aliens have missed is that the regularity of these objects is purely a macroscopic reflection of their microscopic structure. In some sense, they lack the deliberate design that we ascribe to real artifacts. This issue could conceivably be resolved by encoding the relatively small number of possible crystal structures as special cases.

The problem gets significantly more difficult when our alien algorithm is confronted with a beehive. The hive has many hallmarks of artificiality: regularity, geometric structure, symmetry, and precise angles. In fact, if the algorithm were to look at the bees themselves it would likely have difficulty classifying them as any less artificial than a small robot. The purpose of this discussion, adapted from Monod, is to point out the ambiguity inherent in the underlying task. Artificiality and naturalness are

not intrinsic properties of objects, but are as much tied to their origin as they are to their structure and function.

This point echoes the realization that spurred early evolutionary thinking, namely that understanding biology is not simply a task of classifying organisms. We see that *neither* reductionist nor functional categorization is sufficient to capture what separates the living from the non-living world. Reductionism and functionalism appear to be opposing views, but they share a key property: they each assume that an object can be understood independently of its history. The secret of life must lie as much in its origin as in its function. This leads us to the core concept at the heart of *Chance and Necessity*, that life is fundamentally a *teleonomic* process. The term teleonomy was coined in 1958 by Colin Pittendrigh [13], and is perhaps best described by quoting Monod's introduction of the concept directly:

> "Every artifact is a product made by a living being which through it expresses, in a particularly conspicuous manner, one of the fundamental characteristics common to all living beings without exception: that of *objects endowed with a purpose or project*, which at the same time they exhibit in their structure and carry out through their performance (such as, for instance, the making of artifacts).
>
> Rather than reject this idea (as certain biologists have tried to do) it is indispensable to recognize that it is essential to the very definition of living beings. We shall maintain that the latter are distinct from all other structures or systems present in the universe through this characteristic property, which we shall call *teleonomy*."

Where teleology reflects the idea of purpose-driven behavior that is the end result of an agent with intent, teleonomy captures the idea of purpose-driven behavior that emerges from natural law. Though the function of an artifact is derived from the intention of its creator, and thus is strictly external to the artifact's structure,

> "...a living being's structure results from a totally different process, in that it owes almost nothing to the action of outside forces, but everything, from its overall shape down to its tiniest detail, to 'morphogenetic' interactions within the object itself. It is thus a structure giving proof of an autonomous determinism[.]"

Monod goes on the describe life as being fundamentally composed of three components: teleonomy, autonomous morphogenesis, and the invariant transfer of information. The latter two are crucial, as they are the mechanism through which the former can be defined by primarily internal means. Life differs from non-life in that its purpose is derived from its evolutionary lineage, not by an intentional creator. This purpose is of course shaped by the selective pressure of the organism's environment, but the information that captures the result of selective pressure is, ultimately, strictly local.

The idea of teleonomy is useful in its own right, as it succinctly resolves a broad range of philosophical issues surrounding biology. Monod, being first and foremost a scientist, did not treat teleonomy as the end result of his thinking, but rather as the starting point. He sought to put this generic notion on a firm scientific footing. It is worth noting that, while teleonomy has found a place in 20th-century philosophy, it has primarily been applied to evolutionary thought. As far as I can tell, Monod stands alone in the depth and seriousness with which he applies the idea to molecular biology.

The devil is in the details

One of the core innovations of Monod's conception of teleonomy is that it does not sidestep the reductionist argument about biology, i.e. that biology is a purely physical process, but confronts it head on. A key aspect of both teleology and teleonomy is a particular type of causal relationship, specifically that some form of information is translated into behavior. In physical terms, this causality is both borne out and constrained by the laws of thermodynamics.

Monod presents another illustrative thought experiment to show the limits of what a classical thermodynamic description of biology can yield. Imagine filling a calorimeter with a supersatured solution of sucrose. If you were to add a seed crystal, it would grow into a large, highly-ordered crystalline structure. In accordance with the second law of thermodynamics, a commensurate temperature change would be measured by the calorimeter to compensate for the local decrease of entropy in the crystal. This change in temperature should come in at exactly the limit predicted by the second law.

Now imagine a similar setup with a calorimeter filled with a sucrose solution (along with a few other choice molecules), except instead of a seed crystal you instead drop a single *E. coli* cell. If you were then to wait a few days, you would find yourself

with many more *E. coli* cells than you started with. Because of the high efficiency of *E. coli* metabolism, you would expect to again measure a temperature change from the calorimeter that almost exactly matches the displaced entropy predicted by the second law.

We see that both of these experiments are subject to the same constraints, independent of the fact that the underlying processes could not be more wildly different at the molecular level. At the same time it is reasonable to argue that where, in the crystalline case, thermodynamics is the end of the story, for the *E. coli* it is just the beginning. As an analogy, Newton's laws are fundamental to the mechanics of both a projectile launched by a catapult and a rocket leaving Earth. In the former case, Newton's laws can essentially describe the entire story of the projectile, whereas in the latter most of the interesting behavior comes not from what the constraining laws say, but how the engineering of the rocket acts within them.

To Monod, the difference between the sugar crystal and *E. coli* is Maxwell's demon. This demon is derived from a 19th-century thought experiment proposed by James Clerk Maxwell, where he imagined a partitioned chamber containing a collection of molecules, some moving fast and some moving slowly. The molecules are randomly spread between the left and right side of the partition, and thus each side should have the same temperature. The partition contains a small hatch controlled by a demon, who can selectively open and close the hatch to let certain molecules through and not others. In theory, the demon could open the hatch whenever a slow molecule approached from the left or a fast molecule from the right. If this were the case, the demon could somehow reduce the overall entropy of the chamber simply by taking advantage of the thermal properties of the molecules, apparently sidestepping the laws of thermodynamics and passively moving away from thermal equilibrium.

The apparent violation seems to imply that, by the act of some cognitive function, the demon is able to rig things in its own favor without exerting energy. The flaw is that we have not properly accounted for the fact that the simple act of measuring each molecule's velocity and making a decision is inherently costly, and thus must use energy. A common interpretation of this result is that nature is more clever than any demon, and that the universe is stuck abiding by the laws of thermodynamics.

Monod had a somewhat different perspective: rather than casting aside the demon as being too costly, biology has seen fit to employ it many millions of times over. The most salient example might be the enzyme, whose job it is to do exactly what Maxwell's demon does: selectively pick molecules to interact with such that thermal

fluctuations can be translated into chemical kinetics. These interactions generally consume energy, but the payoff is that cells have an enormous cognitive capacity to pick and choose the chemistry that will be carried out. Enzymes not only create order within a cell, they also are responsible for the directed functionality of life:

> "At work here is, quite literally, a microscopic discriminative (if not 'cognitive') faculty. We may say that any teleonomic performance or structure in a living being – whatever it may be – can, in principle at least, be analyzed in terms of stereospecific interactions involving one, several, or a very large number of proteins."

Monod does go on to acknowledge the role of DNA and RNA in this process as well, but most of his discussion focuses on the cognitive role of proteins in carrying out teleonomic function. What is most fascinating is his recognition at the dawn of the molecular era of biology that, fundamentally, "living beings are chemical machines".

Reactionary thinking

While *Chance and Necessity* covers a vast range of philosophical issues in molecular biology, I will restrict the rest of the discussion of Monod's work to the fourth chapter of the book, titled *Microscopic Cybernetics*. In this chapter, Monod lays out a broad vision of molecular biology that is strikingly similar to what has become the field of systems biology. In particular, the perspective presented is surprisingly ambivalent to the details of any particular pathway. Instead he focuses on the general themes that appear to emerge across a wide variety of systems, with a heavy emphasis on the consistent appearance of feedback control. In the context of enzymatic pathways, he points to the apparent 'gratuity' of interactions that are not essential to the synthesis of a final product, but nonetheless serve a crucial role in regulating the cellular function.

In particular he discusses at great length allosteric enzymes, a class of proteins that exemplify the degree to which biological molecules can perform sophisticated computation by having indirect protein-ligand interactions that regulate biological activity. This echoes the developments in his academic work on allosteric regulation, where he helped develop one of the first mechanistic models of protein regulation that was consistent with both biochemical and structural data [14, 15]. The discovery of allostery represented not only progress in our understanding of the

connection between structural and functional aspects of molecular biology, but also the theoretical insight that regulatory processes could be *independent* of the events they regulate.

To contrast, the competing theories of the time proposed direct interaction between either substrates and inhibitors, or between binding sites of the protein. In the former case, the idea was that a regulatory molecule could compete with the substrate for the binding site of the protein. In the latter case, a theory developed by Koshland, Nemethy, and Filmer proposed that one binding site on a protein could directly interact with another to increase or decrease its substrate affinity [16].

Allostery differs fundamentally from these models, in that it assumes that the binding of substrate occurs at a physically distinct location from the binding of regulatory effectors. While this may at first seem like a technical detail that is only relevant to protein structure, the reality is that allosteric regulation essentially creates a virtualization between function and regulation. Many allosteric proteins have several regulators, both positive and negative effectors, each with stereospecific binding. This separation of regulation from function facilitates the development of complex control circuitry that far exceeds what would be possible in a world where, for example, each enzyme could only bind to its primary substrate.

This is why Monod referred to allostery as the 'second secret of life', after the genetic code [17]. By freeing proteins to interact with each other via arbitrary molecular interactions, cells could perform the sophisticated control and computation that are required to ensure that the cell functions properly. The cell may be a chemical machine, but it can only ever be as clever as its programming. Just as Darwin realized that natural selection is sufficient to bring about the purpose-drive behavior of evolution, Monod realized that stereospecific interactions of molecules can bring about the teleonomic behavior that turns a dead collection of proteins and nucleic acids into a living cell.

1.7 The Ship of Modernity

> *Throw Pushkin, Dostoevsky, Tolstoy, etc. overboard from the Ship of Modernity.*
> — Vladimir Mayakovsky, *A Slap in the Face of Public Taste*

Why bother with all of this? Now that we have the end result of this line of inquiry, is there any use in retracing lines of thought that have long outlived their warranty?

More to the point, what does any of this have to do with the actual process of *doing* science?

What has become clear is that science and philosophy have always gone hand in hand. While a great deal of incremental work can be myopic in scope, large changes in thinking rarely occur by accident. Major scientific discoveries are, more often than not, as much a product of a new philosophical perspective as they are of technological innovation. Darwin likely would not have gone to the Galapagos had he not been thinking about the nature of selection and variation, Watson and Crick analyzed DNA not because it has an interesting structure, but because they believed it had the capacity to store the genetic code, and Monod's belief in the teleonomic nature of life most likely led him to search for regulatory interactions throughout the biomolecular world. Each of these steps required scientists to go beyond the intellectual framework used by their predecessors and develop a novel point of view.

With all this in mind, I hope that the work I present in the remaining chapters will be read with a philosophical subtext. In particular, that the language of design, architecture, and tradeoffs is not simply a useful metaphor for discussing biological systems, but that teleonomic language is the *right* way to describe biological phenomena. Once we start to looking at biology through the lens of engineering, it becomes natural to ask questions that are suited to purpose-driven systems. It does not necessarily make sense to ask what is the purpose of the Earth revolving around the Sun or an electron going through a particular slit, but we can learn quite a bit by investigating, for example, the purpose of some biochemical pathway having two feedback loops instead of just one.

To this end, the research presented in the following chapters examines the design, architecture, and function of three molecular processes. The work in Chapter 2 builds directly on the work of Monod, studying functional properties of allosteric proteins. I show that, encoded in the thermodynamics of allostery, is the capacity for pathways to sense and respond to logarithmic changes in signal. In Chapter 3 I will use tools from control theory to analyze the performance of circuits that use a sequestration mechanism to implement robust perfect adaptation (i.e. integral feedback control). Finally, in Chapter 4 I show how a comparative perspective of circuit architecture yields insight into the design of the *E. coli* heat shock response system.

References

[1] Richard P Feynman. "There's plenty of room at the bottom". In: *Engineering and science* 23.5 (1960), pp. 22–36.

[2] Uri Alon. "Network motifs: theory and experimental approaches". In: *Nature Reviews Genetics* 8.6 (2007), pp. 450–461.

[3] Dennis Bray. "Molecular networks: the top-down view". In: *Science* 301.5641 (2003), p. 1864.

[4] Stefano Boccaletti et al. "Complex networks: Structure and dynamics". In: *Physics reports* 424.4 (2006), pp. 175–308.

[5] Mark EJ Newman. "The structure and function of complex networks". In: *SIAM review* 45.2 (2003), pp. 167–256.

[6] Phillip Sloan. "The Concept of Evolution to 1872". In: *The Stanford Encyclopedia of Philosophy*. Ed. by Edward N. Zalta. Spring 2017. Metaphysics Research Lab, Stanford University, 2017.

[7] Jacques Monod. *Chance and Necessity. An Essay on the Natural Philosophy of Modern Biology*. Vintage Books, 1971.

[8] Wikipedia contributors. *Teleology — Wikipedia, The Free Encyclopedia*. [Online; accessed 26-October-2018]. 2018. URL: https://en.wikipedia.org/w/index.php?title=Teleology&oldid=857541893.

[9] Freiherr Christian Friedrich von Wolff. *Philosophia rationalis sive logica*. prostat in Officina libraria Rengeriana, 1740.

[10] Wilhelm Johannsen. "The genotype conception of heredity". In: *The American Naturalist* 45.531 (1911), pp. 129–159.

[11] Horace Freeland Judson. "The eighth day of creation". In: *New York* (1979), p. 550.

[12] Sean B Carroll. *Brave genius: a scientist, a philosopher, and their daring adventures from the French resistance to the Nobel prize*. Crown, 2013.

[13] Colin S Pittendrigh. "Adaptation, natural selection, and behavior". In: *Behavior and evolution* 390 (1958), p. 416.

[14] Jacques Monod, Jean-Pierre Changeux, and Francois Jacob. "Allosteric proteins and cellular control systems". In: *Journal of molecular biology* 6.4 (1963), pp. 306–329.

[15] Jacques Monod, Jeffries Wyman, and Jean-Pierre Changeux. "On the nature of allosteric transitions: a plausible model". In: *Journal of molecular biology* 12.1 (1965), pp. 88–118.

[16] DE Koshland Jr, George Némethy, and David Filmer. "Comparison of experimental binding data and theoretical models in proteins containing subunits". In: *Biochemistry* 5.1 (1966), pp. 365–385.

[17] Aron W Fenton. “Allostery: an illustrated definition for the ‘second secret of life’”. In: *Trends in biochemical sciences* 33.9 (2008), pp. 420–425.

Chapter 2

ALLOSTERIC PROTEINS AS LOGARITHMIC SENSORS

2.1 Introduction

Sensory systems in biology are faced with two seemingly conflicting goals: they must be sensitive in order to detect small changes in signal (Figure 2.1A), and at the same time they must have a broad response range because many natural signals vary over several orders of magnitude (Figure 2.1B) [1]. To achieve these conflicting goals, it has been proposed that many sensory systems have evolved to tune their sensitivity over a wide range (Figure 2.1C). In these systems, the pathway can adapt the regime which it is most sensitive to depending on the magnitude of the signal they receive.

The ability to tune sensitivity over a broad range of signal is a key property of the phenomenon known as fold-change detection, where the change in activity of a system is not a function of the level or absolute difference in signal, but of the ratio of signal to background [2, 3]. For example, a change in signal level from 1 to 3 or from 10 to 30 would yield an identical outcome. Fold-change detection is related to the well-known Weber's Law, which describes how our sensory systems tune their detection thresholds to the background state [4]. Weber's Law has been proposed in many sensory systems, including vision, weight perception, taste, as well as numerical and temporal cognition [5, 6, 4, 7]. Beyond sensory systems in whole organisms, fold-change detection has recently emerged at the cellular level, governing signal transduction in animal cells. Specifically, studies in several signaling pathways have presented evidence that gene transcription responds to the fold change in the level of a transcription factor, rather than its absolute level [8, 9, 10, 11]. Finally, evidence for fold-change detection has also been observed in the sensory response of fungi [12], bacteria [13, 3] and social amoeba [14].

Given its wide-ranging occurrence, it is therefore of interest to understand how fold-change detection is implemented at the molecular level. It has been proposed that fold-change detection can be mediated by specific classes of incoherent feedforward loops (Figure 2.1D) and nonlinear feedback loops (Figure 2.1E) [3, 15]. The authors also hypothesized that fold-change detection can be realized using another type of circuit, where an upstream logarithmic sensor is coupled with linear feedback (Figure

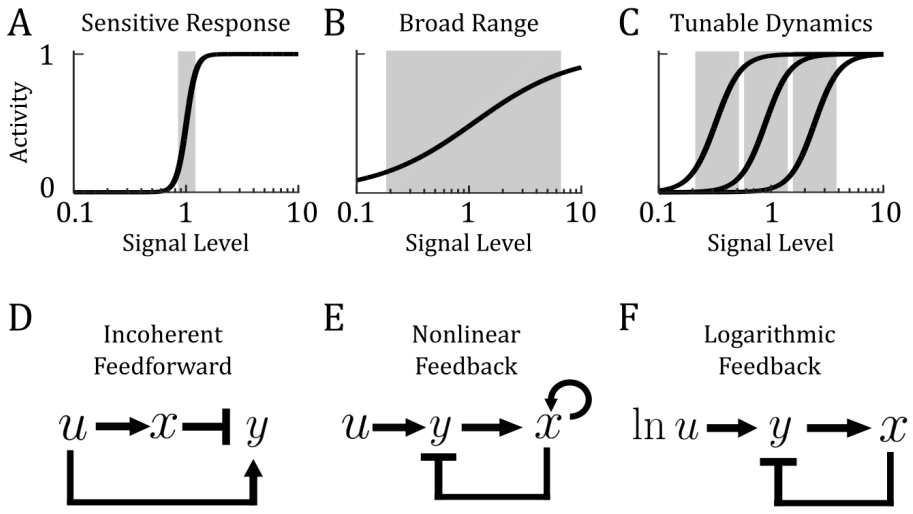

Figure 2.1: Sensory Systems Have Conflicting Goals. A) A sensitive system detects small changes in signal, but has a narrow response range. **B)** A broad-ranged system responds to a large range of signal, but is not sensitive to small changes. **C)** A tunable sensor is both sensitive to small changes in signal, and is capable of adjusting its response curve logarithmically across a broad range.
Proposed molecular circuits for fold-change detection. D) An incoherent feedforward loop is a common motif in gene regulatory systems, where an input activates an output, and at the same time a repressor of the output. **E)** A nonlinear feedback loop has also been proposed as a mechanism for fold-change detection. **F)** A logarithmic-feedback circuit, built from a logarithmic sensor coupled to linear feedback. In this study we ask how a logarithmic sensor might be implemented at the molecular level.

2.1F). Whereas feedforward and feedback circuits are commonly found in biological systems, it is not clear how a logarithmic sensor would be implemented. Here we define a logarithmic sensor as having two properties: (i) it must be able to respond to changes in signal on a logarithmic scale, and (ii) it must be logarithmically tunable, i.e. shift its response curve on a logarithmic scale (see Figure 2.1C). We will rigorously define and analyze these properties in the next section.

In this study we explore the possible roles of allostery in fold-change detection. An allosteric protein is one that has an effector which regulates its activity by acting on a site physically distant from the protein's ligand binding site. Allostery is found in a vast range of processes, including metabolism, signal transduction, oxygen and membrane transport, cell cycle regulation, and transcription [16, 17]. Allostery has been thought to mediate cooperativity, for example in various hemoglobin and metabolic enzymes. Allostery has also been thought to facilitate biological control loops, for example mediating feedback in glycolysis [18].

Notation	Meaning	Units	First Use
$c(t)$	Input ligand concentration	μM	Equation (2.1)
ε_0	Allosteric constant	None	Equation (2.1)
K_A, K_I, K_D	Dissociations constants	μM	Equation (2.1)
N	Number of protein subunits	None	Equation (2.1)
$a(c, \varepsilon_0)$	Fraction of active proteins	None	Equation (2.1)
$S(c, \varepsilon_0)$	Sensitivity function: $c\frac{\delta a}{\delta c}$	None	Equation (2.4)
τ	limits of the logarithmic response range	None	Equation (2.6)
$R, T_{GDP}, T_{GTP}, \alpha_{GDP}, \alpha_{GTP}$	Concentrations in GPCR system	μM	Equation (2.8)
$k_i, i \in [1, 6]$	Rates in GPCR system	s^{-1}	Equation (2.8)

Table 2.1: Description of notation in Chapter 2.

We propose a new function for allosteric proteins as logarithmic sensors. In the context of bacterial chemotaxis, Lazova *et al.* and Tu *et al.* have proposed that a logarithmic transformation can emerge from the aspartate-sensing Tar receptors that follow the Monod-Wyman-Changeux model of allostery [15, 19]. Here we find that logarithmic sensing is a general property of allostery, regardless of whether the conformational change is thermally or kinetically driven, independent of the specific model of allostery (e.g. conformational selection or sequential binding), and can even be implemented in either a single protein or a network of proteins. Essentially, we find that the capacity to act as a logarithmic sensor arises from the fundamental feature of allostery, the ability to tune the activity of a protein without directly affecting its binding kinetics. Given the broad presence of allosteric proteins, this raises the possibility that diverse cellular processes may sense input in a fold-change manner, akin to how our sensory systems work. For convenience, table 2.1 describes the notation used in this chapter.

2.2 Results

To investigate if an allosteric protein can act as a logarithmic sensor, we begin by analyzing a widely used model of allostery, the MWC model, proposed by Monod, Wyman, and Changeux to explain cooperativity in metabolic enzymes and

hemoglobin [20, 21]. The MWC model is based on conformational selection. It considers a large homogeneous population of proteins, where each protein has N identical subunits that can independently bind ligand (Figure 2.2A). Each protein can either be in the active (A) or inactive (I) conformation, each of which have different binding affinities for ligand. Conformational change occurs in an all-or-none fashion when there is no ligand bound, and is regulated by the binding of an allosteric effector.

Let c be the concentration of ligand, K_A and K_I be the dissociation constants associated with the active and inactive conformations and let $e^{\varepsilon_0} = \frac{I_0}{A_0}$ be the equilibrium ratio between the inactive and active conformations when no ligand is bound. This parameter e^{ε_0} is known as the allosteric constant. ε_0 represents the free-energy difference when the system is at thermodynamic equilibrium, or the reaction equilibrium constant when the system is at steady state. The fraction of proteins in the active state $a(c, \varepsilon_0)$ is

$$a(c(t), \varepsilon_0) = \frac{\left(1 + \frac{c(t)}{K_A}\right)^N}{\left(1 + \frac{c(t)}{K_A}\right)^N + e^{\varepsilon_0}\left(1 + \frac{c(t)}{K_I}\right)^N}. \tag{2.1}$$

The MWC model is typically analyzed in a static context. Tu, Shimizu, and Berg analyzed a dynamic version of the model in the context of bacterial chemotaxis [19, 22] by taking partial derivatives with respect to c,

$$\frac{\partial a}{\partial c} = Na(1-a)\frac{K_A^{-1} - K_I^{-1}}{(1 + c/K_A)(1 + c/K_I)}. \tag{2.2}$$

With this dynamic framework, we now examine the range $K_A \ll c \ll K_I$ where the ligand concentration is large enough to facilitate binding to the active conformation, but not so large as to allow binding to the inactive conformation.

This range can be substantial in some proteins, e.g. up to three orders of magnitude in phosphofructokinase [23]. In this range, equations (2.1) and (2.2) simplify respectively to

$$\begin{aligned} a(c, \varepsilon_0) &\approx \frac{e^{-\varepsilon_0}\left(\frac{c}{K_A}\right)^N}{1 + e^{-\varepsilon_0}\left(\frac{c}{K_A}\right)^N}, \\ \frac{\partial a}{\partial c} &\approx N\frac{e^{-\varepsilon_0}(\frac{c}{K_A})^N}{\left(1 + e^{-\varepsilon_0}(\frac{c}{K_A})^N\right)^2}\frac{1}{c} = S(c, \varepsilon_0)\frac{1}{c}, \end{aligned} \tag{2.3}$$

where we define the sensitivity function $S(c, \varepsilon_0)$, which describes the steepness of the activity curve:

$$S(c, \varepsilon_0) \triangleq N \frac{e^{-\varepsilon_0}(\frac{c}{K_A})^N}{\left(1 + e^{-\varepsilon_0}(\frac{c}{K_A})^N\right)^2}. \tag{2.4}$$

Representative plots of $a(c, \varepsilon_0)$ and $S(c, \varepsilon_0)$ are shown in Figure 2.2B and C. We give a detailed analysis in the Supplement and Figures 2.7 and 2.8 of how $S(c, \varepsilon_0)$ varies with c and ε_0 for the full range of ligand concentration.

Examining the dynamics of activity with respect to ligand changing in time, we get the equation

$$\frac{da}{dt} = \frac{\partial a}{\partial c}\frac{dc}{dt} \approx S(c, \varepsilon_0)\frac{K_A}{c}\frac{d}{dt}\left(\frac{c}{K_A}\right) = S(c, \varepsilon_0)\frac{d}{dt}\left(\ln \frac{c}{K_A}\right). \tag{2.5}$$

This shows explicitly that the rate of change in the activity of an MWC protein is a function of the logarithm of ligand concentration c.

The logarithmic dependence of an MWC protein occurs within a certain range,

$$\frac{\varepsilon_0 - \ln(\tau)}{N} < \ln\left(\frac{c}{K_A}\right) < \frac{\varepsilon_0 + \ln(\tau)}{N}, \tag{2.6}$$

where τ parametrizes the limits of the logarithmic range. This range is illustrated by the gray regions in Figure 2.2B and C, where we have chosen as an example $\tau = 6$. We provide a detailed derivation in the Supplement for how the range (2.6) translates into the gray regions in Figure 2.2B and C.

τ can be related to the deviation of the MWC response curve from a hypothetical ideal logarithmic sensor (the blue line in Figure 2.2B, derived in the Supplement). If we tolerate, for example, at most 10% error (at the lower and upper limits of the range (2.6) when $\tau = 6$) then an MWC protein with cooperativity $N = 4$ (e.g. hemoglobin and phosphofructokinase), would have a logarithmic range of $\sim$ 2.5-fold change in ligand concentration. A monomeric protein without any cooperativity ($N = 1$) would have a logarithmic range of 36-fold change in ligand concentration. Therefore, the range over which the activity of an MWC protein is logarithmically dependent on ligand concentration can be quite substantial. We see further that this range can be increased at the expense of cooperativity, telling us that there is an intrinsic trade-off between sensitivity and logarithmic range.

The logarithmic dependence of activity on ligand concentration is, however, not a unique feature of MWC proteins. Any monotonic binding curve, e.g. that of a Hill

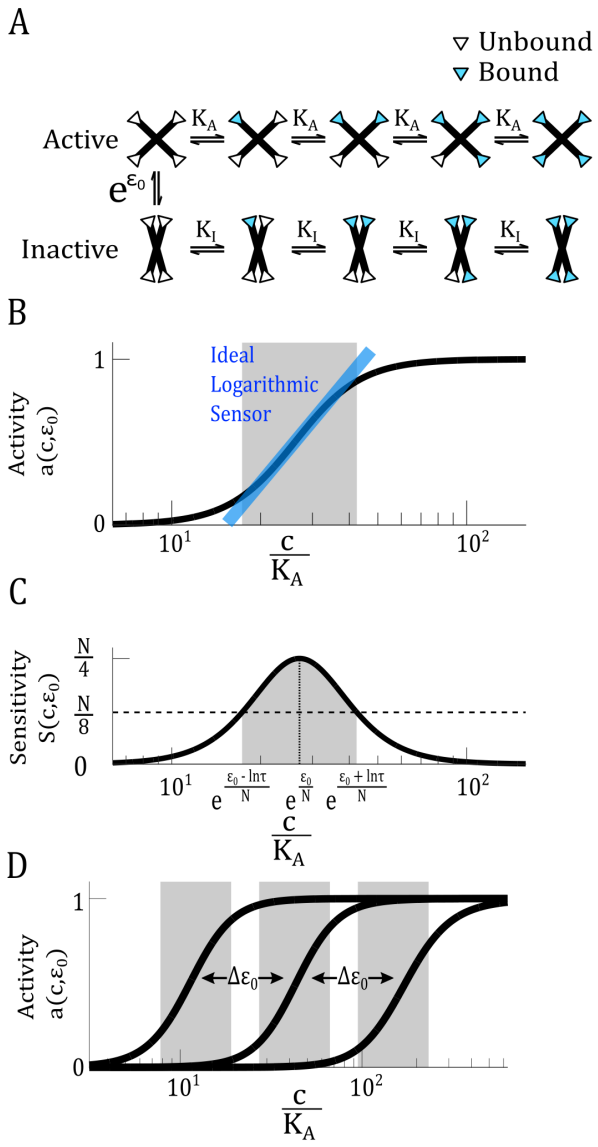

Figure 2.2: An MWC Protein Can Act as a Logarithmic Sensor. **A)** The MWC model describes a protein that can switch between an active and inactive conformation at a rate determined by the allosteric constant e^{ε_0}. The active state has a ligand binding affinity K_A and the inactive state has an affinity K_I. The white and blue triangles represent binding sites unoccupied and occupied by ligand, respectively. **B)** Within a certain range, activity of the MWC protein, $a(c, \varepsilon_0)$, depends logarithmically on the ligand concentration. The blue line indicates the ideal logarithmic sensor, whose activity directly corresponds to the logarithm of ligand concentration. The gray range indicates the range where activity of the MWC protein coincides with that of the ideal logarithmic sensor with a certain tolerable error. In this illustration, we set the error to be at most 10% (corresponding to $\tau = 6$ in equation (2.20)) **C)** The Sensitivity function $S(c, \varepsilon_0)$ is related to the derivative of the activity function, $a(c, \varepsilon_0)$. It allows us to define a range (in gray) where the sensitivity is above a certain threshold. In this illustration, the threshold is set to $\frac{N}{8}$, corresponding approximately to $\tau = 6$. In both B and C we use $N = 4$, $K_A = 10^{-3}\mu M$, $K_I = 10^{2}\mu M$, and $\varepsilon_0 = 13$. **D)** The activity curve of an MWC protein can be tuned on a logarithmic scale, by modulating the allosteric parameter ε_0.

model

$$a(c) = \frac{\left(\frac{c}{K_D}\right)^N}{1 + \left(\frac{c}{K_D}\right)^N}, \tag{2.7}$$

would also show some range for which activation depends logarithmically on ligand. The requirement for a logarithmic sensor we are considering here is a more stringent one: the activity of the protein must also be logarithmically tunable (Figure 2.1C). This will allow a protein which can already sense logarithmically over some regime of ligand to extend its responsiveness to a much greater range.

MWC proteins have the additional feature of logarithmic tunability, facilitated by the presence of an allosteric effector. Inequality (2.6) shows that the net effect of varying the allosteric parameter ε_0 is a shift in the midpoint of the logarithmic range, without changing its width (Figure 2.2D). The logarithmic tuning of the activity curve comes from the independent multiplicative relationship between e^{ε_0} and c in equation (2.3). To contrast, a Hill protein with a fixed K_D has no capacity to tune its response curve logarithmically. This can be seen in equation (2.7), which is analogous to the activation of an MWC protein in equation (2.3), except that there is no allosteric parameter ε_0. Allosteric regulation, which modulates the structural conformation of a protein, produces logarithmic tuning in the protein's response range.

Now we may ask, is the capacity to act as a logarithmic sensor a unique feature of the MWC model? First, we find that logarithmic tuning of the response curve does not depend on the specific form of the equilibrium ratio e^{ε_0}. Either an exponential form or a polynomial form of this function, as originally used by Monod, Wyman, and Changeux, work equally well (See Supplement) [21]. This means that an MWC protein can act as a logarithmic sensor whether it is thermally or kinetically driven.

Second, we find that other models of allostery also show the capacity for logarithmic sensing. An alternative model of allostery was proposed by Koshland, Nemethy, and Filmer, known as the KNF or sequential binding model [24]. In this model, ligand binding induces processive conformational changes, as opposed to the all-or-none transition in the MWC model. We find that activity of the KNF model can be tuned logarithmically, though it requires the regulation of more parameters (see derivation in Supplement and Figure 2.9).

Finally, beyond a single protein, we find that a network of proteins with appropriate connectivity can act as a logarithmic sensor. We illustrate this by analyzing the G protein-coupled receptor (GPCR) system (Figure 2.3A). GPCRs are a large family of seven-transmembrane domain receptor that couples to a G protein. The G proteins are composed of α, β, and γ subunits. Ligand binding induces a conformational change in the receptor, which results in the exchange of GDP to GTP in the alpha

subunit. This causes the α subunit to break off and activate downstream targets.

The GPCR system is described by a mass-action model (Figure 2.3A) [25]:

$$\dot{R} = k_1 c(1 - R) - k_2 R \tag{2.8a}$$

$$\dot{T}_{GDP} = k_3 \alpha_{GDP} - k_4 T_{GDP} R \tag{2.8b}$$

$$\dot{T}_{GTP} = k_4 T_{GDP} R - k_5 T_{GTP} \tag{2.8c}$$

$$\dot{\alpha}_{GTP} = k_5 T_{GTP} - k_6 \alpha_{GTP} \tag{2.8d}$$

$$\dot{\alpha}_{GDP} = k_6 \alpha_{GTP} - k_3 \alpha_{GDP}, \tag{2.8e}$$

where R is the fraction of active receptors, c is the ligand concentration, T_{GDP} and T_{GTP} are the concentrations of G protein with GDP and GTP bound, and α_{GDP} and α_{GTP} are the concentrations of α subunits dissociated from the G protein complex with GDP and GTP bound. Additionally, let $T_{tot} = T_{GDP} + T_{GTP} + \alpha_{GDP} + \alpha_{GTP}$ be the total concentration of G protein.

Although this system of differential equations appears unrelated to the MWC model, we find upon solving the equations that the steady-state activity of the GPCR system is

$$\hat{\alpha}_{GTP}(c) = \frac{\alpha_{GTP}}{T_{tot}} = \frac{c}{(1 + \frac{k_6}{k_3} + \frac{k_6}{k_4} + \frac{k_6}{k_5})c + \frac{k_6}{k_4}\frac{k_2}{k_1}}, \tag{2.9}$$

which is analogous to equation (2.3) in the MWC model (see detailed derivation in Supplement). The effective allosteric parameter here is k_6/k_4, which regulates the availability of G proteins. As plotted in Figure 2.3B, varying k_4 logarithmically tunes the activity curve of the GPCR. This eventually breaks down when k_4 becomes too low. In a later section, we will discuss the physiological significance of tuning the rate k_4.

Therefore the capacity to act as a logarithmic sensor can be realized when conformational changes in an allosteric protein are either thermally or kinetically driven, whether allosteric regulation is manifested through all-or-none or processive conformational change, and whether allosteric regulation is realized by a single protein with multiple subunits or a network of many proteins. We formally define a logarithmic sensor as a system that satisfies the property

$$a(c, \varepsilon_0 + \Delta\varepsilon) = a(e^{-\kappa\Delta\varepsilon}c, \varepsilon_0), \tag{2.10}$$

where κ is a scaling factor that corresponds to the rate at which logarithmic shifting occurs. The particular value of κ will depend on the parameters of the underlying

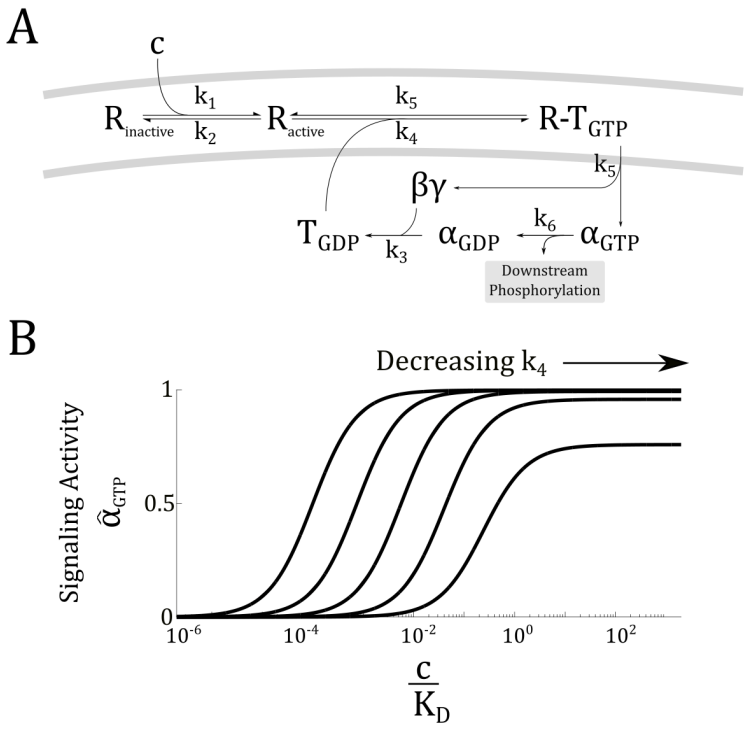

Figure 2.3: The Regulatory Circuit of the G Protein-Coupled Receptors Can Act as a Logarithmic Sensor. **A)** Upon activation by ligand (c), the receptor (R) changes conformation and activates a G protein (T), which then break into an α and a $\beta\gamma$ subunit. The α subunit is responsible for downstream signaling, after which it recombines with a $\beta\gamma$ subunit and recover the pool of G proteins. **B)** Activity of the GPCR system, i.e. the concentration of $\hat{\alpha}_{GTP}$, is logarithmically tuned by $\frac{k_6}{k_4}$, the effective allosteric constant in the system. The logarithmic tuning breaks down when k_4 is much slower than k_6. In this plot, $k_1 = 1, k_2 = 10, k_3 = 10, k_5 = 50, k_6 = .01$, and $k_4 \in [10^{-2}, 10^2]$.

system. With some manipulation, we get

$$\begin{aligned} a(c, \varepsilon_0 + \Delta\varepsilon) &= a(e^{-\kappa\Delta\varepsilon} c, \varepsilon_0) \\ &= a(e^{-\kappa\Delta\varepsilon} e^{\ln(c)}, \varepsilon_0) \\ &= a(e^{\ln(c) - \kappa\Delta\varepsilon}, \varepsilon_0). \end{aligned} \tag{2.11}$$

In any system where equation (2.10) holds, a linear shift in ε results in a logarithmic tuning of the response curve. We show in the Supplement that the different models we have considered satisfy these requirements in equation (2.10) (e.g. the MWC model, the GPCR network, the KNF model).

How might a logarithmic sensor be used in biological systems? A logarithmic sensor can mediate fold-change detection if it is coupled to a downstream feedback module (Figure 2.4A and B). For example, consider a system that experiences a two-

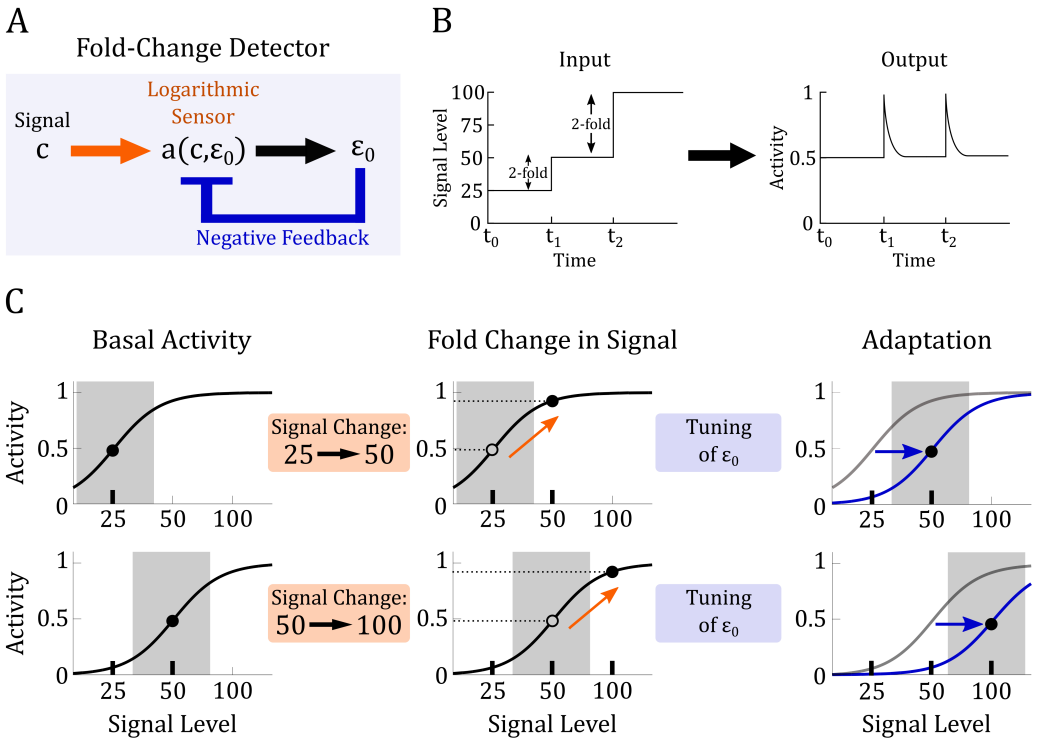

Figure 2.4: Logarithmic-Feedback Circuit. A) A logarithmic sensor can produce fold-change detection when coupled with negative feedback. In our model, the logarithmic sensor is an allosteric protein and the feedback comes from downstream modulation of an allosteric effector. **B)** In fold-change detection a step increase in signal from 25 to 50, or from 50 to 100 will produce identical outputs. **C)** An illustration of how the logarithmic-feedback circuit can produce fold-change detection. In the first row: a logarithmic sensor experiences a two-fold change in signal from 25 to 50. This produces a change in the sensor's activity (orange arrow). The change in activity turns on downstream feedback which allosterically tunes the activation curve on a logarithmic scale (blue arrow), returning the sensor's activity to its basal level. In the second row: the same sensor now experiences another 2-fold change in signal, from 50 to 100. Despite the different in signal magnitude, this 2-fold change produces a change in activity that is identical to the previous one (dashed lines). Feedback will eventually take effect and the system will return again to its basal level of activity.

fold change in signal, from 25 to 50 (Figure 2.4C, row 1). The logarithmic sensor computes a two-fold change, and produces an activity change of Δa. Subsequently, the feedback module adapts the system to the new signal level by allosterically tuning the response curve and restoring the protein to the original level of activity. The system is now poised to respond to signal changes again. If, from the basal activity of 50, the system experiences another change in signal to 100 (Figure 2.4C, row 2), the logarithmic sensor will again compute a two-fold change, producing an identical

change in activity of Δa, and the feedback module again adapts the system to the new signal level. We simulate the interaction of allostery and negative feedback, and confirm that they can indeed produce fold-change detection (see Supplement and Figures 2.10 and 2.11). Therefore, the combination of a logarithmic sensor and adaptive feedback produces fold-change detection by continually tuning the response curve to a new background level, avoiding saturation and maintaining sensitivity to subsequent changes in signal.

Evidence that allosteric proteins are used as logarithmic sensors

While our theoretical results show that allosteric proteins can act as logarithmic sensors, in practice there may be physical limitations where the systems may not operate in an appropriate parameter regime to facilitate this behavior. For example, it may be that the inactive conformation is so heavily preferred that ligand binding follows a Michaelis-Menten model. Alternatively, the binding of allosteric effectors may be saturated, making it impossible to tune the activity curve.

We therefore explored evidence in the literature to see if known allosteric proteins act as logarithmic sensors in physiological contexts. We found two lines of evidence. First, we found many measurements of allosteric proteins show response curves that are logarithmically tunable. Second, we find examples where allosteric proteins play a prominent role in processes where fold-change detection has been proposed or established.

Shown in Figure 2.5 are measured activity curves of some allosteric proteins. We reproduced these measurements with original data when available, or by retrieving data with the application Web Plot Digitizer. In some instances the curves were originally plotted in linear scale, and we have replotted them here in logarithmic scale to examine if they are logarithmically tunable. Although there is wide literature on allosteric proteins, we present here examples where quantitative measurements have been performed over a broad range of ligand concentrations.

Not only do some allosteric proteins tune their response on logarithmic scale, they can do so over a substantial range. One striking example we found is the glycolytic enzyme phosphofructokinase (PFK1), whose response can be tuned over a remarkable 2000-fold range of ligand concentration. This eventually fails at low concentrations, where leaky enzyme activity begins to appear. More examples are summarized in the table (Figure 2.5G). Presented in the table is the approximate range of ligand concentrations over which allosteric proteins tune their response

logarithmically. We found examples across a wide range of biological processes including metabolism, ion transport, neurotransmission, insulin signaling, and olfaction.

In addition to evidence that some allosteric proteins operate in the parameter regime where they are logarithmically tunable, we find that they play a prominent role in systems where fold-change detection has been proposed. Further, in each example, the allosteric proteins are coupled to feedback mechanisms, suggesting that their capacity as a logarithmic sensor is functionally utilized. We describe three examples here.

Bacterial Chemotaxis

Bacterial cells detect and track chemical gradients in their environment. Mesibov *et al.* [13] first observed that the bacterial motile behavior depended on fold changes in attractant concentration. The fold-change detection was later confirmed through elegant FRET experiments [15, 28, 34].

Structural studies have now established a physical basis for MWC allostery in the aspartate-sensing Tar receptors (Figure 2.5D) [35, 22]. Further, the allosteric receptor is connected to a well established feedback mechanism. Feedback is largely mediated by methylation and demethylation of the Tar receptors, which yields precise adaptation [36, 37, 38].

Vision

Logarithmic response is well established in vision, in particular in the context of dark adaptation in rod photoreceptors [5, 39]. Light detection is mediated by the GPCR rhodopsin in retinal photoreceptor cells. Examining the rhodopsin regulation network, we found two possible roles for allostery. First, recent studies find evidence that GPCRs follow the MWC model, existing in distinct conformational states, containing physically distant regulatory sites, and forming oligomers [29, 40, 41, 42, 43]. Indeed, several regulators tune activity curves of GPCRs on a logarithmic scale (Figure 2.5E). Second, as described earlier, the regulatory network of interactions between GPCRs and G proteins can give the net effect of allosteric regulation (Figure 2.3).

Moreover, the allosteric rhodopsin is coupled to a known feedback mechanism mediated by β-arrestin. Activation of rhodopsin induces receptor phosphorylation and binding of arrestin, which blocks further binding of transducin and results in

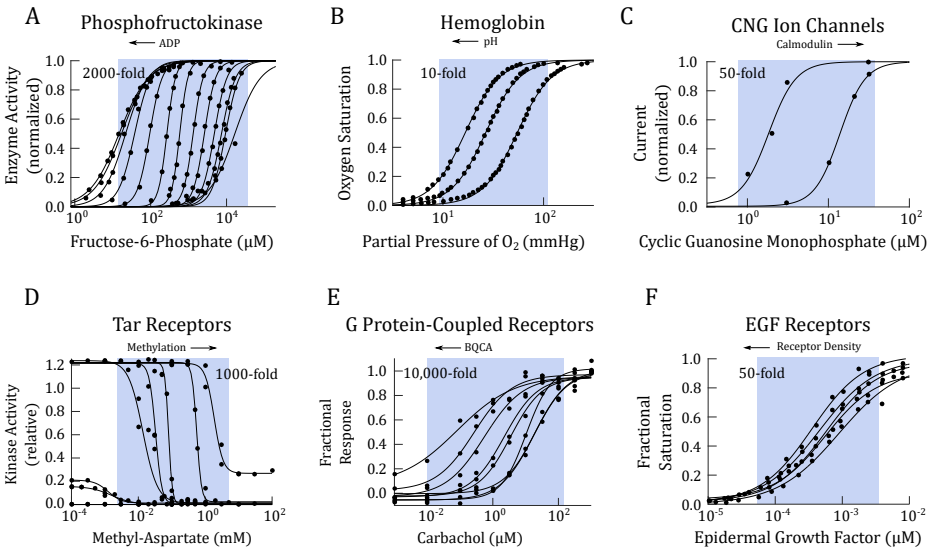

G

Protein	Biological Process	Experimental System	Range of Log Tuning	Reference
(**A**) Phosphofructokinase	Glycolysis	Purified Protein	2,000-fold	Blangy *et al.*
(**B**) Hemoglobin	Oxygen Transport	Purified Protein	10-fold	Imai *et al.*
(**C**) CNG Ion Channels	Olfaction	HEK Cells	50-fold	Müller *et al.*
CNG Ion Channels	Phototransduction	*Xenopus* Oocytes	10-fold	Molokanova *et al.*
(**D**) Tar Receptors	*E. coli* Chemotaxis	*E. coli*	1000-fold	Shimizu *et al.*
(**E**) GPCR (M_1 mAChR)	Nervous System Regulation	CHO Cells	10,000-fold	Canals *et al.*
GPCR (M_2 mAChR)	Heart Rate Regulation	CHO Cells	100-fold	Wootten *et al.*
GPCR (A_1-AR)	Neurotransmitter Signaling	CHO Cells	10-fold	Wootten *et al.*
GPCR (GLP-1)	Insulin Regulation	CHO Cells	10-fold	Wootten *et al.*
(**F**) EGF Receptors	Signal Transduction	CHO Cells	50-fold	Macdonald *et al.*
lac Repressor	Metabolic Regulation	*E. coli*	100-fold	Lewis *et al.*

Figure 2.5: Biophysical Measurements Show That Allosteric Proteins are Logarithmically Tunable. In A-F, activity of an allosteric protein is plotted against ligand concentration. Within each plot, each activity curve corresponds to a different level of allosteric modulation. The arrow indicates modulation of the concentration of allosteric effectors. Data points (black circles) were extracted from the original studies using Web Plot Digitizer, except in panels A and B where the original data were available. The data were fit with Hill equations using a nonlinear least-square fit in MATLAB. The range of logarithmic tuning is defined as the ratio of $\frac{K_A}{K_I}$, which we estimated from the published measurements with empirical K_Ds from the Hill equation and is depicted in the blue regions. These regions are meant to be a visual aid to highlight the effects of allosteric regulation, and are not analytical. **A)** Phosphfructokinase is a key enzyme in glycolysis and is allosterically regulated by ADP and ATP. In this study, ADP was varied from 0 to $2mM$ [23]. **B)** Hemoglobin is the primary oxygen transport protein in vertebrates. It is allosterically regulated by blood pH. In this study, pH was varied from 6.6 to 7.8 [26]. **C)** Cyclic Nucleotide-Gate Ion Channels are allosterically modulated by calmodulin. In this study, the ion channels were treated with 0 and $.5\mu M$ calmodulin [27]. **D)** The Tar Receptor in the *E. coli* chemotaxis pathway is allosterically regulated by methylation level. In this study, the methylation level was varied through receptor mutants [28]. **E)** Muscarinic Acetylcholine Receptors are a G protein-coupled receptor responsible for signaling often found in neurons. They are allosterically regulated by benzyl quinolone carboxylic acid (BQCA). In this study, BQCA was varied from 0 to $10\mu M$ [29]. **F)** Epidermal Growth Factor Receptors are allosterically regulated by receptor density [30]. In this study, receptor density was varied by overexpression from 2×10^4 to 1.2×10^6 receptors per cell. G) A table summary of more allosteric proteins, whose measured activity shows logarithmically tuning. When measurements were performed *in vivo*, the systems was either Chinese Hamster Ovary (CHO) cells, Human Embryonic Kidney (HEK) cells, *Xenopus* oocytes, or *E. coli*. Data for CNG ion channels in phototransduction comes from Molokanova *et al.* [31], data for M_2 mAChR, A_1-AR, and GLP-1 GPCRs come from Wootten *et al.* [32], and data for the *lac* repressor comes from Lewis *et al.* [33].

adaptation to the pre-stimulus state. The action of arrestin modulates k_4 in Figure 2.3A, the regulatory step that facilitates logarithmic tuning of the GPCR response curves (Figure 2.3B).

Epidermal Growth Factor Signaling

The EGF receptor (EGFR) pathway is a major signaling pathways in animal cells. Cohen-Saidon *et al.* showed that upon ligand stimulation, single cells show a precise fold-change response relative to the basal level, despite large variation in the absolute magnitude of the response [9]. Recent evidence suggests that the EGFR is allosterically regulated [30]. The EGFR exists in monomeric and dimeric forms. Binding of the ligand stabilizes the dimers, leading to activation of downstream effectors. It is proposed that modulation of dimerization rate results in allosteric regulation, which produced logarithmic tuning in the receptor activity (Figure 2.5F).

Moreover, the allosteric receptor is upstream from various known feedback mechanisms, including ubiquitylation and endocytosis of receptors [44, 45], dephosphorylation of active receptors [46], and feedback by ERK [47]. Interestingly, one member of the EGFR family, ErbB2 receptor, lacks a ligand-binding domain but can dimerize with other receptors. Overexpression of ErbB2 has been associated with therapy-resistant cancers [48], suggesting that disrupting the allosteric regulation of the EGF receptors may play a role in disease.

2.3 Discussion

In this study, we set out to search for a molecular implementation of a logarithmic sensor that can mediate fold-change detection in sensory systems. We identify that a ubiquitous class of regulation, allostery, has the necessary properties to act as a logarithmic sensor. Allostery has traditionally been thought as a mechanism for generating cooperativity and implementing feedback in signaling systems. Our analysis suggests a new role for allosteric proteins, namely as logarithmic sensors. We find that the capacity for logarithmic sensing is not dependent on the specific physical implementations of allostery. Rather, it arises from the basic feature of allostery: the presence of an independent regulation to tune the protein's activity without altering the ligand binding kinetics. It is remarkable that the seemingly complex task of computing a logarithm can be encoded within a single protein, and further that this can be accomplished through such a pervasive form of regulation in biological systems. Moreover, beyond proteins, allostery also applies to RNAs. For instance, there is recent evidence that riboswitch activity can be tuned via

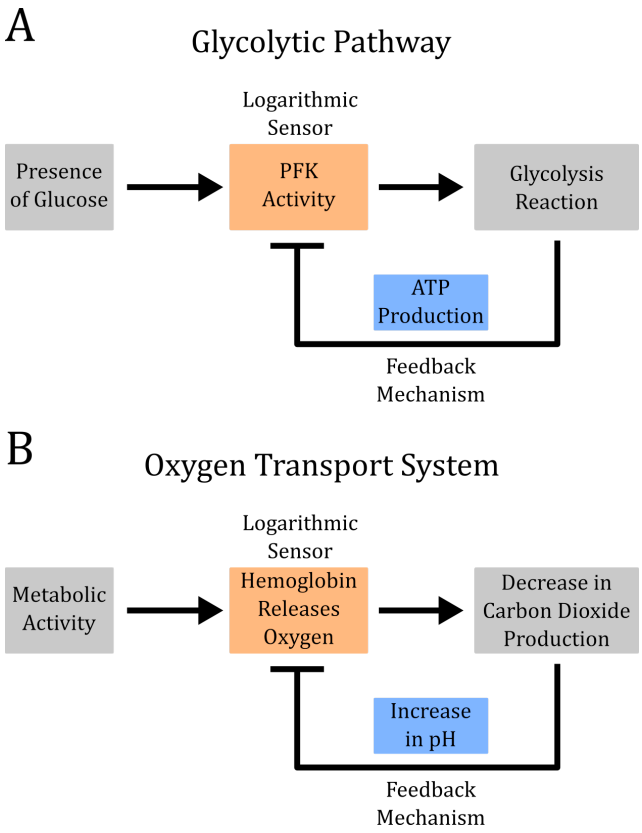

Figure 2.6: Allostery and Feedback in Glycolysis and Oxygen Regulation. A) Phosphofructokinase (PFK) is a key enzyme in glycolysis. PFK both catalyzes downstream production of ATP and is allosterically regulated by ATP itself. This system of interactions resembles a logarithmic-feedback circuit, which has the capacity to produce fold-change detection. **B)** Oxygen transport in vertebrates is mediated by hemoglobin and feedback via multiple effectors (including carbon dioxide level). This system of interactions forms a logarithmic-feedback circuit, which can produce fold-change detection.

conformational selection [49]. This opens up the possibility of an RNA-based logarithmic sensor that senses metabolite concentration.

When allosteric regulation is coupled with linear feedback, it can produce fold-change detection (Figure 2.4A). This logarithmic-feedback circuit is an appealing architecture because feedback regulation is another ubiquitous feature of biological systems, and raises the questions of whether logarithmic sensing and the related phenomenon of fold-change detection occurs more broadly in biological processes than is currently appreciated. For instance in glycolysis, phosphofructokinase is inhibited by ATP and ADP, end products of the pathway, producing a logarithmic-feedback circuit (Figure 2.6A) [18]. We imagine that fold-change detection might be beneficial in glycolysis to maintain sensitive metabolic activity across a broad range of glucose concentrations. In another example, hemoglobin is regulated by blood

pH, in what is known as the Bohr effect [26, 50]. High levels of carbon dioxide cause changes in blood pH, which in turn regulate the activity of hemoglobin, producing a logarithmic-feedback motif (Figure 2.6B). We imagine that fold-change detection might be beneficial for hemoglobin to maintain sensitivity across a range of altitude, metabolic state, physical activity, lifestyle, or body size, where oxygen level varies.

Therefore, beyond their commonly thought of roles as enzymes, transporters, it would be interesting to see if allosteric proteins may also generally act as quantitative sensors, adjusting detection on a logarithmic scale to maintain sensitivity over a broad response range.

2.4 Supplemental Material

Analysis of the Sensitivity and Error Functions

We now define the sensitivity function $S(c, \varepsilon_0)$, which summarizes the steepness of the slope of the activity curve is as a function of c and ε_0,

$$S(c, \varepsilon_0) \triangleq N \frac{e^{-\varepsilon_0}(\frac{c}{K_A})^N}{\left(1 + e^{-\varepsilon_0}(\frac{c}{K_A})^N\right)^2}. \tag{2.12}$$

Looking at the dynamics of activity with respect to ligand changing in time, we get the equation

$$\frac{da}{dt} = \frac{\partial a}{\partial c}\frac{dc}{dt} \approx S(c, \varepsilon_0)\frac{K_A}{c}\frac{d}{dt}\left(\frac{c}{K_A}\right) = S(c, \varepsilon_0)\frac{d}{dt}\left(\ln\frac{c}{K_A}\right). \tag{2.13}$$

Here we see the first requirements for a protein to give rise to logarithmic sensing: the rate of change of activity is naturally a function of the logarithm of the ligand concentration c. Equation (2.5) is complicated by the sensitivity function $S(c, \varepsilon_0)$, which varies with c and is therefore not a simple proportional factor. An ideal logarithmic sensor requires that the activity function depends strictly on $\ln c$, as illustrated by the blue dashed line in Figure 2.2B. To measure how well an MWC protein can act as a logarithmic sensor, let us quantify the extent to which $S(c, \varepsilon_0)$ varies as a function of c.

First we note that an ideal logarithmic sensor coincides exactly with an MWC protein at the midpoint of the activity curve ($a = 1/2$, at the inflection point of a). This also corresponds to the maximum of the sensitivity function $S_{\max} = \frac{N}{4}$ in equation (2.4), i.e. the peak in Figure 2.2C. Any variation in ligand which pushes activity away from the midpoint will lower the sensitivity, and will do so in a nonlinear way.

Our first task here is to define a regime of the sensitivity curve (the gray region in Figures 2.2B, C and D) where the MWC protein can approximate a logarithmic sensor, and compute the corresponding error.

To parametrize variation from $S_{\max}$, we define the effective ligand concentration to be

$$\mathcal{L}(c, \varepsilon_0) = e^{-\varepsilon_0}(c/K_A)^N. \tag{2.14}$$

Deriving equation (2.4) in terms of $\mathcal{L}$, we obtain a natural representation of the sensitivity function,

$$S(\mathcal{L}) = \frac{da}{d\mathcal{L}} = \frac{\mathcal{L}}{(1+\mathcal{L})^2}. \tag{2.15}$$

In this representation, the sensitivity is now maximized at $\mathcal{L} = 1$. Next, we derive a lower limit on the sensitivity function. Let us define the parameter τ, such that for distance $\tau > 1$ from the midpoint of the activity curve, we have a minimum sensitivity,

$$S_{\min}(\tau) = \frac{\tau}{(1+\tau)^2}. \tag{2.16}$$

With these lower and upper limits on sensitivity, we now define the regime in the response curve over which the MWC protein approximates a logarithmic sensor as

$$S_{\min} < S(\mathcal{L}) < S_{\max}. \tag{2.17}$$

Using equation (2.14), we can derive a corresponding lower limit on for the range of $\mathcal{L}$ over which the bound holds, $\frac{1}{\tau} < \mathcal{L} < \tau$. These limits give the ligand concentration range over which an MWC protein behaves as a logarithmic sensor,

$$\frac{\varepsilon_0 - \ln(\tau)}{N} < \ln\left(\frac{c}{K_A}\right) < \frac{\varepsilon_0 + \ln(\tau)}{N}. \tag{2.18}$$

This range is shown in Figure 2.2B and C, where the sensitivity regimes for different values of ε_0 are shaded in gray. We see that the range of ligand over which the MWC systems functions as a logarithmic sensor is set by a threshold for sensitivity $S_{\min}$. The error between the MWC activity curve and the idealized sensor is parametrized by τ. The range over which the MWC protein behaves as a logarithmic sensor depends on how much error the system can tolerate.

To derive the error, we first write the formal expression for an ideal logarithmic sensor,

$$a^*(\mathcal{L}) = \frac{1}{4}\ln\mathcal{L} + \frac{1}{2}. \tag{2.19}$$

We will now use this expression to define an error function $r = 1 - \frac{a}{a^*}$ to quantify the deviation of the actual activity function a from the idealized one a^*. Combining equations (2.3) and (2.19), we have

$$r(\mathcal{L}) = 1 - \frac{a(\mathcal{L})}{a^*(\mathcal{L})} = 1 - \frac{2\mathcal{L}}{(1+\mathcal{L})(1+\frac{1}{2}\ln\mathcal{L})}. \tag{2.20}$$

At the midpoint of activity ($\mathcal{L} = 1$) the error function is minimized at $r(1) = 0$, since this is the point where MWC activity coincides exactly with the ideal logarithmic sensor. We observe that the error $r(\mathcal{L})$ increases as $\mathcal{L}$ moves away from 1. Consequently, the error at the threshold τ, $r(\tau)$, corresponds to the worst case error in the sensitive regime. For example in Figure 2.2E where we set $\tau = 6$, we have $r(\tau) \approx .1$, so the MWC response differs by at most $\sim 10\%$ from the ideal logarithmic response in the sensitive regime. The threshold τ serves as a way to analyze how much the response of an MWC protein differs from an ideal logarithmic sensor as we expand the range of ligand concentration over which it is used. The maximum error $r(\tau)$ increases at an asymptotic rate of

$$\lim_{\tau \gg 1} = 1 - \frac{4}{\ln\tau}.$$

This means that the error increases slowly with τ, and that the MWC protein can approximate well an ideal logarithmic sensor over a wide range of the activity curve.

With the error function, we can now define the logarithmic regime of an MWC protein, as the ratio of the maximum and minimum ligand concentrations in the sensitive regime

$$c_S(\tau) = \frac{c_{\max}}{c_{\min}} = \frac{e^{\frac{\varepsilon_0 + \ln(\tau)}{N}}}{e^{\frac{\varepsilon_0 - \ln(\tau)}{N}}} = e^{\frac{2}{N}\ln(\tau)} = \tau^{\frac{2}{N}}. \tag{2.21}$$

If we tolerate, for example, 10% error from the ideal logarithmic sensor (corresponding to $\tau \approx 6$), then an MWC protein with cooperativity $N = 4$ (as is the case, for example, with hemoglobin and phosphofructokinase), we have $c_S(\tau) = \sqrt{\tau} \approx 2.45$, so the protein can act as a logarithmic sensor over a 2.45 range of fold change in signal. If, for example, the protein of interest were a monomer (i.e. $N = 1$) that lacks cooperativity, we would have $c_S(\tau) = \tau^2 = 36$, so the protein can act as a logarithmic sensor over a 36-fold range of signal. We see from this that an MWC protein can approximate an ideal logarithmic sensor over a substantial range of ligand concentration. Reducing cooperativity effectively increases the regime over which an MWC protein responds logarithmically to ligand. Equation (2.21) tells

us that there is an intrinsic trade-off between sensitivity and signaling range. Since N corresponds to cooperativity and c_s corresponds to the width of the sensitivity regime, we see directly that increasing N for a given τ narrows the range over which the sensor can function.

Effects of the Allosteric Constant on the Sensitivity Function

We first analyze the effects of ε_0 on $S(c, \varepsilon_0)$ when c is in the range $K_A \ll c \ll K_I$, and then analyze the general case where c could be near saturation. In the former case, as we derive in the main text,

$$S(c, \varepsilon_0) \triangleq N \frac{e^{-\varepsilon_0}(\frac{c}{K_A})^N}{\left(1 + e^{-\varepsilon_0}(\frac{c}{K_A})^N\right)^2}.$$

Figure 2.7 shows that $S(c, \varepsilon_0)$ shifts logarithmically as ε_0 is varied, in the same way as the activity curve $a(c, \varepsilon_0)$ does.

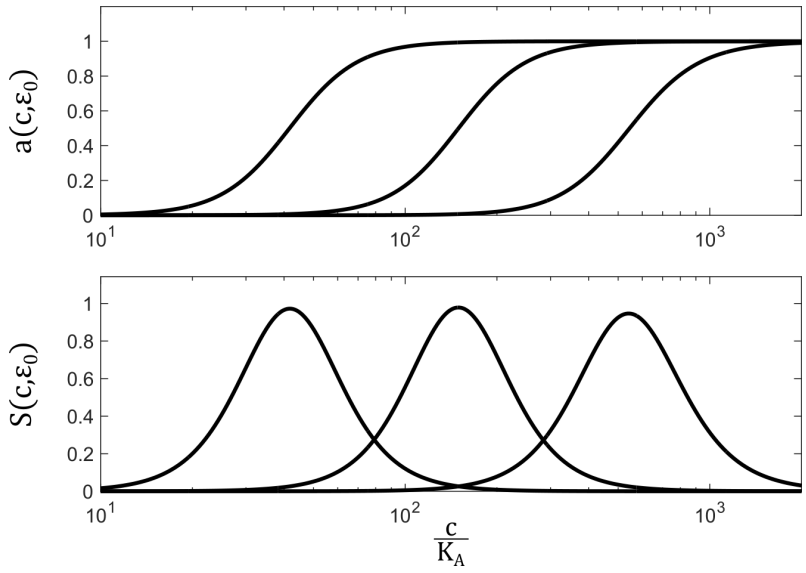

Figure 2.7: Effects of ε_0 on the Sensitivity Function. A) Activation curves for the MWC model in equation (2.1). The parameters used here are $K_A = 10^{-2}, K_I = 10^2, N = 4, \varepsilon_0 \in [15, 25]$. B) Sensitivity functions corresponding to the MWC activation curves in panel A.

Next, we analyze the general case for all values of ligand concentration c. The general sensitivity function $S(c, \varepsilon_0)$ is defined in terms of the expression,

$$\frac{\partial a}{\partial t} = S(c, \varepsilon_0) \frac{d \log c}{dt}. \tag{2.22}$$

For an MWC protein, we have from equation (2.2) that

$$\frac{\partial a}{\partial t} = Na(1-a)\frac{K_A^{-1}-K_I^{-1}}{(1+c/K_A)(1+c/K_I)}\frac{dc}{dt} \tag{2.23}$$

$$= Nca(1-a)\frac{K_A^{-1}-K_I^{-1}}{(1+c/K_A)(1+c/K_I)}\frac{d\log c}{dt}$$

$$\implies S(c,\varepsilon_0) = Nca(1-a)\frac{K_A^{-1}-K_I^{-1}}{(1+c/K_A)(1+c/K_I)}. \tag{2.24}$$

Next, assuming that $K_A \ll K_I$, we can rewrite the sensitivity function as

$$S(c,\varepsilon_0) = Na(1-a)\frac{c/K_A}{(1+c/K_A)(1+c/K_I)}. \tag{2.25}$$

As a sanity check, we see that in limit $K_A \ll c \ll K_I$ (i.e. $\frac{c}{K_A} \gg 1, \frac{c}{K_I} \ll 1$), equation (2.25) reduces to the sensitivity function we derive in the main text,

$$S(c,\varepsilon_0) = Na(1-a) = N\frac{e^{-\varepsilon_0}(\frac{c}{K_A})^N}{\left(1+e^{-\varepsilon_0}(\frac{c}{K_A})^N\right)^2}.$$

Logarithmic tuning fails for very high or low values of ε_0, when c is near saturation. To see this, we derive the limit of $S(c,\varepsilon_0)$ as $c \approx K_A$, corresponding to the ligand concentration being near the lower saturation limit. We can make the simplification $\frac{c}{K_I} \ll 1$, which yields

$$S_{lower}(c,\varepsilon_0) = Na(1-a)\frac{c/K_A}{1+c/K_A}. \tag{2.26}$$

Figure 2.8B shows the full sensitivity function (equation (2.25)) as a solid black line and the approximation in equation (2.26) as a blue dotted line. We see that, as c/K_A approaches 1, $S(c,\varepsilon_0)$ is scaled down by a factor of $\frac{c/K_A}{1+c/K_A}$ (shown as a dotted black line). This will become a noticeable effect when ε_0 is small enough to push the center of the sensitivity function close to K_A.

At the upper limit, as $c \approx K_I$, which give the simplification $\frac{c}{K_A} \gg 1$, we can derive

$$S_{upper}(c,\varepsilon_0) = Na(1-a)\frac{1}{1+c/K_I}. \tag{2.27}$$

Figure 2.8C shows the equation (2.27) in red. As c approaches K_I, $S(c,\varepsilon_0)$ scales down by a factor of $\frac{1}{1+c/K_I}$. This will become a noticeable effect when ε_0 is large enough to push the center of the sensitivity function close to K_I.

This analysis shows how c and ε_0 combine to determine the shape of the full sensitivity function, and how logarithmic sensing breaks down as ligand concentration nears saturation.

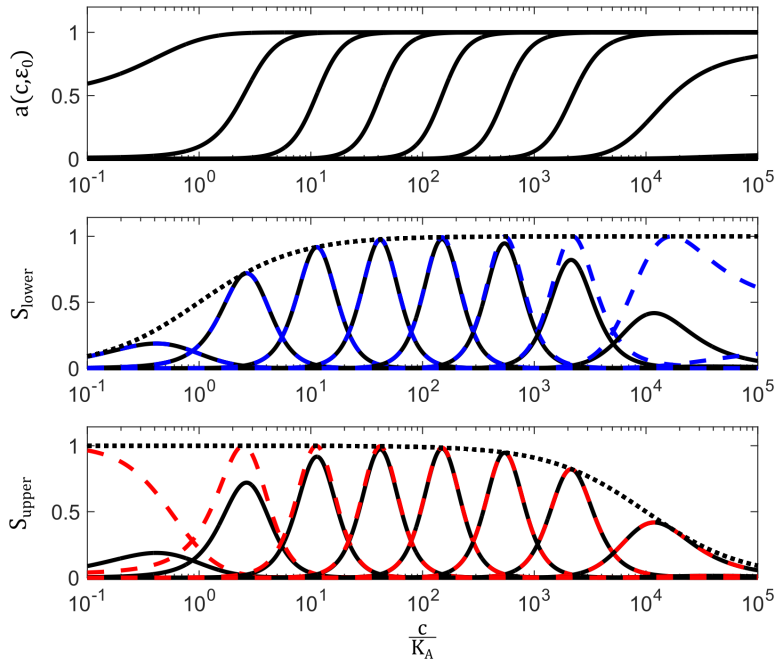

Figure 2.8: Saturation Effects in the Sensitivity Function. A) Activation curves for the MWC model in equation (2.1), across a full range of ligand concentration, c. The parameters used here are $K_A = 10^{-2}, K_I = 10^2, N = 4, \varepsilon_0 \in [0, 60]$. B) $S(c, \varepsilon_0)$ as c nears lower saturation. The solid black curves are $S(c, \varepsilon_0)$ for the same parameters as in panel A, the dashed blue line is $S_{lower}(c, \varepsilon_0)$ from equation (2.26), and the dotted black line is the scaling function $\frac{N}{4}\frac{c/K_A}{1+c/K_A}$. C) $S(c, \varepsilon_0)$ as c nears upper saturation. The solid black curves are plots of $S(c, \varepsilon_0)$ for the same parameters as in panel A, the dashed red line is from equation (2.27), and the dotted black line is the scaling function $\frac{N}{4}\frac{1}{1+c/K_I}$.

Allosteric Activators and Inhibitors in the MWC Model

In their original model, Monod *et al.* did not express their "allosteric constant" in the general form e^{ε_0}, but rather proposed a more detailed model where the binding of allosteric activators and inhibitors are explicitly accounted for, in much the same way as the primary ligand. In terms of our notation, their model can be expressed in the form

$$a(c, c_a, c_i) = \frac{\left(1 + \frac{c}{K_A}\right)^N}{\left(1 + \frac{c}{K_A}\right)^N + L\left(1 + \frac{c}{K_I}\right)^N}, \tag{2.28}$$

where $L = e^{\varepsilon_0}\frac{(1+\frac{c_i}{K_i})^{n_i}}{(1+\frac{c_a}{K_a})^{n_a}}$. This version of the model assumes that the activator and inhibitor have n_a and n_i binding sites with dissociation constants K_a and K_i, respectively. Rewriting the expression for L, we get

$$L = \exp\left(\varepsilon_0 + n_i \ln\left(1 + \frac{c_i}{K_i}\right) - n_a \ln\left(1 + \frac{c_a}{K_a}\right)\right). \tag{2.29}$$

If the allosteric effectors are far from saturation, then from the Taylor expansion of $\ln(1+x)$ we have

$$L \approx \exp\left(\varepsilon_0 + n_i \frac{c_i}{K_i} - n_a \frac{c_a}{K_a}\right). \tag{2.30}$$

This approximation gives a mechanism for the linear dependence of free-energy on the concentrations of allosteric regulators. Shimizu *et al.* found just such a dependence in experiments on receptor methylation in the bacterial chemotaxis pathway [28].

Logarthmic Tuning in the KNF Model

Shortly after Monod, Wyman, and Changeux published their MWC model of allostery via conformational selection, Koshland *et al.* put forth what is now called the induced fit or KNF model of allostery to explain hemoglobin binding kinetics [24]. This model proposes that instead of undergoing spontaneous comformational change, that individual binding events in one subunit could directly change the binding kinetics of another. This model has the advantage that it can both encapsulate positive cooperativity (like the MWC model) and negative cooperativity, where a given binding even could potentially inhibit the next. In the years after both models of hemoglobin were published, structural work by Perutz gave evidence that the MWC model was indeed more accurate. In reference to the work of Monod *et al.*, Perutz wrote, "These words ring prophetically if we look at the mechanism in terms of quaternary structure" [51].

Be that as it may, the concept of induced fit proved useful for describing other classes of allosteric systems, in particular those in which negative cooperativity plays an important role [52]. Here we show under what conditions the KNF model can be logarithmically tuned. The KNF model differs from other models of binding typically discussed because the specific geometry of the protein plays an important role, we will use as an example the tetrahedral geometry discussed in the original paper by Koshland *et al.* which results in the saturation function

$$Y(c, K_{BB}) = \frac{K_{AB}^3 \frac{c}{K_D} + 3K_{AB}^4 K_{BB} (\frac{c}{K_D})^2 + 3K_{AB}^3 K_{BB}^3 (\frac{c}{K_D})^3 + K_{BB}^6 (\frac{c}{K_D})^4}{1 + 4K_{AB}^3 \frac{c}{K_D} + 6K_{AB}^4 K_{BB} (\frac{c}{K_D})^2 + 4K_{AB}^3 K_{BB}^3 (\frac{c}{K_D})^3 + K_{BB}^6 (\frac{c}{K_D})^4}, \tag{2.31}$$

where K_D is the ligand dissociation constant, and the subunit conformations are denoted A and B. By convention, A will be the low affinity inactive state and B will be the high affinity active state. The interaction strengths K_{AB} and K_{BB} represent

the relative strengths of interactions between the A and B conformations and the B conformation with itself, respectively. Here we allow allosteric effects to enter through K_{BB}. The motivation for this is the underlying model that the allosteric effectors alter the stability of the bonds between the active conformation.

The authors use $K_{AA} = 1$ as a reference interaction strength against which to measure the other two, so it does not have to be explicitly accounted for in equation (2.31). In this model, high cooperativity comes from high stability of the active state B, i.e. $K_{BB} \gg 1$ and $K_{AB} \approx K_{AA} = 1$. Under these conditions, the intermediate terms in the

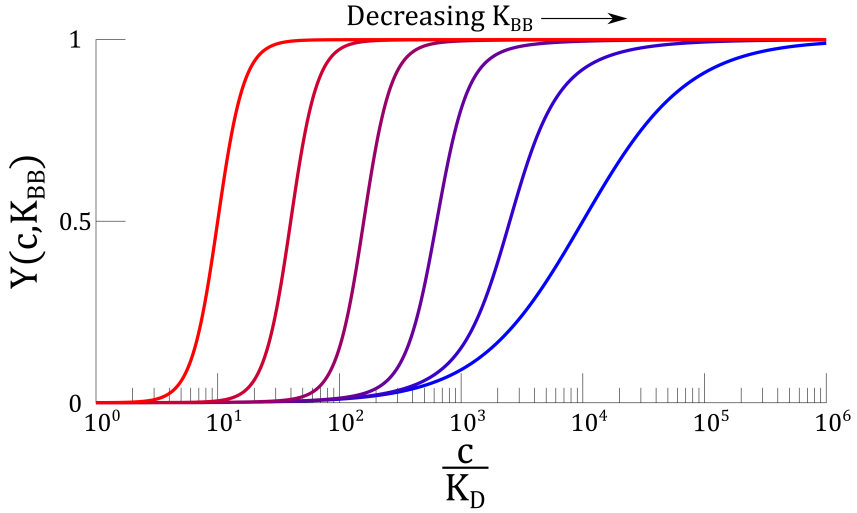

Figure 2.9: Logarithmic Tuning in the KNF Model. Here we show the capacity of the KNF model to be logarithmically tuned. This plot uses $K_D = 10^2, K_{ab} = 1, K_{bb} \in [10^0, 10^2]$. For these parameters, we observe approximately three orders-of-magnitude in logarithmic shifting before the response curve begins to change shape. Much like the MWC and GPCR models, the KNF model can pontentialy act as a logarithmic sensor over a broad range of signal.

KNF model drop out the saturation function and we have the simplified expression

$$Y(c, K_{BB}) \approx \frac{K_{BB}^6 (\frac{c}{K_D})^4}{1 + K_{BB}^6 (\frac{c}{K_D})^4} = \frac{e^{\varepsilon_0} (\frac{c}{K_D})^4}{1 + e^{\varepsilon_0} (\frac{c}{K_D})^4}, \tag{2.32}$$

where $\varepsilon_0 = 6 \ln (K_{BB})$. Here we see that, in the limits of strong cooperativity, the KNF model satisfies the logarithmic tuning requirement in relationship (2.10). This is consistent with the data originally fitted by Koshland *et al.*, where they use $K_{AA} = K_{AB} = 1$ and, for the tetrahedral case, find $K_{BB} \in [1.8, 6.8]$. Even for the lower end of this range, we have $K_{BB}^6 \approx 34$, which is much greater than the next largest coefficient in equation (2.31), $K_{AB}^3 K_{BB}^3 \approx 5.8$.

Detailed Analysis of the GPCR Model

Here we present a more detailed derivation of the activation function derived in equation (2.9). We begin again from the system of differential equations for GPCR activation:

$$\begin{aligned}
\dot{R} &= k_1 c(1-R) - k_2 R \\
\dot{T}_{GDP} &= k_3 \alpha_{GDP} - k_4 T_{GDP} R \\
\dot{T}_{GTP} &= k_4 T_{GDP} R - k_5 T_{GTP} \\
\dot{\alpha}_{GTP} &= k_5 T_{GTP} - k_6 \alpha_{GTP} \\
\dot{\alpha}_{GDP} &= k_6 \alpha_{GTP} - k_3 \alpha_{GDP}.
\end{aligned}$$

From this, we will solve for $\hat{\alpha}_{GTP}$, the relative level α_{GTP} compared to the total level of G protein $T_{tot} = T_{GDP} + T_{GTP} + \alpha_{GDP} + \alpha_{GTP}$. Just by setting derivatives equal to zero, we get

$$\begin{aligned}
\hat{\alpha}_{GTP} &= \frac{\alpha_{GTP}}{T_{tot}} \\
&= \frac{\alpha_{GTP}}{T_{GDP} + T_{GTP} + \alpha_{GDP} + \alpha_{GTP}} \\
&= \frac{\frac{k_5}{k_6} T_{GTP}}{T_{GDP} + T_{GTP} + \alpha_{GDP} + \frac{k_5}{k_6} T_{GTP}} \\
&= \frac{\frac{k_4}{k_6} T_{GDP} R}{T_{GDP} + \frac{k_4}{k_5} T_{GDP} R + \alpha_{GDP} + \frac{k_4}{k_6} T_{GDP} R} \\
&= \frac{\frac{k_4}{k_6} R}{1 + \frac{k_4}{k_5} R + \frac{k_4}{k_3} R + \frac{k_4}{k_6} R} \\
&= \frac{R}{\frac{k_6}{k_4} + R(\frac{k_6}{k_5} + \frac{k_6}{k_3} + 1)}.
\end{aligned}$$

We then use the fact steady-state relationship

$$R = \frac{c}{\frac{k_2}{k_1} + c}$$

to find

$$\begin{aligned}\hat{\alpha}_{GTP} &= \frac{\frac{c}{\frac{k_2}{k_1}+c}}{\frac{k_6}{k_4}+\frac{c}{\frac{k_2}{k_1}+c}(\frac{k_6}{k_5}+\frac{k_6}{k_3}+1)} \\ &= \frac{c}{\frac{k_6}{k_4}(\frac{k_2}{k_1}+c)+c(\frac{k_6}{k_5}+\frac{k_6}{k_3}+1)} \\ &= \frac{c}{(1+\frac{k_6}{k_3}+\frac{k_6}{k_4}+\frac{k_6}{k_5})c+\frac{k_6}{k_4}\frac{k_2}{k_1}},\end{aligned}$$

just as in equation (2.9). Since $\frac{k_2}{k_1}$ is effectively a K_D for the receptors, it is taken as a fixed quantity. On the other hand, β-arrestin signaling alters the rate (k_4) at which T_{GDP} binds to active receptors. To this end, we will rewrite equation (2.9) to see if it can be made to look like the form for the LAS requirement defined in relationship (2.10), with the definition $K_D = \frac{k_2}{k_1}$,

$$\hat{\alpha}_{GTP} = \frac{c}{(1+\frac{k_6}{k_3}+\frac{k_6}{k_4}+\frac{k_6}{k_5})c+\frac{k_6}{k_4}\frac{k_2}{k_1}} = \frac{\frac{k_4}{k_6}\frac{c}{K_D}}{1+(1+\frac{k_6}{k_3}+\frac{k_6}{k_4}+\frac{k_6}{k_5})\frac{k_4}{k_6}\frac{c}{K_D}}. \tag{2.33}$$

Here we see that, if we allow $\frac{k_4}{k_6}$ to play the role that e^{ε_0} plays in the MWC model, with variations in β-arrestin signaling effectively shifting the free energy ε, then the GPCR model almost fits the logarithmic tuning requirement in relation (2.10). The confounding element is the factor of $(1+\frac{k_6}{k_3}+\frac{k_6}{k_4}+\frac{k_6}{k_5})$ that depends on k_4 and thus could potentially complicate things. Rearranging this term, we get

$$\left(1+\frac{k_6}{k_3}+\frac{k_6}{k_4}+\frac{k_6}{k_5}\right) = \left(1+k_6\left(\frac{1}{k_3}+\frac{1}{k_4}+\frac{1}{k_5}\right)\right).$$

From this we see that there dependence on k_4 will vanish so long as either $\frac{1}{k_4} \ll \frac{1}{k_3}+\frac{1}{k_5}$ or $k_6 \ll k_4$, and consequently under these conditions the system will behave as a logarithmic sensor. In terms of the biochemistry of the GPCR pathway, this means that β-arrestin binding is far from saturation so that T_{GDP} is alway able to find active receptors, be it at an attenuated rate.

Fold-Change Detection Arises From Logarithmic Sensing and Negative Feedback

We present here simulations showing fold-change detection arising from a circuit containing allosteric regulation and negative feedback. We use as specific examples

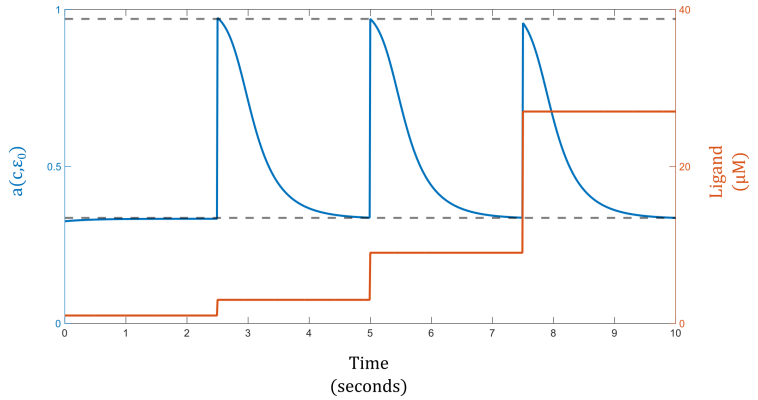

Figure 2.10: Fold-Change Detection with an MWC Tar/Tsr Sensor. In this simulation, $K_A = 10^{-2}, K_I = 10^2, N = 4, m = 10, a_0 = \frac{1}{3}$. The blue line indicates the activity of the Tar/Tsr receptor. The orange line indicates ligand concentration, varied by 3-fold at each step increase.

the Tar/Tsr receptor system (discussed in the second half of the Result section) and the GPCR system.

Tar/Tsr receptor and negative feedback. We model the allosteric regulation of the receptor using the MWC model, and the negative feedback as described in Shimizu *et al.* [28] and Pontius *et al.* [38]. The negative feedback via methylation acts on a slower time scale than receptor activation, such that $a(c, \varepsilon_0)$ instantaneously responds to changes in ligand and allosteric effector concentrations. Further, ε_0 and a are related by a linear feedback coupling, such that

$$\begin{aligned} a(c, \varepsilon_0) &= \frac{\left(1 + \frac{c}{K_A}\right)^N}{\left(1 + \frac{c}{K_A}\right)^N + e^{\varepsilon_0}\left(1 + \frac{c}{K_I}\right)^N} \\ \dot{\varepsilon}_0 &= m(a - a_0), \end{aligned} \tag{2.34}$$

where a_0 is the basal activation level to which the system adapts and m is a constant corresponding to the rate of adaptation. When $\dot{\varepsilon}_0 = 0$, we have $a = a_0$, and the system will show precise adaptation, as expected. Figure 2.10 shows the change in Tar/Tsr receptor activity (blue) in response to sequential 3-fold step increases in ligand concentration (orange). The system gives identical responses for all three steps, performing fold-change detection.

GPCR receptor and negative feedback. The dynamics of the GPCR system are described in the main text (equations (2.8)). As described in the main text, allosteric regulation is implemented through k_4, which characterizes the rate of receptor phosphorylation and β-arrestin binding. While we could express feedback in terms

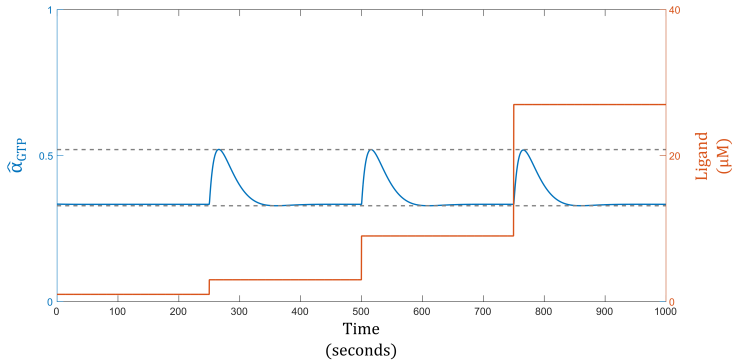

Figure 2.11: Fold-Change Detection with a GPCR Sensor. In this simulation, $k_1 = .01, k_2 = 15, k_3 = 10, k_5 = 20, k_6 = .05, \beta = 1, m = .15, a_0 = \frac{1}{3}$. The blue line indicates the activity of the GPCR system. The orange line indicates ligand concentration, varied by 3-fold at each step increase.

of k_4 directly, we may run into problems because k_4 is a reaction rate and therefore must be non-negative. To avoid running into negative values, we rewrite $k_4 = \beta e^{\varepsilon_0}$, for some constant β. The differential equations describing the GPCR system are now

$$\begin{aligned} \dot{R} &= k_1 c(1-R) - k_2 R \\ \dot{T}_{GDP} &= k_3 \alpha_{GDP} - \beta e^{\varepsilon_0} T_{GDP} R \\ \dot{T}_{GTP} &= \beta e^{\varepsilon_0} T_{GDP} R - k_5 T_{GTP} \\ \dot{\alpha}_{GTP} &= k_5 T_{GTP} - k_6 \alpha_{GTP} \\ \dot{\alpha}_{GDP} &= k_6 \alpha_{GTP} - k_3 \alpha_{GDP} \\ \dot{\varepsilon}_0 &= m(a_0 - \hat{\alpha}_{GTP}), \end{aligned} \tag{2.35}$$

where $\hat{\alpha}_{GTP} = \frac{\alpha_{GTP}}{T_{tot}}$. Figure 2.11 shows the response of the GPCR system to sequential 3-fold step increase in signal. We see again that a logarithmic sensor coupled with negative feedback yields fold-change detection.

References

[1] BM Martins and Peter S Swain. "Trade-offs and constraints in allosteric sensing". In: *PLoS Comput Biol* 7.11 (2011), e1002261.

[2] Lea Goentoro et al. "The incoherent feedforward loop can provide fold-change detection in gene regulation". In: *Molecular cell* 36.5 (2009), pp. 894–899.

[3] Oren Shoval et al. "Fold-change detection and scalar symmetry of sensory input fields". In: *Proceedings of the National Academy of Sciences* 107.36 (2010), pp. 15995–16000.

[4] Ernst Heinrich Weber, Helen Elizabeth Ross, and David J Murray. *EH Weber on the tactile senses*. Psychology Press, 1996.

[5] EN Pugh, S Nikonov, and TD Lamb. "Molecular mechanisms of vertebrate photoreceptor light adaptation". In: *Current opinion in neurobiology* 9.4 (1999), pp. 410–418.

[6] Stanislas Dehaene. "The neural basis of the Weber–Fechner law: a logarithmic mental number line". In: *Trends in cognitive sciences* 7.4 (2003), pp. 145–147.

[7] Eric R Kandel, James H Schwartz, Thomas M Jessell, et al. *Principles of neural science*. Vol. 4. McGraw-Hill New York, 2000.

[8] Lea Goentoro and Marc W Kirschner. "Evidence that fold-change, and not absolute level, of β-catenin dictates Wnt signaling". In: *Molecular cell* 36.5 (2009), pp. 872–884.

[9] Cellina Cohen-Saidon et al. "Dynamics and variability of ERK2 response to EGF in individual living cells". In: *Molecular cell* 36.5 (2009), pp. 885–893.

[10] Kevin Thurley et al. "Reliable encoding of stimulus intensities within random sequences of intracellular Ca2+ spikes". In: *Science signaling* 7.331 (2014), ra59.

[11] Robin EC Lee et al. "Fold change of nuclear NF-κB determines TNF-induced transcription in single cells". In: *Molecular cell* 53.6 (2014), pp. 867–879.

[12] Max Delbrück, W Reichardt, and D Rudnick. "System analysis for the light growth reactions of Phycomyces". In: *Fourteenth Symposium of the Society for the Study of Development and Growth 1955*. Princeton University Press. 1956, pp. 3–44.

[13] Robert Mesibov, George W Ordal, and Julius Adler. "The range of attractant concentrations for bacterial chemotaxis and the threshold and size of response over this range Weber law and related phenomena". In: *The Journal of general physiology* 62.2 (1973), pp. 203–223.

[14] Miri Adler, Avi Mayo, and Uri Alon. "Logarithmic and Power Law Input-Output Relations in Sensory Systems with Fold-Change Detection". In: *PLoS Computational Biology* 10.8 (2014), e1003781.

[15] Milena D Lazova et al. "Response rescaling in bacterial chemotaxis". In: *Proceedings of the National Academy of Sciences* 108.33 (2011), pp. 13870–13875.

[16] Sarah Marzen, Hernan G Garcia, and Rob Phillips. "Statistical mechanics of Monod–Wyman–Changeux (MWC) models". In: *Journal of molecular biology* 425.9 (2013), pp. 1433–1460.

[17] Jean-Pierre Changeux. "Allostery and the Monod-Wyman-Changeux model after 50 years". In: *Annual review of biophysics* 41 (2012), pp. 103–133.

[18] Fiona A Chandra, Gentian Buzi, and John C Doyle. “Glycolytic oscillations and limits on robust efficiency”. In: *science* 333.6039 (2011), pp. 187–192.

[19] Yuhai Tu, Thomas S Shimizu, and Howard C Berg. “Modeling the chemotactic response of Escherichia coli to time-varying stimuli”. In: *Proceedings of the National Academy of Sciences* 105.39 (2008), pp. 14855–14860.

[20] Jacques Monod, Jean-Pierre Changeux, and Francois Jacob. “Allosteric proteins and cellular control systems”. In: *Journal of molecular biology* 6.4 (1963), pp. 306–329.

[21] Jacque Monod, Jeffries Wyman, and Jean-Pierre Changeux. “On the nature of allosteric transitions: a plausible model”. In: *Journal of molecular biology* 12.1 (1965), pp. 88–118.

[22] Bernardo A Mello and Yuhai Tu. “Effects of adaptation in maintaining high sensitivity over a wide range of backgrounds for Escherichia coli chemotaxis”. In: *Biophysical journal* 92.7 (2007), pp. 2329–2337.

[23] Daniel Blangy, H Buc, and J Monod. “Kinetics of the allosteric interactions of phosphofructokinase from Escherichia coli”. In: *Journal of molecular biology* 31.1 (1968), pp. 13–35.

[24] DE Koshland Jr, G Nemethy, and D_ Filmer. “Comparison of experimental binding data and theoretical models in proteins containing subunits”. In: *Biochemistry* 5.1 (1966), pp. 365–385.

[25] James Keener and James Sneyd. *Mathematical physiology I: Cellular Physiology*. Vol. 1. Springer Science & Business Media, 2009, pp. 905–907.

[26] Kiyohiro Imai and GA Gilbert. “The Monod-Wyman-Changeux allosteric model describes haemoglobin oxygenation with only one adjustable parameter”. In: *Journal of molecular biology* 167.3 (1983), pp. 741–749.

[27] Frank Müller et al. “Phosphorylation of mammalian olfactory cyclic nucleotide-gated channels increases ligand sensitivity”. In: *The Journal of neuroscience* 18.1 (1998), pp. 164–173.

[28] Thomas S Shimizu, Yuhai Tu, and Howard C Berg. “A modular gradient-sensing network for chemotaxis in Escherichia coli revealed by responses to time-varying stimuli”. In: *Molecular systems biology* 6.1 (2010), p. 382.

[29] Meritxell Canals et al. “A Monod-Wyman-Changeux mechanism can explain G protein-coupled receptor (GPCR) allosteric modulation”. In: *Journal of Biological Chemistry* 287.1 (2012), pp. 650–659.

[30] Jennifer L Macdonald-Obermann and Linda J Pike. “The intracellular juxtamembrane domain of the epidermal growth factor (EGF) receptor is responsible for the allosteric regulation of EGF binding”. In: *Journal of Biological Chemistry* 284.20 (2009), pp. 13570–13576.

[31] Elena Molokanova et al. “Modulation of rod photoreceptor cyclic nucleotide-gated channels by tyrosine phosphorylation”. In: *The Journal of neuroscience* 17.23 (1997), pp. 9068–9076.

[32] Denise Wootten, Arthur Christopoulos, and Patrick M Sexton. “Emerging paradigms in GPCR allostery: implications for drug discovery”. In: *Nature Reviews Drug Discovery* 12.8 (2013), pp. 630–644.

[33] Mitchell Lewis. “Allostery and the lac Operon”. In: *Journal of molecular biology* 425.13 (2013), pp. 2309–2316.

[34] Yevgeniy V Kalinin et al. “Logarithmic sensing in Escherichia coli bacterial chemotaxis”. In: *Biophysical journal* 96.6 (2009), pp. 2439–2448.

[35] Juan E Keymer et al. “Chemosensing in Escherichia coli: two regimes of two-state receptors”. In: *Proceedings of the National Academy of Sciences of the United States of America* 103.6 (2006), pp. 1786–1791.

[36] Martin S Springer, Michael F Goy, and Julius Adler. “Sensory transduction in Escherichia coli: two complementary pathways of information processing that involve methylated proteins”. In: *Proceedings of the National Academy of Sciences* 74.8 (1977), pp. 3312–3316.

[37] Robert G Endres and Ned S Wingreen. “Precise adaptation in bacterial chemotaxis through “assistance neighborhoods””. In: *Proceedings of the National Academy of Sciences* 103.35 (2006), pp. 13040–13044.

[38] William Pontius, Michael W Sneddon, and Thierry Emonet. “Adaptation dynamics in densely clustered chemoreceptors”. In: *PLoS Comput Biol* 9.9 (2013), e1003230.

[39] Gordon L Fain et al. “Adaptation in vertebrate photoreceptors”. In: *Physiological reviews* 81.1 (2001), pp. 117–151.

[40] J Robert Lane et al. “A new mechanism of allostery in a G protein-coupled receptor dimer”. In: *Nature chemical biology* (2014).

[41] Ruth Nussinov and Chung-Jung Tsai. “Allostery in disease and in drug discovery”. In: *Cell* 153.2 (2013), pp. 293–305.

[42] Ruth Nussinov, Chung-Jung Tsai, and Buyong Ma. “The underappreciated role of allostery in the cellular network”. In: *Annual review of biophysics* 42 (2013), pp. 169–189.

[43] Sudarshan Rajagopal, Keshava Rajagopal, and Robert J Lefkowitz. “Teaching old receptors new tricks: biasing seven-transmembrane receptors”. In: *Nature reviews Drug discovery* 9.5 (2010), pp. 373–386.

[44] Graham Carpenter and Stanley Cohen. “125I-labeled human epidermal growth factor. Binding, internalization, and degradation in human fibroblasts.” In: *The Journal of Cell Biology* 71.1 (1976), pp. 159–171.

[45] Roi Avraham and Yosef Yarden. “Feedback regulation of EGFR signalling: decision making by early and delayed loops”. In: *Nature reviews Molecular cell biology* 12.2 (2011), pp. 104–117.

[46] Matthew Stuible et al. “PTP1B Targets the Endosomal Sorting Machinery DEPHOSPHORYLATION OF REGULATORY SITES ON THE ENDOSOMAL SORTING COMPLEX REQUIRED FOR TRANSPORT COMPONENT STAM2”. In: *Journal of Biological Chemistry* 285.31 (2010), pp. 23899–23907.

[47] Michele K Dougherty et al. “Regulation of Raf-1 by direct feedback phosphorylation”. In: *Molecular cell* 17.2 (2005), pp. 215–224.

[48] Dennis J Slamon et al. “Studies of the HER-2/neu proto-oncogene in human breast and ovarian cancer”. In: *Science* 244.4905 (1989), pp. 707–712.

[49] Ross C Wilson et al. “Tuning riboswitch regulation through conformational selection”. In: *Journal of molecular biology* 405.4 (2011), pp. 926–938.

[50] Ron Milo et al. “The relationship between evolutionary and physiological variation in hemoglobin”. In: *Proceedings of the National Academy of Sciences* 104.43 (2007), pp. 16998–17003.

[51] MF Perutz. “Stereochemistry of Cooperative Effects in Haemoglobin: Haem-Haem Interaction and the Problem of Allostery”. In: *Nature* 228 (1970), pp. 726–734.

[52] Daniel E Koshland and Kambiz Hamadani. “Proteomics and models for enzyme cooperativity”. In: *Journal of Biological Chemistry* 277.49 (2002), pp. 46841–46844.

Chapter 3

HARD LIMITS AND PERFORMANCE TRADEOFFS IN A CLASS OF SEQUESTRATION FEEDBACK SYSTEMS

3.1 Introduction

One of the central goals of systems biology is to gain insight into the design, function, and architecture of biomolecular circuits. When systems biology emerged as a field, there was a focus on the precise measurement of parameters in canonical pathways, for example those that govern glucose metabolism [1] and developmental signaling [2, 3]. As both our understanding of these pathways and our quantitative measurements improved, it became apparent that many of the underlying circuit parameters are subject to large amounts of variability, despite the circuit's overall performance being robust [4, 5, 6, 7]. These observations led to the important insight that signaling networks have evolved sophisticated feedback control mechanisms that confer robustness, similar to those developed for classical engineering systems [8, 9, 10, 11, 12]. To this end, understanding the architecture and constraints of these regulatory processes is essential both to assessing the range of biological functions that they can implement and to building functional synthetic systems [13, 14, 15].

For many systems, the key to achieving robust performance is feedback control, which can provide robustness to both external noise and disturbances and to internal system variability [16, 17, 9, 18]. When the system undergoes a change, such as an external disturbance or a variation in parameters, feedback can ensure that the system returns to its desired steady state with a small error [18]. Additionally, feedback control can stabilize and speedup unstable or slow processes [19, 8, 20]. However, feedback must be correctly designed and tuned, as it can inadvertently amplify noise and exacerbate instability [21, 18]. Despite some limitations, feedback control is ubiquitous in natural biological systems, where it serves to regulate diverse processes such as body temperature, circadian rhythms, calcium dynamics, and glycolysis [22, 23, 17, 8, 16].

There are a variety of circuit architectures capable of implementing feedback control in a biomolecular network. However, the time scale and dynamic range of their response can vary greatly depending on implementation details, such as whether the circuit relies on gene regulation [24] or post-translational modification [7].

Similarly, some circuits are robust over a broad range of inputs [25], while others may have a more modest functional range of response [4].

A particularly interesting class of biological control circuits was recently proposed by Briat et al. [26]. The authors showed that feedback implemented with a molecular sequestration mechanism is equivalent to integral feedback control [18], which guarantees perfect steady-state adaptation of the output of a network to an input signal [16]. An endogenous biological system that uses sequestration feedback to achieve perfect adaptation relies on the binding of sigma factor σ^{70} to anti-sigma factor Rsd [27]. Examples of synthetic biological systems that employ sequestration feedback include a concentration tracker [28, 29], two bacterial cell growth controllers [30], and a gene expression controller [31].

While integral control is a powerful tool, its stability and performance are not guaranteed to be well-behaved. Even if both the controller and the network being controlled are stable, their closed-loop dynamics may be either stable (Figure 3.1A) or unstable (Figure 3.1B). If the closed-loop system is stable, performance can be characterized by metrics such as tracking error, response time, leakiness, and sensitivity to disturbances. Although these metrics can be optimized individually, they can rarely all yield good results simultaneously due the constraints imposed by performance tradeoffs. These hard limits have been studied in a variety of contexts, for example in general stochastic biological control systems [32] and in the particular context of metabolic control in the yeast glycolysis system [8, 12].

Though many biomolecular circuits of interest are too complex to yield clear theoretical results that describe system-level dynamics and performance, we show in section 3.2 that a class of sequestration feedback networks can be precisely analyzed using techniques from control theory. In particular, we find that there exists an analytic stability criterion for a class of sequestration feedback systems (described in Figure 3.1C). This stability criterion gives rise to performance tradeoffs, for example between speed and sensitivity, since fast responding controllers are intrinsically less robust. We prove these results both in the case where there is no controller degradation (section 3.2), as in the model from [26], and in the more biologically realistic context where there is such degradation (section 3.2) [33]. Though we determine many different classes of tradeoffs for the circuit, we find that they can all be viewed as different aspects of Bode's integral theorem, which states a conservation law for the sensitivity of feedback control systems [18].

These theoretical tools provide novel insight into both the analysis of endogenous

Notation	Meaning	Units	First Use
x_1, x_2	Process species concentration	nM	Equation (3.1)
z_1, z_2	Controller species concentration	nM	Equation (3.1)
k	Synthesis rate for x_2	h^{-1}	Equation (3.1)
θ_1, θ_2	Synthesis rates for z_1 and x_2	h^{-1}	Equation (3.1)
γ_p, γ_c	Degradation rates for process and controller species	h^{-1}	Equations (3.1) and (3.11)
μ	Synthesis rate for z_1	$nM\,h^{-1}$	Equation (3.1)
η	Sequestration rate for z_1 and z_2	$nM^{-1}\,h^{-1}$	Equation (3.1)
$\mathbf{x}$	Linearized state vector (4x1)	h^{-1}	Equation (3.3)
M	Linearized system matrix (2x2)	nM	Equation (3.3)
α	Open-loop system gain	h^{-1}	Equation (3.3)
β	Linearized feedback strength	h^{-2}	Equation (3.3)
ω	Frequency of oscillation at stability boundary	h^{-1}	Equation (3.6)
$S(i\omega)$	Sensitivity function	None	Equation (3.7)
$\mathcal{M}$	Stability measure	None	Equation (3.8)
$\mathcal{F}$	Fragility measure	None	Equation (3.10)
ε	Steady-state error of x_2	None	Equation (3.13)

Table 3.1: Description of notation in Chapter 3.

biological systems and the design of synthetic systems, which we demonstrate by applying our results to a synthetic bacterial growth control circuit in section 3.2. Finally, we demonstrate in section 3.2 that it is possible to develop control architectures that will stabilize an otherwise unstable chemical reaction process. This result points towards new application domains, such as autocatalytic metabolic networks, for sequestration-based controllers that have yet to be explored in detail. Table 3.1 describes the most common notation used throughout this chapter.

3.2 Results

Our goal here will be to develop a mathematical framework to investigate the general constraints that shape the structure of the closed-loop sequestration feedback

network. For the sake of clarity we focus the results here on the simplest examples of a network regulated by sequestration feedback, however many of the results presented in this section generalize to a broader class of systems (e.g. the case with more network species and the case with controller degradation).

Model Description

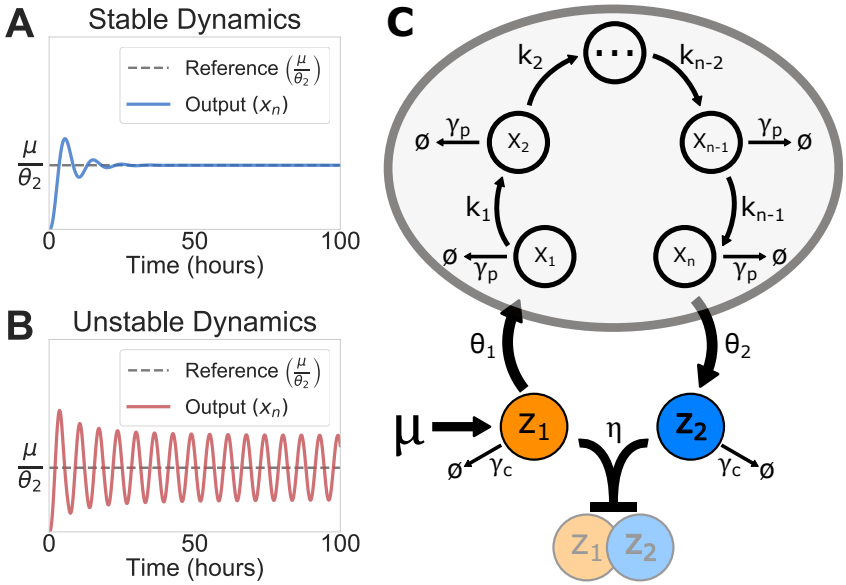

Figure 3.1: The Sequestration Feedback Network. A) Stable dynamics of a sequestration feedback system, where the output (solid line) precisely adapts to a reference signal (dashed line). **B)** Unstable dynamics of the same circuit, where the system is now in a parameter regime that results in sustained oscillations. **C)** A class of sequestration feedback networks. This general model has two control species, z_1 and z_2, and n process species. The two controller species are subject to a sequestration reaction with binding rate η. Additionally, we assume that the binding of the two controller species is much faster than their unbinding. The process species production rates are denoted as $\theta_1, \theta_2, k_1, \ldots, k_{n-1}$. For simplicity, the process species degradation rate γ_p is assumed to be equal for each x_i, as is the controller species degradation rate γ_c. This class of networks is defined by a simple set of possible processes where each species is only involved in the production of the next species.

We first describe the simple sequestration feedback model proposed by Briat et al. [26] with two control species (z_1 and z_2) and two species in the open-loop network (x_1 and x_2), which corresponds to the case of $n = 2$ in the general circuit diagram presented in Figure 3.1C with $\gamma_c = 0$. In the control theory literature the network being controlled is often referred to as the process, a convention we will use in the rest of the chapter.

We model the full closed-loop network using the following system of ordinary

differential equations:

$$\dot{x}_1 = \theta_1 z_1 - \gamma_p x_1, \tag{3.1a}$$

$$\dot{x}_2 = k x_1 - \gamma_p x_2, \tag{3.1b}$$

$$\dot{z}_1 = \mu - \eta z_1 z_2, \tag{3.1c}$$

$$\dot{z}_2 = \theta_2 x_2 - \eta z_1 z_2. \tag{3.1d}$$

The rates k and γ_p are production and degradation rates that are internal to the process. The parameters θ_1 and θ_2 are production rates that provide an interface between the network and the controller. An external reference inducer μ determines production rate of z_1, and the two control species z_1 and z_2 sequester each other at the rate η.

While realistic models of biological circuits often have both more complex interactions and many more states, this model captures much of the important structural information about the sequestration feedback system. In particular, Briat et al. found that the network defined by (3.1) implements precise adaptation of x_2 via integral feedback [26], as shown by the following relationship:

$$\dot{z}_1 - \dot{z}_2 = \mu - \theta_2 x_2 \implies (z_1 - z_2)(t) = \theta_2 \int_0^t \left(\frac{\mu}{\theta_2} - x_2(t') \right) dt'. \tag{3.2}$$

This ensures that, *if* the system is stable (i.e. $\dot{z}_1 - \dot{z}_2 \to 0$), then at steady state (denoted with a $*$) $x_2^* = \mu/\theta_2$. The parametric conditions that guarantee stability are not, however, obvious at first glance. Briat et al. showed general algebraic conditions that prove the existence of both stable and unstable dynamics of the linearized sequestration feedback system (using Descartes' rule of sign), however it is not trivial to use their methods to explicitly describe stability in general.

We find that, in the limit of strong feedback (large η), there is a simple closed-form criterion for system-level stability. Later, we will show that a one-state network is intrinsically stable for all parameters, and that there exists a simple stability criterion for the general class of networks with many states represented in Figure 3.1C. For the analysis, we assume both that a set of process parameters (k and γ_p) and a desired set point (determined by μ and θ_2) are given, and we study how stability and performance relate to the rest of the control parameters (θ_1 and η).

Linear Stability Analysis

In this section, we derive an analytic criterion for the stability of sequestration feedback networks. For simplicity, we assume strong sequestration binding of the controller species (which we define mathematically later in the section).

A key difficulty in studying sequestration is the nonlinear term $\eta z_1 z_2$ that mediates feedback in equations (3.1c) and (3.1d). Though there exist techniques to study nonlinear feedback systems, there are far more general tools available to study linear ones. While analysis of the linear system does not give guarantees about global behavior, it does allow us to characterize the local stability of the steady state to which we would like x_2 to adapt. To this end, we linearize the sequestration feedback network around the non-zero steady-state value derived from equation (3.1):

$$\dot{\mathbf{x}} = M\mathbf{x},$$
$$\mathbf{x} = \begin{bmatrix} x_1 \\ x_2 \\ z_1 \\ z_2 \end{bmatrix}, M = \begin{bmatrix} -\gamma_p & 0 & \theta_1 & 0 \\ k & -\gamma_p & 0 & 0 \\ 0 & 0 & -\alpha & -\beta/\alpha \\ 0 & \theta_2 & -\alpha & -\beta/\alpha \end{bmatrix}, \tag{3.3}$$

where $\alpha = \theta_1\theta_2 k/\gamma_p^2$ and $\beta = \eta\mu$. We can think of α as representing the open-loop gain of the system, and β as representing the feedback gain.

In general, stability of linear systems is determined by the sign of the real parts of its eigenvalues. If they are all strictly negative, then the dynamical system is stable and the system will converge to the equilibrium point. Ideally, we would be able to directly compute the eigenvalues of M, however this computation corresponds to finding the roots of a fourth-order polynomial $p(s) = \det(sI - M)$. While this is difficult to do in general, it is possible to study stability by finding what has to be true of the parameters for the system to have a pair of purely imaginary eigenvalues, which characterizes the boundary between stable and unstable behavior. We find that, in the limit of strong sequestration (specifically $\eta \gg \max(\alpha, \gamma_p) \cdot \alpha/\mu$), M will have purely imaginary eigenvalues $\lambda = \pm i\omega$ when $\omega = \gamma_p = \sqrt[3]{\frac{\theta_1\theta_2 k}{2}}$. More generally, we find that the criterion for stability is

$$\sqrt[3]{\frac{\theta_1\theta_2 k}{2}} < \gamma_p, \tag{3.4}$$

a relationship we refer to as the production-degradation inequality (proved in section 3.4).

This implies that the closed-loop system will be stable so long as the degradation rate is larger than a constant that is proportional to the geometric mean of the production rates ($\sqrt[3]{\theta_1\theta_2 k}$). We note that, in this strong sequestration limit, inequality (3.4) is independent of the controller variables μ and η. Thus, this relationship tells us that stability is purely a function of the parameters describing the process and its

connection to the controller, and is independent of the controller itself. Intuitively, the degradation rate sets the rate of adaptation of x_1 and x_2, so inequality (3.4) tells us that, so long as the species have a rate of adaptation that is faster than the rate of change in production, the system will be stable.

Through a more technical argument (also in section 3.4), we find that a generalized system with a chain of n process species has a production-degradation inequality of the form

$$\sqrt[n+1]{\frac{\theta_1\theta_2\prod_{i=1}^{n-1}k_i}{\Omega_n}} < \gamma_p, \tag{3.5}$$

where Ω_n is a constant that is only a function of the number of process species. When the system has purely imaginary eigenvalues, each species will oscillate at the frequency

$$\omega = \tan\left(\frac{\pi}{2n}\right)\gamma_p. \tag{3.6}$$

For $n = 1$ we get $\omega = \tan(\pi/2)\gamma_p = \infty$, corresponding to an intrinsically stable system (i.e. it cannot oscillate or become otherwise unstable). At $n = 2$ we find $\omega = \gamma_p$, so the frequency of oscillation is equal to the process degradation rate. Since $\tan(\pi/(2n))$ is a decreasing function of n, the frequency of oscillation will monotonically decrease as the system grows (assuming a fixed value of γ_p).

Alternatively, we can interpret the parameter α as the open-loop gain between z_1 and z_2. Rearranging inequality (3.5), we get the inequality

$$\alpha < \Omega_n\gamma_p,$$

which says that the degradation rate γ_p sets a bound on how large α can be, which can be interpreted as the open-loop gain between z_1 and z_2, while still maintaining stability.

For simplicity, the results so far focus only on the strong feedback regime. However, we show in the supplement that there are also tractable and interesting results in the regime of weak feedback (η small). The results have a similar form to that of the strong feedback limit, however the direction of the inequality is reversed. The stability condition for weak feedback is

$$\sqrt[n-1]{\frac{\Omega_n\theta_1\theta_2\prod_{i=1}^{n-1}k_i}{\beta}} > \gamma_p.$$

One interpretation of these results as a whole is that stability is achieved when either feedback *or* process degradation are sufficiently large, but not when both are.

Bode's integral theorem and The Anatomy of a Sensitivity Function

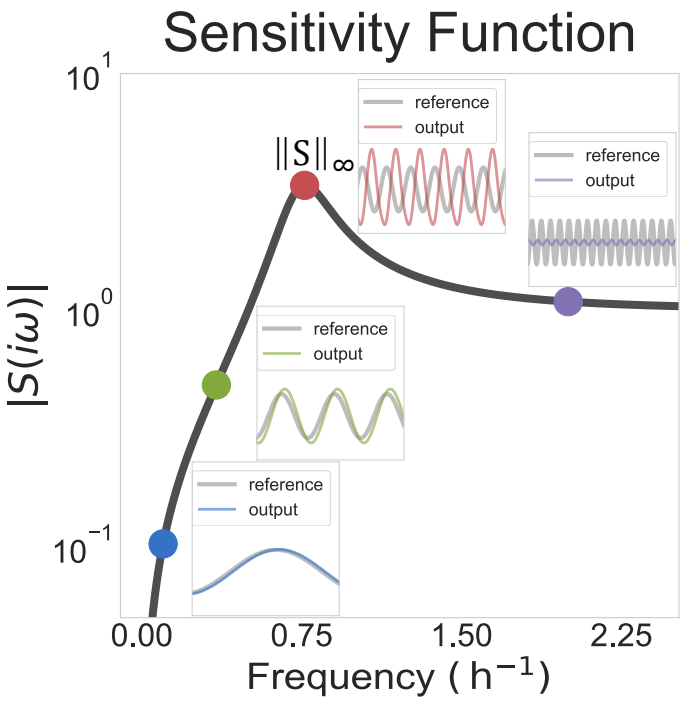

Figure 3.2: The Sensitivity Function. The sensitivity function for a system, with simulations of reference tracking dynamics for various inputs. We see that when $|S(i\omega)| < 1$, the system has small error and performs well (blue and green). At the peak $|S(i\omega)| = \|S\|_\infty$ (red), we see that the output magnitude is not only amplified, but also phase shifted such that it is almost exactly out of sync with the reference. At high frequencies (purple), the reference is changing so quickly that the system can barely track it.

The primary goal of any control system is to ensure that a process has a desirable response to an input signal, while minimizing the effect of external disturbances (such as noise and systematic modeling errors). While we often think of the time evolution of the full state of a dynamical system $x(t)$, it is often useful to study the input-output relationship of a dynamical system using the (one-sided) Laplace transform

$$X(s) = \int_0^\infty x(t)e^{-st}dt,$$

where it becomes straightforward to mathematically analyze the input-output relationship of given process. Here s is a complex number.

We call functions that describe the input-output response of a system in the Laplace domain **transfer functions**, and in particular the transfer function between a reference and the output error of a system is the **sensitivity function** of a system $S(s)$. If we take $y(t)$ as the output state of the system (in the sequestration circuit $y(t) = x_2(t)$), we denote the Laplace transform of the output $Y(s)$. We can similarly

define an input or reference signal $r(t)$ (corresponding to μ) with a corresponding transformed signal $R(s)$. We then define the error of the closed-loop system as $E(s) = R(s) - Y(s)$, and ask how large the error of the system will be when tracking a given reference. This is given by the function

$$S(s) = \frac{E(s)}{R(s)} = \frac{1}{1 + P(s)C(s)},$$

where $P(s)$ and $C(s)$ are the transfer functions for the open-loop process and controller, respectively.

Intuitively, when the magnitude of this function $|S(s)|$ is small, then there will be a small tracking error between the reference signal $r(t)$ and the output $y(t)$. Conversely when $|S(s)|$ is large, then there is a large tracking error. If we assume $r(t) = A\sin(\omega t)$, then we can study the **frequency response** of the system $|S(i\omega)|$ to a sinusoidal input with frequency ω.

$|S(i\omega)|$ provides a way to measure system robustness, by quantifying how well a system attenuates errors to a given input. The worst-case robustness can be described by the maximum value of $|S(i\omega)|$, denoted $\|S\|_\infty$. Ideally we would have $|S(i\omega)| \ll 1$ for all ω. However, a deep result known as Bode's integral theorem (proved by Hendrik Bode in 1945 [34]) states that, for an open-loop stable process, the following is true of the closed-loop response:

$$\int_0^\infty |\log(S(i\omega))| d\omega = 0. \tag{3.7}$$

This implies that in order to reduce error in one frequency range, it *must* be increased elsewhere. This is known as the waterbed effect, and sets a fundamental limitation on the performance of any feedback control system.

Performance Tradeoffs and Hard Limits

While inequality (3.4) gives us a binary condition that determines stability, it does not directly tell us about overall performance of the system. We know when the system becomes unstable, but it is unclear how the system behaves as it approaches instability. Let

$$\mathcal{M} = 1 - \frac{\theta_1\theta_2 k}{2\gamma_p^3} \tag{3.8}$$

be a measure of how far the system is from going unstable that we will refer to as a *stability measure* of the system. For simplicity the analysis here will focus on the $n = 2$ species case, however the results naturally generalize for arbitrary n.

From inequality (3.4), we have that $\mathcal{M} = 0$ implies instability, and that the larger $\mathcal{M}$ is the further the system is from becoming unstable. Intuitively it seems that the system should become increasingly fragile to disturbances as $\mathcal{M}$ approaches zero. Conversely, we can increase $\mathcal{M}$ by decreasing the production rates θ_1, θ_2, and k, but this will slow down the dynamics of the system and could potentially hurt performance.

To analyze this problem, we will study the sensitivity function $S(s)$, which is the transfer function between the reference signal and the output error of the system [18]. This transfer function captures the effect of external disturbances on the output error of a system, in this case, x_2. The sensitivity function is described in greater detail in the box above.

While there are many different ways to characterize robustness, generally we consider a system to be robust if there no small change in parameters that would cause it to become unstable. A mathematically equivalent interpretation is that a system is robust when its worst-case error when tracking references (i.e. the maximum value of S) is small [18]. For the $n = 2$ case of the circuit in Figure 3.1, we have (see section 3.4):

$$|S(i\omega)| = \frac{\gamma_p^2 + \omega^2}{\sqrt{\left(\frac{1}{\omega}\theta_1\theta_2 k - 2\omega\gamma_p\right)^2 + (\gamma_p^2 - \omega^2)^2}}. \tag{3.9}$$

The robustness of a system can be formally quantified by $\|S\|_\infty = \max_\omega |S(i\omega)|$, the maximum magnitude of the sensitivity function across all frequencies (in mathematics, the quantity $\|\cdot\|_\infty$ is referred to as the infinity norm of a function). The quantity $\|S\|_\infty$ describes the worst-case disturbance amplification for the system to an oscillatory input. If $\|S\|_\infty$ is in some sense small enough to be manageable, then values of $|S|$ across all frequencies are also small and the system is robust to any disturbance. If $\|S\|_\infty$ is large enough to be problematic, then there is at least one disturbance against which the system is fragile.

Directly computing $\|S\|_\infty$ in terms of the parameters of a system is difficult in general, but it is sometimes possible to compute good lower bounds that yield insight into a system's robustness. To this end, we find that (see Section 3.4 for a detailed proof):

$$\|S\|_\infty \geq \mathcal{F} = \frac{1 + \frac{\alpha}{2\gamma_p}}{1 - \frac{\alpha}{2\gamma_p}} = \frac{2\gamma_p^3 + \theta_1\theta_2 k}{2\gamma_p^3 - \theta_1\theta_2 k}, \tag{3.10}$$

with equality when

$$\mathcal{M} = 0 \iff \gamma_p = \sqrt[3]{\frac{\theta_1 \theta_2 k}{2}} \iff \|S\|_\infty = \mathcal{F} = \infty.$$

The fragility bound $\mathcal{F}$ is constructive, in that we can write down the frequency ω^* that achieves it:

$$|S(i\omega^*)| = \mathcal{F} \iff \omega^* = \sqrt{\frac{\alpha\gamma_p}{2}}.$$

For a given constant reference μ/θ_2, we use equation (3.10) to derive a tradeoff between fragility and response time (which we quantify with $1/\theta_1$). Figure 3.3A shows this tradeoff curve for a particular set of parameters as θ_1 varies, with the corresponding dynamics shown in Figure 3.3B. We see from the latter plots that the response time ($1/\theta_1$) and fragility ($\mathcal{F}$) correspond directly to the rise times and oscillatory behavior of simulations in Figure 3.3B. Figure 3.3C shows the corresponding sensitivity functions, with colored dots corresponding to values of $\mathcal{F}$. Here we can clearly see Bode's integral theorem (equation (3.7)) at work, in that the area above and below the dashed line (corresponding to $\log |S(i\omega)| = 0$) is always equal. We see that, as dynamics become more oscillatory, $\|S\|_\infty$ becomes large.

Because we have fixed μ/θ_2 and assumed that η is large, the only remaining control parameter to vary is θ_1, so there will only ever be one meaningful tradeoff dimension to study for this system. In the next section, we present results for the case with non-zero controller degradation rates. This model is both more biologically realistic and provides a richer tradeoff space to analyze.

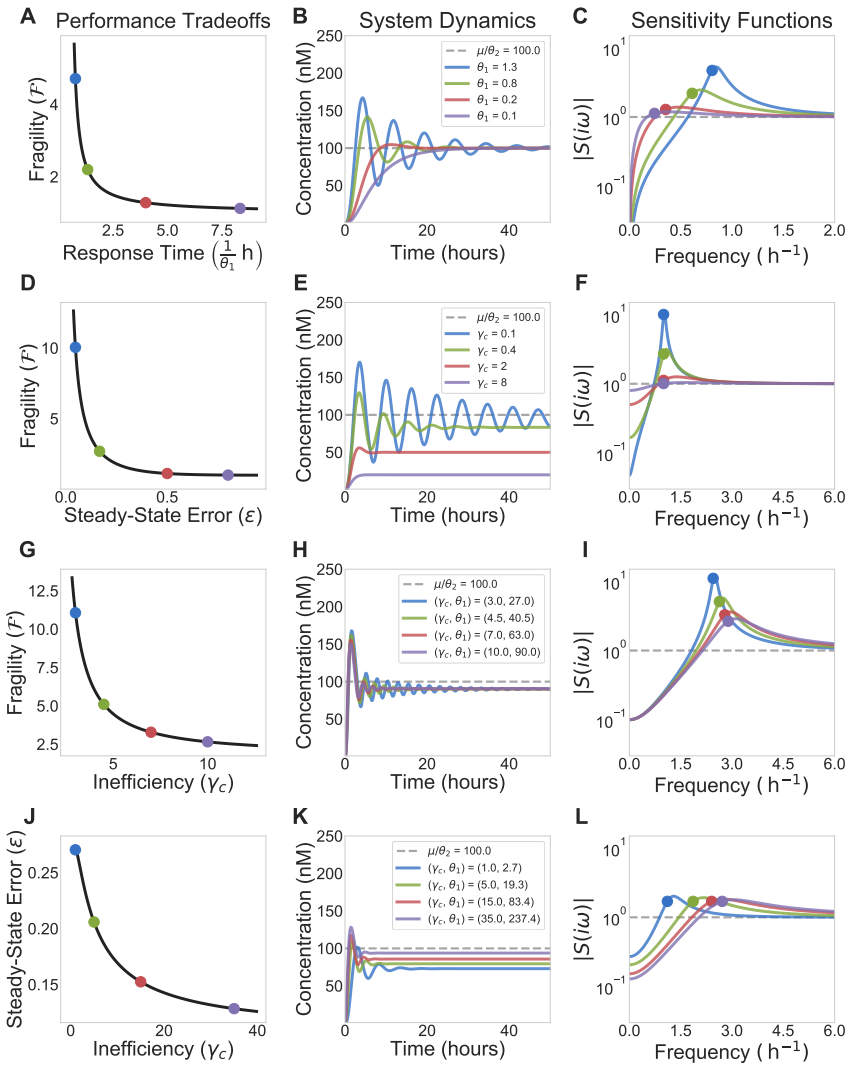

Figure 3.3: Hard Limits and Performance Tradeoffs in Sequestration Feedback Circuits. **A)** We see the relationship between speed and fragility in the sequestration feedback system. Speed can be characterized in terms of any of the production rates of the system (here we vary θ_1^{-1}), where higher production rates lead to a faster response. Fragility is defined as a lower bound on the maximum value of the sensitivity function $\|S\|_\infty$ as defined in equation (3.10). **B)** Time-domain simulations corresponding to different points on the tradeoff curve in **A**. We see that speed and fragility naturally relate to the rise time and settling time of the system. **C)** Sensitivity functions for various parameter values. We see what is known in control theory as a waterbed effect, where better attenuation of disturbances at low frequencies necessarily implies worse amplification of disturbances at higher frequencies as a result of equation (3.7). The colored dots correspond to values of $\mathcal{F}$ computed using equation (3.10). **D)** Here we set $\gamma_c > 0$ and observe the effects of controller degradation being varied on its own. We set $\theta_1 = 2\,\text{h}^{-1}$ so that, if $\gamma_c = 0$, the system would be unstable. We see that increasing γ_c decreases fragility, at the cost of introducing steady-state error, which is illustrated in the dynamics shown in panel **E**. **F)** The corresponding sensitivity functions also illustrate the tradeoff, where the peak of $|S(i\omega)|$ (fragility) decreases as the value of $|S(0)|$ (steady-state error) increases. $\mathcal{F}$ is now computed using equation (3.15). **G-I)** In these plots we vary both γ_c and θ_1 such that $\theta_1/\gamma_c = 9$, corresponding to $\varepsilon = .1$ in equation (3.13). We now observe a tradeoff between fragility and leakiness, the latter being captured by how much turnover of z_1 and z_2 is introduced by γ_c. **K-L)** Finally, we can instead hold $\mathcal{F}$ constant and numerically solve for θ_1 given a value of γ_c. This introduces a tradeoff between steady-state error and leakiness. In all simulations $k = \theta_2 = \gamma_p = 1\,\text{h}^{-1}$, $\eta = 1000\,\text{h}^{-1}\,\text{nM}^{-1}$, and $\mu = 100\,\text{nM}\,\text{h}^{-1}$.

The Effects of Controller Species Degradation

In the previous sections, we assumed that the controller species does not degrade and we derived an analytic stability criterion for closed-loop sequestration feedback networks. Fulfilling the stability criterion ensures that the sequestration feedback network precisely adapts. As discussed, perfect adaptation is a desirable property because it facilitates disturbance rejection and robustness despite variability process dynamics. However, the literature suggests that implementing sequestration feedback with no controller species degradation is challenging [35, 36]. Because of this, we will now extend our analysis of stability, performance, and tradeoffs to sequestration feedback networks with nonzero controller species degradation rates.

To model the effects of controller species degradation, we modify equations (3.1c) and (3.1d) such that,

$$\dot{z}_1 = \mu - \eta z_1 z_2 - \gamma_c z_1, \tag{3.11a}$$

$$\dot{z}_2 = \theta_2 x_2 - \eta z_1 z_2 - \gamma_c z_2, \tag{3.11b}$$

where γ_c is the degradation rate of the control species z_1 and z_2.

Including the controller species degradation rate in the sequestration feedback network model changes its properties of stability and performance. In particular, the closed-loop sequestration feedback network has zero steady-state error for $\gamma_c = 0$, whereas if $\gamma_c > 0$ then there will generally be some non-zero error in x_2.

In the limit of strong sequestration, we can analytically compute the steady-state values of the system species and bound its sensitivity function. While it is somewhat more complicated to compute even the steady-state values of each species for this system, we show (see section 3.4) that, in the limit of large η, it is possible to derive a simple approximate formula for x_2^*:

$$x_2^* \approx \frac{\mu}{\theta_2} \frac{1}{1 + \frac{\gamma_c}{\alpha}}, \tag{3.12}$$

from which all other steady-state values can be derived. Under the strong feedback assumption, x_2 no longer precisely adapts to the set point μ/θ_2, but rather will have some amount of steady-state error determined by the ratio γ_c/α. The relative error in x_2^* can be quantified by the relationship

$$\varepsilon = \frac{\mu/\theta_2 - x_2^*}{\mu/\theta_2} = \frac{1}{1 + \frac{\alpha}{\gamma_c}}. \tag{3.13}$$

We see that $\gamma_c = 0 \implies \varepsilon = 0$, corresponding to our previously results that precise adaptation is achieved when there is no controller degradation. Using this simplified expression, the relative steady-state error function can be bounded. For example, if we are interested in obtaining $\varepsilon < .1$, then we can choose a controller degradation rate such that $\gamma_c < \frac{\alpha}{9}$.

Moreover, we can also derive the corresponding stability criterion (see section 3.4). Here we present the stability criterion for the two process species case, which was proved in [37] by Yoke Peng Leong:

$$\frac{\theta_1 \theta_2 k}{2} < \gamma_p(\gamma_c + \gamma_p)^2. \tag{3.14}$$

This reduces to inequality (3.4) when $\gamma_c = 0$, and shows that $\gamma_c > 0$ leads to a increased stability measure. If we only consider variations in γ_c, then the combination of equation (3.13) and inequality (3.14) yields yet another tradeoff. As γ_c increases, the system becomes increasingly stable at the cost of worse steady-state error (see Figure 3.3D and E).

In section 3.4, we derive a general stability criterion that depends on comparing the controller and the process species degradation rates for $n > 2$ process species. When the process degradation rate is much larger that the controller degradation rate or the two are comparable, then the stability criterion is the same as the production-degradation inequality. However, when the process degradation rate is much smaller than the controller degradation rate, then the stability criterion relies on the controller degradation term to compensate for the slow process degradation rate. Since the process network is slow, the sequestration feedback network is challenging to stabilize and its performance can be very poor.

We now focus on analyzing the properties of the sensitivity function and the tradeoff it introduces. Figure 3.3F shows the corresponding sensitivity function for this system. One major difference between these sensitivity functions and those in Figure 3.3C is that we now have $|S(0)| > 0$. This is directly related to the steady-state error in equation (3.12), as we can think of a signal with frequency $\omega = 0$ as a constant reference. A convenient property of the sensitivity function is that $|S(0)| = \varepsilon$, so the previously mentioned tradeoff between robustness and steady-state error can be recast as a tradeoff between $|S(0)|$ and $\|S\|_\infty$. In Figure 3.3C we see that $\log|S(0)| = -\infty$, corresponding to $|S(0)| = 0$, implying $\varepsilon = 0$ steady-state error. Because of the waterbed effect, increasing $|S(0)|$ has a tendency to reduce $\|S\|_\infty$.

This can be seen directly by deriving a bound similar to the one in equation (3.10) for the case $\gamma_c > 0$:

$$\|S\|_\infty > \mathcal{F} = \frac{(\gamma_p^2 + \omega^{*2})\sqrt{1 + \left(\frac{\gamma_c}{\omega^*}\right)^2}}{(\gamma_p^2 - \omega^{*2}) + 2\gamma_c\gamma_p}, \tag{3.15}$$

$$\omega^* = \gamma_p\sqrt{\frac{\alpha + \gamma_c}{2\gamma_p + \gamma_c}}. \tag{3.16}$$

Though $\mathcal{F}$ is now more complicated, we can see that it will scale as $O(1/\gamma_c)$ for small γ_c. This tells us that increasingly γ_c has the potential to reduce $\mathcal{F}$. In Figure 3.3D we see this effect, where $\mathcal{F}$ asymptotically decreases to 1 as γ_c (and consequently ε) increases. It is also straightforward to check that $\mathcal{F}$ reduces to equation (3.10) when $\gamma_c = 0$.

So far we have shown what happens when the control parameters θ_1 and γ_c are varied individually, however it is also interesting to study what happens when they are varied such that a particular performance characteristic is held constant. Figure 3.3G, H and I demonstrate the system's response when we vary θ_1 and γ_c such that the steady-state error ε is fixed. This sort of variation can be interpreted as changing the turnover rate, and consequently the leakiness, of the controller. This leakiness can also be thought of decreasing efficiency, as it means that control molecules are degraded before ever being involved in feedback. By increasing γ_c, we make the system less efficient because the controller spends resources producing and then degrading molecules of z_1 and z_2. Figure 3.3G shows that highly efficient controllers are more fragile than less efficient ones. We can also see this in Figure 3.3I, where the integrated area of $|S(i\omega)|$ gets spread out over high frequencies, rather than having a large and narrow peak. This leads to a lower value of $\|S\|_\infty$ and a corresponding increase in robustness. Conversely, we can fix $\mathcal{F}$ and see how ε changes with leakiness. In Figure 3.3J and K we see that highly efficient controllers have worse steady-state error, and as the controller becomes less efficient ε improves. This can be observed in Figure 3.3L, where $|S(0)|$ is reduced as γ_c increases. Because $|S(0)|$ is decreasing and $\|S\|_\infty$ is fixed, we see that $|S(i\omega)|$ stays large at higher frequencies rather than falling off quickly after its peak.

While any of these tradeoffs could be studied in their own right, the important conceptual takeaway is that what underlies all of them is Bode's integral theorem. In the same way that conservation laws provide a broad understanding of the constraints

on physic quantities (like momentum and energy), Equation (3.7) gives us a unifying framework for understanding the fundamental performance limitations of control systems. With this result in hand, we see that the performance tradeoffs shown here are simply different ways of tuning parameters to shape the function $|S(i\omega)|$. In the next section, we will apply some of these theoretical concepts to a particular biological circuit model. Though this model is more complex and nonlinear than those we have discussed so far, we will see that the same essential theoretical approach applies.

A Synthetic Growth Control Circuit

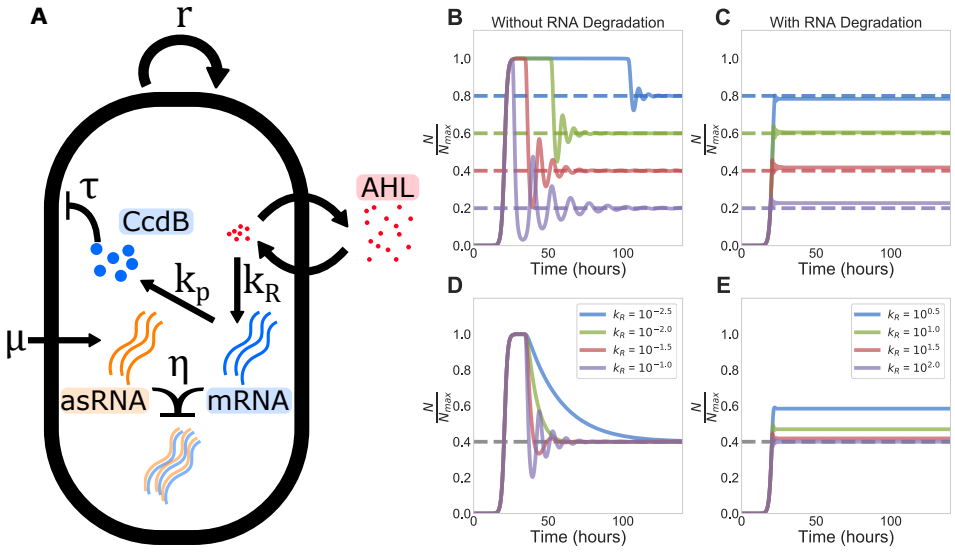

Figure 3.4: A Synthetic Growth Control Circuit. A) The circuit diagram for the dynamics described in equation (3.17). **B)** Simulations of the growth control circuit without RNA degradation (solid lines) for various set points μ (dashed lines). This architecture exhibits the precise adaptation property, though the response is relatively slow and oscillatory. **C)** Here we see the same circuit simulated with RNA degradation. The response is much faster and more robust, however there is non-zero steady-state error for each trajectory. **D)** Here we again simulate the circuit without degradation, but now vary k_R. We see qualitatively similar performance tradeoffs to those in Figure 3.3. **E)** As before, we see that adding controller degradation yields a very fast and consistent response. For these particular parameters, the circuit can achieve this performance with relatively little steady-state error. For all circuits we use the parameters $N_m = 10^9$, $r = 1\ \mathrm{h}^{-1}$, $\eta = 20\ \mathrm{nM}^{-1}\,\mathrm{h}^{-1}$, $k_p = 10\ \mathrm{h}^{-1}$, $\gamma_p = 3\ \mathrm{h}^{-1}$, $G_a = 10^{-6}$ nM, and $\tau = 4 \times 10^{-3}\ \mathrm{nM}^{-1}\,\mathrm{h}^{-1}$. Panel **B** uses $k_R = 0.1\ \mathrm{h}^{-1}$ and **C** uses $k_R = 10\ \mathrm{h}^{-1}$ and $\gamma_R = 20\ \mathrm{h}^{-1}$.

Here we will use the results from previous sections to study a simple model of a synthetic sequestration feedback circuit based on the work in [38, 30], illustrated in Figure 3.4A. The intended function of this circuit is to regulate the population level

Species	Steady State	Exact Form $\gamma_R = 0$	Approximate Form, $\gamma_R > 0$
N/N_m	N^*/N_m	$\frac{\mu}{N_m \hat{k}_R}$	$\frac{\frac{\mu}{N_m \hat{k}_R} + \frac{\gamma_R}{\alpha}}{1+\frac{\gamma_R}{\alpha}}$
[CcdB]	$\frac{r}{\tau}\left(1 - \frac{N^*}{N_m}\right)$	$\frac{r}{\tau}\left(1 - \frac{\mu}{N_m \hat{k}_R}\right)$	$\frac{r}{\tau}\frac{1}{1+\frac{\gamma_c}{\alpha}}\left(1 - \frac{\mu}{N_m \hat{k}_R}\right)$
[mRNA]	$\frac{\gamma_p}{k_p}[\text{CcdB}]^*$	$\frac{\gamma_p r}{k_p \tau}\left(1 - \frac{\mu}{N_m \hat{k}_R}\right)$	$\frac{\gamma_p r}{k_p \tau}\frac{1}{1+\frac{\gamma_c}{\alpha}}\left(1 - \frac{\mu}{N_m \hat{k}_R}\right)$
[asRNA]	$\frac{\mu}{\eta}\frac{1}{[\text{mRNA}]^*}$	$\frac{\mu k_p \tau}{\eta \gamma_p r}\left(1 - \frac{\mu}{N_m \hat{k}_R}\right)^{-1}$	$\frac{\mu k_p \tau}{\eta \gamma_p r}(1 + \frac{\gamma_c}{\alpha})\left(1 - \frac{\mu}{N_m \hat{k}_R}\right)^{-1}$

Table 3.2: Steady-state parameter values derive from equation (3.17). For the case $\gamma_R = 0$ these solutions are exact, while they are approximated (assuming η large) for $\gamma_R > 0$.

of a colony of *E. coli* via an external reference signal such as an inducer. We model the circuit with the following set of differential equations:

$$\frac{d}{dt}[\text{CcdB}] = k_p[\text{mRNA}] - \gamma_p[\text{CcdB}] \tag{3.17a}$$

$$\frac{d}{dt}N = rN\left(1 - \frac{N}{N_m}\right) - \tau[\text{CcdB}]N \tag{3.17b}$$

$$\frac{d}{dt}[\text{mRNA}] = k_R G_a N - \eta[\text{mRNA}][\text{asRNA}] - \gamma_R[\text{mRNA}] \tag{3.17c}$$

$$\frac{d}{dt}[\text{asRNA}] = \mu - \eta[\text{mRNA}][\text{asRNA}] - \gamma_R[\text{asRNA}]. \tag{3.17d}$$

Quantities of the form $[\cdot]$ represent intracellular concentrations for each cell, and N represents the total number of cells. N follows logistic dynamics with an additional death rate due to toxicity τ proportional to the concentration of [CcdB] per cell. [CcdB] is a protein that is toxic to the cell, [mRNA] is the corresponding messenger RNA, the transcription of which we model as being induced by a quorum sensing ligand that is produced at a rate proportional to N, and [asRNA] is a short antisense RNA that has a complementary sequence to the CcdB mRNA, thus acting as a sequestering partner. The term $G_a = 10^{-6}$ nM captures the gain between N and mRNA induction mediated by the quorum-sensing molecule AHL.

As before, we will analyze a linearized version of this circuit. To do this we must first compute the steady-state values, shown in table 3.2. The linearized dynamics

can now be written as

$$\dot{\mathbf{x}} = M\mathbf{x},$$

where

$$\mathbf{x} = \begin{bmatrix} [\text{CcdB}] \\ N \\ [\text{mRNA}] \\ [\text{asRNA}] \end{bmatrix}, M = \begin{bmatrix} -\gamma_p & 0 & k_p & 0 \\ -T & -\gamma_N & 0 & 0 \\ 0 & \hat{k}_R & -\nu - \gamma_R & -\rho \\ 0 & 0 & -\nu & -\rho - \gamma_R \end{bmatrix},$$

and $\hat{k}_R = k_R G_a$, $T = \tau N^*$, $\gamma_N = rN^*/N_m$, $\alpha = (\hat{k}_R \tau N_m)/(\gamma_R r)$, $\nu = [\text{asRNA}]^*$, and $\rho = [\text{mRNA}]^*$. From this, we can again derive stability results in the limit of large η. In terms of the parameters in M, we get a similar relationship to that of inequality (3.14), with the introduction of heterogeneous degradation rates:

$$k_p \hat{k}_R T < (\gamma_p + \gamma_R)(\gamma_N + \gamma_R)(\gamma_p + \gamma_N), \tag{3.18}$$

and the corresponding stability measure

$$\mathcal{M} = 1 - \frac{k_p \hat{k}_R T}{(\gamma_p + \gamma_R)(\gamma_N + \gamma_R)(\gamma_p + \gamma_N)}.$$

A notable difference about this circuit is that stability is implicitly dependent on μ. This is because μ appears in N^*, which determines the values of γ_N and T. Given that the function of this circuit is to control cell proliferation, it is natural to ask what steady-state levels of N^* are achievable for a given set of parameters. Because the scale of N^* is set by N_m, we can non-dimensionalize the population size with the term N^*/N_m. In the case $\gamma_R = 0$, we can recast equation (3.18) as

$$\frac{N^*}{N_m} = \frac{\mu}{\hat{k}_R N_m} > \frac{k_p}{\gamma_p} \frac{\tau \hat{k}_R N_m}{r^2} - \frac{\gamma_p}{r}. \tag{3.19}$$

One immediate result of inequality (3.19) is that, if the following holds:

$$\frac{k_p}{\gamma_p} \frac{\tau \hat{k}_R N_m}{r^2} < \frac{\gamma_p}{r} \implies \frac{\tau \hat{k}_R N_m}{r} < \frac{\gamma_p^2}{k_p},$$

then the steady-state N^* is stable for any μ such that $\frac{\mu}{\hat{k}_R} < N_m$ (the steady-state value of N^* cannot exceed the carrying capacity N_m in equation (3.17b) from the nonlinear model). This constraint is also implicit in the steady-state value $[\text{asRNA}]^*$, which is infinite if $\frac{\mu}{\hat{k}_R} = N_m$. Because the right-hand side of the inequality has a factor of γ_p^2/k_p, it is possible to improve performance without changing the steady-state

concentration of [CcdB] by increasing both k_p and γ_p simultaneously, effectively increasing the protein's turnover rate. If the right-hand side of inequality (3.19) is positive, then we see that the system's performance is constrained, in that there is a certain population threshold below which N^* cannot be set. Just as in the previous section, as the system approaches this threshold it will become increasingly oscillatory. These effects were observed experimentally in [39], which uses the same general growth control architecture as in [38].

Figure 3.4B demonstrates how the growth control circuit adapts to various steady-state population levels when there is no controller degradation ($\gamma_R = 0$). The steady state is set by varying μ. When possible, parameters for this model are taken from [38]. What is clear across all set points is that the population first grows to carrying capacity before the circuit is activated. Intuitively, the blue curve in Figure 3.4B has a large amount of asRNA that sequesters mRNA. Because of this, it takes longer to accumulate enough mRNA to make CcdB and lower the population level. In contrast, the purple curve has comparatively little asRNA, effectively increasing the rate at which CcdB can be produced. Qualitatively similar long-term oscillatory behavior in a CcdB-based growth control circuit was observed in [39].

Since [38] does not explicitly model transcription, we would ideally pick realistic transcription and translation timescales for bacteria. If we were to naively assume that we could model asRNA and mRNA as if they were like z_1 and z_2 in section 4.4, i.e. neglecting controller degradation and assuming they are only removed via sequestration, then we run into an issue. Because the sequestration mechanism modeled in section 4.4 assumes that controller degradation is negligible, we must use a very small mRNA synthesis rate to achieve stable dynamics, assuming all other parameters are fixed in a biologically plausible regime, even if sequestration is fast. This leads to a slow circuit response and a large transient overshoot. This is demonstrated in Figure 3.4B, where CcdB production is so slow that the population reaches carrying capacity before the circuit can become active. In Figure 3.4D we see similar dynamics to those in Figure 3.3, where the circuit faces harsh tradeoffs between speed and robustness.

We see from Figure 3.4C and E that good performance requires not only that RNA is removed via sequestration, but also that it is degraded at a nontrivial rate. At the cost of a lack of precise adaptation, these circuits display dramatically improved performance. In Figure 3.4C and E, the transient overshoot from Figure 3.4B and D has almost entirely disappeared, and each system adapts on a nearly identical time

scale, independent of μ. Figure 3.4D and E compare performance for various values of k_R in each system. Figure 3.4E shows that the introduction of γ_R makes the system's dynamics extremely robust to variations in k_R over a wide range of values. We can interpret γ_R as introducing a third tradeoff dimension, namely steady-state error. By allowing the system flexibility along this axis, its speed and robustness are greatly improved.

This section illustrates two key points, the first being that the general theoretical results from our initial analysis can be adapted to specific biological-motivated models of control. The second more general takeaway is that systems that look on the surface to be both biologically and mathematical distinct, e.g. a linear model of a chemical reaction network and a nonlinear population-level growth control circuit, have the same underlying structure. We often think of linearization simply as a method of approximation, but its real power often lies in showing us the connection between seemingly different mathematical models. In this case, it becomes clear what the analogous production and degradation rates are in equation (3.1) and equation (3.17). This type of system-level theory allows us to abstract away details to see that seemingly different problems can be tackled with the same class of tools.

Controlling Autocatalytic Processes

The general approach of the results presented so far has been to analyze in detail the simplest classes of networks that can be controlled by sequestration feedback. Going forward, it will be important to study networks where both the process and controller have more complex architecture. At the controller level, the sequestration mechanism alone only implements integral feedback. It will be useful to investigate mechanisms that could robustly implement proportional and derivative control mechanisms with the ultimate goal of synthesizing full proportional-integral-derivative (PID) controller [18, 40] in synthetic circuits.

It will also likely be essential to explore other mechanisms of implementing feedback control in living systems. Several mechanisms for biological control that are currently being explored include: paradoxical extracellular signaling inspired by process regulation [41] and post-translation mechanisms such as multi-protease regulation. Using control theoretical tools, it will be important to develop models for these biological controllers and assess their stability and performance. Researchers in bioengineering will likely benefit from having multiple mechanisms of feedback control to choose from, depending on the particular application.

Our results thus far has focused on the application of sequestration feedback to processes that are open-loop stable. It will likely be important to study the case of unstable processes, which can occur in autocatalytic networks such as the one involved in glycolysis and other metabolic processes. In control theory, unstable processes lead to a modified version of Bode's integral theorem:

$$\int_0^\infty \ln(|S(i\omega)|)d\omega = \pi \sum_k Re(p_k), \tag{3.20}$$

where $Re(p_k)$ is the real part of the unstable eigenvalues. Larger values of $\pi \sum_k Re(p_k)$ correspond to more global sensitivity to disturbances and harsher performance trade-offs.

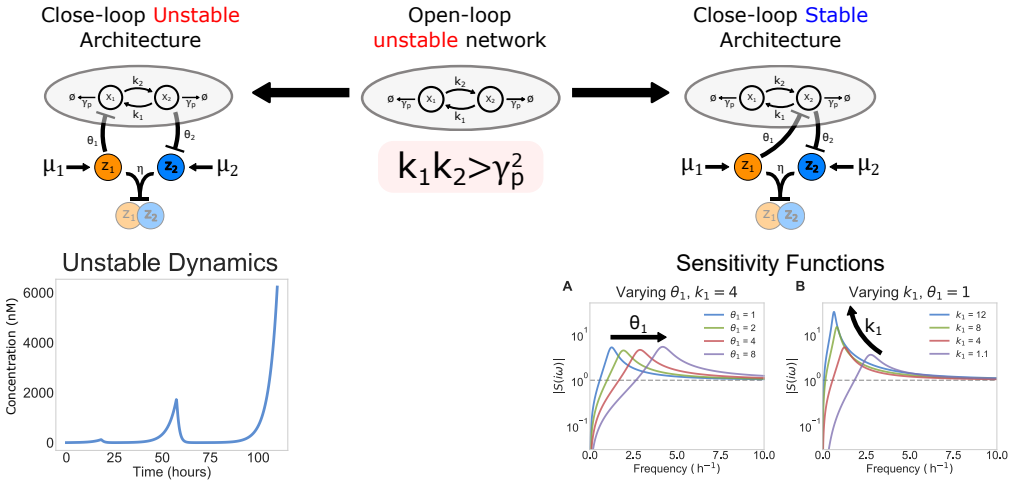

Figure 3.5: Using Sequestration to Control an Unstable Network. Here we take an unstable process (center) and study two different sequestration-based control architectures (left and right). This network is unstable so long as $k_1 k_2 > \gamma^2$. The repressive architecture on the left is *intrinsically* unstable, in that there are no values of the the control parameters that lead to the system reaching a stable steady state. A representative simulation of the unstable dynamics is presented below the architecture diagram. In contrast, the repressive architecture on the right is not only stabilizing, but *intrinsically* stabilizing. Any non-zero parameter values that result in positive steady-state concentrations of species will yield a stable closed-loop network. Panel **A** shows the sensitivity function as θ_1 varies for a fixed value of $k_1 = 4$ h^{-1}. In this case, equation (3.7) tells us that the integrated area of the $|S(i\omega)|$ will be constant as θ_1 varies, because θ_1 does not effect the location of unstable poles. In panel **B**, $\theta_1 = 1$ h^{-1} is fixed and k_1 varies. This will change the location of the unstable pole, and we see a consequent change in integrated area of $|S(i\omega)|$, with large values of k_1 leading to higher overall sensitivity of the system. In all simulations we take $\theta_2 = k_2 = \gamma_p = 1$ h^{-1}, $\eta = 1000$ h^{-1} nM^{-1}, $\mu_1 = 10$ nM h^{-1}, and $\mu_2 = 110$ nM h^{-1}.

To demonstrate the nuance and complexity added by unstable processes, we demonstrate two seemingly similar control architectures that yield diametrically opposed

behavior. As a simple model of an unstable process, we will use the process described in Figure 3.5, which has the following dynamics:

$$\begin{aligned}\dot{x}_1 &= k_2 x_2 - \gamma_p x_1,\\ \dot{x}_2 &= k_1 x_1 - \gamma_p x_2.\end{aligned}$$

Since the system is linear, it is straightforward to check that the system is unstable when $k_1 k_2 > \gamma_p^2$. Because of the instability of the process, our controller will need to be repressive rather than activating, as it has been throughout the chapter. The left panel of Figure 3.5 describes a plausible control architecture for such a system:

$$\begin{aligned}\dot{x}_1 &= \frac{k_2 x_2}{1+\theta_1 z_1} - \gamma_p x_1,\\ \dot{x}_2 &= k_1 x_1 - \gamma_p x_2,\\ \dot{z}_1 &= \mu_1 - \eta z_1 z_2,\\ \dot{z}_2 &= \frac{\mu_2}{1+\theta_2 x_2} - \eta z_1 z_2.\end{aligned}$$

Here z_1 represses x_1 and x_2 represses z_2. Intuitively, if x_2 is large then z_1 will be reduced, increasing the amount of z_1 which in turns reduces the amount of x_1 and x_2. We prove that this controller is actually *incapable* of stabilizing an unstable process, in that there are no parameters for which the closed-loop system is stable (section 3.4). If, however, we instead have z_1 directly repress x_2 (Figure 3.5, right):

$$\begin{aligned}\dot{x}_1 &= k_2 x_2 - \gamma_p x_1,\\ \dot{x}_2 &= \frac{k_1 x_1}{1+\theta_1 z_1} - \gamma_p x_2,\\ \dot{z}_1 &= \mu_1 - \eta z_1 z_2,\\ \dot{z}_2 &= \frac{\mu_2}{1+\theta_2 x_2} - \eta z_1 z_2.\end{aligned}$$

It is not only possible to stabilize the closed-loop system, but the system is *intrinsically* stable. So long as the system has positive parameter values and steady-state concentrations, we recover robust precise adaptation as presented in the earlier sections (section 3.4). While the stable process architecture could either be stable or unstable in closed-loop, this unstable process architecture confers a sort of inherent

closed-loop stability that is quite surprising. If the system were linear, this would not be possible. Stability is a direct result of the nonlinearity introduced by repression. There is, however, a limitation: equation (3.20) tells us that a very unstable process ($k_1 k_2 \gg \gamma_p^2$) must exhibit extreme disturbance amplification. In terms of reference tracking, this implies that even the intrinsically stable controller will potentially have very bad transient behavior (e.g. extreme overshoot and ringing as the system stabilizes). While we can use the techniques developed in this chapter to mathematically prove why these two architectures behave so differently, we have little biological insight into the architectural requirements for a stabilizing sequestration feedback controller. In the future we hope to develop a more general theoretical understanding of which architectures can confer stability to unstable networks.

3.3 Discussion

The development of synthetic biomolecular controllers could enable bioengineering to yield new solutions to problems in drug synthesis, immune system engineering, waste management, and industrial fermentation [42, 43, 44]. In their current state, however, most current synthetic circuits lack the requisite robustness and scalability required of industrial technologies. The application of control theory to synthetic biological controllers aims to ensure that they function robustly in different host organisms and signaling contexts, despite perturbations from an uncertain environments.

The recent development of sequestration feedback controllers represents a promising step towards a general framework for implementing control in biological networks. This is best demonstrated by the rapid experimental progress towards implementing these controllers in a variety of contexts and with different sequestration mechanisms [30, 28, 45, 46, 47]. As these controllers become widely used, we believe that the theoretical results in this chapter will not only provide a broad theoretical perspective on how the parameters of these networks interact to determine circuit performance, but also provide practical design rules that will tune circuit behavior in order to meet performance requirements.

In the first half of the 20th century, the development of a cohesive theory of feedback control by Hendrik Bode, Harry Nyquist, and many other foundational thinkers facilitated the rapid development and proliferation of control systems in fields such as aerospace, electrical, and chemical engineering. The work presented here provides a link between the tools from classical control theory and contemporary problems in

synthetic biology. In particular, we showed that it is possible to explicitly describe parametric conditions that determine stability, performance tradeoffs, and hard limits for a class of sequestration feedback controllers. While these limits can each be evaluated on their own, we observe that they can all be interpreted as different aspect of Bode's integral theorem. This result acts like a fundamental conservation law for the performance of feedback control systems. By understanding these general theoretical constraints, we can gain a broad understanding of what is and is not achievable with a given control architecture.

3.4 Supplemental Information

The Stability Criterion

We consider the mathematical model of the sequestration network described in equation (3.1). This mathematical model has a nonlinear term introduced by the sequestration dynamics. To evaluate its properties of stability and performance, we first linearize its dynamics. We can then describe the block structure of the linearized system in terms of the following matrices:

$$A = \begin{bmatrix} -\gamma_p & 0 & \cdots & 0 \\ k_1 & -\gamma_p & \cdots & 0 \\ 0 & \ddots & \ddots & \vdots \\ 0 & \cdots & k_{n-1} & -\gamma_p \end{bmatrix}, B = \begin{bmatrix} \theta_1 & 0 \\ \vdots & \vdots \\ 0 & 0 \end{bmatrix},$$

$$C = \begin{bmatrix} 0 & \cdots & 0 \\ 0 & \cdots & \theta_2 \end{bmatrix}, D = \begin{bmatrix} -\alpha & -\beta/\alpha \\ -\alpha & -\beta/\alpha \end{bmatrix},$$

$$M = \left[\begin{array}{c|c} A & B \\ \hline C & D \end{array}\right],$$

where $\alpha = \frac{\theta_1\theta_2\prod_{i=1}^{n-1} k_i}{\gamma_p^n}$ and $\beta = \beta$. The linearized dynamics will then be of the form

$$\dot{\mathbf{x}} = M\mathbf{x},$$

where

$$\mathbf{x} = \begin{bmatrix} x_1 \\ \vdots \\ x_n \\ z_1 \\ z_2 \end{bmatrix}$$

To prove our main stability result, we will analyze the characteristic polynomial of M, $p(s)$. The roots of $p(s)$ correspond to eigenvalues of M. In general it is difficult to analyze these roots, however we will see that the $p(s)$ has a great deal of useful structure which we can exploit. First, we have to write down what $p(s)$ actually is.

Lemma 1. *The characteristic polynomial of M is*

$$p(s) = \det(sI - M) = (s + \gamma_p)^n \left[s^2 + \left(\alpha + \frac{\beta}{\alpha} \right) s \right] + \gamma_p^n \beta.$$

Proof. We start by using the result that, for a block matrix such as M, we can use the classical result from linear algebra

$$\begin{aligned} p(s) &= \det(sI - M) \\ &= \det \left[\begin{array}{c|c} sI - A & -B \\ \hline -C & sI - D \end{array} \right] \\ &= \det(sI - A) \det[(sI - D) - C(sI - A)^{-1} B]. \end{aligned}$$

Since A is lower-triangular, we see immediately that the first term is

$$\det(sI - A) = (s + \gamma_p)^n.$$

To analyze the second term, we first focus on computing $C(sI - A)^{-1} B$. Because of the sparse structure of B and C, we have

$$C(sI - A)^{-1} B = \begin{bmatrix} 0 & 0 \\ \theta_1 \theta_2 (sI - A)^{-1}_{n1} & 0 \end{bmatrix},$$

where $(sI - A)^{-1}_{n1}$ is the bottom-left most entry of $(sI - A)^{-1}$. Using Cramer's rule, we can compute

$$\begin{aligned} (sI - A)^{-1}_{n1} &= \frac{1}{(s + \gamma_p)^n} (-1)^{n+1} \det \begin{bmatrix} -k_1 & s + \gamma_p & \cdots & 0 \\ \vdots & \ddots & \ddots & \vdots \\ 0 & \cdots & -k_{n-2} & s + \gamma_p \\ 0 & 0 & \cdots & -k_{n-1} \end{bmatrix} \\ &= \frac{1}{(s + \gamma_p)^n} (-1)^{n+1} (-1)^{n-1} \prod_{i=1}^{n-1} k_i \\ &= \frac{\prod_{i=1}^{n-1} k_i}{(s + \gamma_p)^n}. \end{aligned}$$

Combing these results, we see that

$$\begin{aligned} p(s) &= (s+\gamma_p)^n \det \begin{bmatrix} s+\alpha & \frac{\beta}{\alpha} \\ \alpha - \frac{\theta_1\theta_2\prod_{i=1}^{n-1} k_i}{(s+\gamma_p)^n} & s+\frac{\beta}{\alpha} \end{bmatrix} \\ &= (s+\gamma_p)^n \left[(s+\alpha)\left(s+\frac{\beta}{\alpha}\right) - \beta + \frac{\gamma_p^n \beta}{(s+\gamma_p)^n} \right] \\ &= (s+\gamma_p)^n \left[s^2 + \left(\alpha + \frac{\beta}{\alpha}\right) s \right] + \gamma_p^n \beta. \end{aligned} \tag{3.23}$$

□

We can now use this result about $p(s)$ to analyze the stability of the linearized sequestration feedback system.

Theorem 2 (Eigenvalue Classification Theorem)**.** *For a given n and $\beta \gg \alpha^2, \alpha\gamma_p$, the eigenvalues λ of M has a parameter-independent classification of the form $\left|\arg\left(\frac{\lambda}{\gamma_p}\right) + \arg\left(\frac{\lambda}{\gamma_p}+1\right)\right| = m\pi$, for an integer m.*

Proof. To study the eigenvalues of M, we will analyze the roots of $p(s)$. We begin by substituting $s = \gamma_p\sigma$ in equation (3.23) and setting $p(\sigma) = 0$:

$$\gamma_p^2\sigma(1+\sigma)^n \left[\sigma + \frac{\alpha^2+\beta}{\alpha\gamma_p}\right] = -\beta.$$

Taking the limit of strong feedback ($\beta \gg \alpha^2, \alpha\gamma_p$), this equation reduces to

$$\sigma(1+\sigma)^n \left[1 + \sigma\frac{\alpha\gamma_p}{\beta}\right] = -\frac{\alpha}{\gamma_p}.$$

From this relationship we see that $p(\sigma)$ has one large real root at $\sigma \approx -\frac{\beta}{\alpha\gamma_p}$. If we plug this into the phase constraint equation, this gives a phase of $(n+1)\pi$. We will say the index of this root is $n+1$. If $|\sigma| \ll \frac{\beta}{\alpha\gamma_p}$, we get the simplified magnitude constraint

$$|\sigma||1+\sigma|^n = \frac{\alpha}{\gamma_p}$$

and the phase constraint

$$\arg(\sigma) + n\arg(1+\sigma) = \pi + 2k\pi = (2k+1)\pi.$$

We can see from this that the maximum phase possible is $n+1$ and that any each of the indices will be of the form $2k+1$ (i.e., odd integers). Because the magnitude

constraint is independent of k, fundamentally we can have phase indices for any odd integer m such that $|m| \leq n + 1$.

First we will see what conditions can produce purely real roots. If σ is real and $\sigma > 0$, then

$$\arg(\sigma) + n \arg(1 + \sigma) = 0,$$

which violates the phase constraint. This implies that, if there are unstable roots, they are not purely real. If $-1 < \sigma < 0$, then

$$\arg(\sigma) + n \arg(1 + \sigma) = \pi,$$

and we can have stable real roots with index 1. The magnitude constraint tells us that we will have a pair of these real roots if $\frac{\alpha}{\gamma_p} < \frac{n^n}{(n+1)^{n+1}}$ (which have index 1) with a bifurcation that generates conjugate pairs of roots when $\frac{\alpha}{\gamma_p} \geq \frac{n^n}{(n+1)^{n+1}}$. These conjugate roots will have indices ± 1.

An immediate result of these observations is that, for any positive odd integer m such that $1 < m < n + 1$, roots cannot be purely real and must come in conjugate pairs $\pm m$. If n is odd, then we will have a conjugate pair of roots for each $m \in [3, n - 1]$, either a pair of small real roots or a conjugate pair for $m = 1$, and a single large negative real root for $m = n + 1$.

If n is odd, then the situation will be almost the same except for the fact that there will be a second real root with index $n+1$. By some simple accounting, this analysis accounts for all $n + 1$ roots of $p(\sigma)$, which correspond to roots of $p(s)$ by a simple rescaling by $\frac{1}{\gamma_p}$. □

Theorem 3 (Production-Degradation Inequality)**.** *Let M be the matrix corresponding to a linearization of the sequestration feedback system with two control molecules (z_1 and z_2) and n process species. In the limit of strong feedback ($\beta \gg \alpha^2, \alpha\gamma_p$), the system is stable if and only if $\sqrt[n+1]{\frac{\theta_1\theta_2 \prod_{i=1}^{n-1} k_i}{\Omega_n}} < \gamma_p$, where Ω_n is a constant that only depends on n. Further, when the system has purely imaginary eigenvalues the frequency of oscillation will be $\omega = \tan(\frac{\pi}{2n})\gamma_p$.*

Proof. We will prove the results by finding parametric conditions that will result in purely imaginary eigenvalues, and then study what happens to the stability of the system when those parametric conditions do not hold (i.e. equalities become inequalities). To do this, we generalize a technique from [26], where we evaluate $p(s) = 0$ on the imaginary axis. In particular, we pick the change of variable

$s = i\omega^* \gamma_p$, where ω^* is a positive real number (which we can assume without loss of generality because complex roots come in conjugate pairs), and evaluate $p(\omega^*)$. This yields the equations

$$p(\omega^*) = 0 \implies \gamma_p^2 i\omega^*(1 + i\omega^*)^n(\phi + i\omega^*) = -\beta, \tag{3.24}$$

where $\phi = \frac{\alpha^2+\beta}{\alpha\gamma_p}$. If we take the magnitude and phase of the the left-hand side of equation (3.24), we get the constraints

$$\gamma_p^2 \omega^*(1 + \omega^{*2})^{\frac{n}{2}} \sqrt{\phi^2 + \omega^{*2}} = \beta \tag{3.25}$$

$$n \tan^{-1}(\omega^*) + \tan^{-1}\left(\frac{\omega^*}{\phi}\right) = \frac{\pi}{2} + 2k\pi. \tag{3.26}$$

From theorem 2 we know that, in the limit of strong feedback, all complex eigenvalues have magnitude much less than ϕ, therefore $\tan^{-1}(\omega^*/\phi) \to 0$. From these observations, we get the simplified relationship

$$n \tan^{-1}(\omega^*) = \frac{\pi}{2} + 2k\pi \implies \omega^* = \tan\left(\frac{\pi}{2n} + \frac{2k}{n}\pi\right),$$

and equation (3.25) becomes

$$\omega^*(1 + \omega^{*2})^{\frac{n}{2}} \frac{\gamma_p}{\alpha} = 1$$

$$\implies \gamma_p = \sqrt[n+1]{\frac{\theta_1\theta_2 \prod_{i=1}^{n-1} k_i}{\Omega_n}}, \tag{3.27}$$

where $\Omega_n = \omega^*(1+\omega^{*2})^{\frac{n}{2}}$. We can think of the parametric constrain equation (3.27) as the boundary between stable and unstable behavior in the system. Because the left-hand side of equation (3.25) is monotone in ω^*, we can infer that ω^* is unique and consequently there can only be one point in parameter space where there exist purely imaginary eigenvalues.

The final step is to study what happens when equation (3.27) does not hold. First we look at the regime $\sqrt[n+1]{\frac{\theta_1\theta_2 \prod_{i=1}^{n-1} k_i}{\Omega_n}} < \gamma_p$. Again using the uniqueness of ω^*, if we understand the stability behavior of the system for a particular value of γ_p in this regime, the same stability behavior must hold for all γ_p in this range. Because of this, we can first examine the range where γ_p is large. Intuitively, if degradation is sufficiently stronger than production then all species subject to degradation should converge to 0. To prove this rigorously, we will first search for roots with a large

magnitude. If we apply the strong feedback limit to the characteristic equation from equation (3.23), we get

$$p(s) = s(s+\gamma_p)^n(s+\frac{\beta}{\alpha}) + \gamma_p^n\beta = 0$$

$$\implies s\left(\frac{s}{\gamma_p}+1\right)^n\left(s\frac{\gamma_p\alpha}{\beta}+1\right) + \gamma_p\alpha = 0.$$

When $|s| \gg \gamma_p\alpha$, the characteristic equation will have the approximate form

$$\left(\frac{s}{\gamma_p}+1\right)^n\left(s\frac{\gamma_p\alpha}{\beta}+1\right) = 0,$$

which gives us n roots at $-\gamma_p$ and one root at $-\frac{\beta}{\gamma_p\alpha}$. Since equation (3.23) is order $n+2$, we know there is one remaining root outside of this regime. Next, we search for the final small root ($|s| \ll \min(\gamma_p, \frac{\beta}{\gamma_p\alpha})$, which gives the relationship

$$s + \gamma_p\alpha = 0,$$

which gives a final small root at $-\gamma_p\alpha$. Since each of the $n+2$ roots is negative, the system is stable for all $\sqrt[n+1]{\frac{\theta_1\theta_2\prod_{i=1}^{n-1}k_i}{\Omega_n}} < \gamma_p$.

Now we examine the regime $\sqrt[n+1]{\frac{\theta_1\theta_2\prod_{i=1}^{n-1}k_i}{\Omega_n}} > \gamma_p$. Here we will use a different technique, as taking the analogous limit of very small γ_p is less straight-forward to analyze. To start, we will perform a change of variable $s = \gamma_p\sigma$, where $\sigma \in \mathbb{C}$. We will again using the strong feedback limit, and study roots near the stability boundary, such that the characteristic equation still has the general form

$$\sigma(1+\sigma)^n = -\frac{\alpha}{\gamma_p}. \tag{3.28}$$

If we write $\sigma = a + ib$, we have the magnitude constraint

$$(a^2+b^2)[(1+a)^2+b^2]^n = \left(\frac{\alpha}{\gamma_p}\right)^2 > \Omega_n^2.$$

We also get the phase relationship

$$\tan^{-1}\left(\frac{b}{a}\right) + n\tan^{-1}\left(\frac{b}{1+a}\right) = \pi$$

$$\implies \frac{b}{1+a} < \omega^*.$$

Combining these relationships, we get

$$[a^2 + \omega^{*2}(1+a)^2](1+\omega^{*2})^n(1+a)^{2n} > \Omega_n^2.$$

$$\implies \left[\left(\frac{a}{\omega^*}\right)^2 + (1+a)^2\right](1+a)^{2n} > 1.$$

Since $a = 0$ at the stability boundary, there must be a regime of parameters sufficiently close to the boundary such that $|a| \ll \omega^*$, for which we have the relationship

$$(1+a)^{2(n+1)} > 1 \implies a > 0.$$

This proves the existence of an unstable point when $\sqrt[n+1]{\frac{\theta_1\theta_2\prod_{i=1}^{n-1}k_i}{\Omega_n}} > \gamma_p$, which implies that all parameters in this regime will yield unstable dynamics (so long as the strong feedback assumption still holds). □

We note that, though previous results studied the regime of strong feedback (β large), the core assumption that was made is that the quantity

$$\frac{\alpha^2+\beta}{\alpha\gamma_p} \gg 1.$$

We note that there is an entirely different way to achieve this, by making $\alpha^2 \gg \beta, \alpha\gamma_p$. In this regime, all of the previous results follow in almost exactly the same way, except for changes to the constants involved. It is relatively straightforward to show that the characteristic equation for the system reduces to

$$\sigma(1+\sigma)^n = -\frac{\beta\gamma_p}{\alpha}.$$

Following the same steps from the previous proofs, we can find that instability now occurs when

$$\sqrt[n-1]{\frac{\Omega_n\theta_1\theta_2\prod_{i=1}^{n-1}k_i}{\beta}} = \gamma_p.$$

Interestingly, the stable regime is now

$$\sqrt[n-1]{\frac{\Omega_n\theta_1\theta_2\prod_{i=1}^{n-1}k_i}{\beta}} > \gamma_p,$$

the opposite of what occurs in the strong feedback limit. One interpretation of these results as a whole is that stability is achievable when either controller sequestration or process degradation are individually large, but not when both are large simultaneously.

The Sensitivity Function

The sensitivity function $S(s), s \in \mathbb{C}$ is the transfer function between an input reference to a system and output error [18]. It is particularly useful to examine $|S(i\omega)|$, which corresponds to the magnitude of S given a purely oscillatory disturbance. If $|S(i\omega)| > 1$, then the system will amplify disturbances at a frequency ω. Conversely, if $|S(i\omega)| < 1$ then the system will attenuate disturbances at frequency ω.

Define $P(s)$ and $C(s)$ to be the transfer function between inputs and outputs of the process and controller, respectively. It is a standard result in control theory that

$$S = \frac{1}{1 + PC}.$$

In general, for a linear system

$$\begin{aligned} \dot{x} &= Ax + Bu \\ y &= Cx, \end{aligned}$$

the transfer function has the form $H(s) = C(sI - A)^{-1}B$. For the sequestration feedback system, we have that

$$P(s) = [0, \cdots, 1](sI - A)^{-1} \begin{bmatrix} 0 \\ \vdots \\ \theta_1 \end{bmatrix} = \frac{\theta_1 \prod_{i=1}^{n-1} k_i}{(s + \gamma_p)^n},$$

where just as before we use

$$A = \begin{bmatrix} -\gamma_p & 0 & \cdots & 0 \\ k_1 & -\gamma_p & \cdots & 0 \\ 0 & \ddots & \ddots & \vdots \\ 0 & \cdots & k_{n-1} & -\gamma_p \end{bmatrix}.$$

Similarly, we have that

$$C(s) = [1, 0](sI - D)^{-1} \begin{bmatrix} 0 \\ \theta_2 \end{bmatrix} = \frac{1}{s} \frac{\theta_2 \frac{\beta}{\alpha}}{[s + \left(\alpha + \frac{\beta}{\alpha}\right)]},$$

where

$$D = \begin{bmatrix} -\alpha & -\beta/\alpha \\ -\alpha & -\beta/\alpha \end{bmatrix}.$$

Note that $C(s)$ has a factor if $\frac{1}{s}$, indicating that it corresponds to an integrator. From P and C, we see that

$$S(s) = \frac{1}{1 + \frac{\frac{\beta}{\alpha}\theta_1\theta_2\prod_{i=1}^{n-1} k_i}{s(s+\gamma_p)^n\left[s+\left(\alpha+\frac{\beta}{\alpha}\right)\right]}} = \frac{s(s+\gamma_p)^n\left[s+\left(\alpha+\frac{\beta}{\alpha}\right)\right]}{s(s+\gamma_p)^n\left[s+\left(\alpha+\frac{\beta}{\alpha}\right)\right] + \beta\gamma_p^n}.$$

If we again take the limit $\frac{\alpha+\frac{\beta}{\alpha}}{\gamma_p} \gg 1$ and substitute $s = \gamma_p\sigma$ we get the approximation

$$S(\sigma) \approx \frac{\sigma(1+\sigma)^n}{\sigma(1+\sigma)^n + \frac{\alpha}{\gamma_p}}.$$

Ideally we would like to analyze $\|S(i\omega)\|_\infty = \max_\omega |S(i\omega)|$, however this is difficult to compute in general. A lower bound for this term can, however, be easily computed by evaluating a particular value of ω close to the maximum. Specifically, we will use $\omega = \tan(\frac{\pi}{2n})\gamma_p = \omega^*\gamma_p$. At $\sigma = i\omega^*$, we get

$$|S(i\omega^*)| \approx \frac{\omega^*(1+\omega^{*2})^{\frac{n}{2}}}{\omega^*(1+\omega^{*2})^{\frac{n}{2}} - \frac{\alpha}{\gamma_p}} = \frac{\Omega_n}{\Omega_n - \frac{\alpha}{\gamma_p}}.$$

From our previous results, we know that the system is purely oscillatory when $\Omega_n = \frac{\alpha}{\gamma_p}$, which corresponds to $|S(i\omega^*)| = \|S(i\omega)\|_\infty = \infty$. This gives the intuitive result that the system is infinitely sensitive to a periodic disturbance at $\omega = \omega^*\gamma_p$ when $\Omega_n = \frac{\alpha}{\gamma_p}$. In general, we will have that

$$\|S(i\omega)\|_\infty \geq \frac{\Omega_n}{\Omega_n - \frac{\alpha}{\gamma_p}}. \tag{3.29}$$

For the special case of $n = 2$, we can explicitly derive an even tighter bound than the one in inequality (3.29). First, we can explicitly compute

$$\begin{aligned}
|S(i\omega^*)| &\approx \frac{|i\omega^*(1+i\omega^*)^2|}{|i\omega^*(1+i\omega^*)^2 + \frac{\alpha}{\gamma_p}|} \\
&= \frac{\omega^*(1+\omega^{*2})}{\left|\left(\frac{\alpha}{\gamma_p} - 2\omega^{*2}\right) + i\omega^*(1-\omega^{*2})\right|} \\
&= \frac{\omega^*(1+\omega^{*2})}{\sqrt{\left(\frac{\alpha}{\gamma_p} - 2\omega^{*2}\right)^2 + (\omega^*(1-\omega^{*2}))^2}}.
\end{aligned}$$

Much of the complexity in this equation comes from the denominator, which can be simplified if we pick ω^* such that either the real or imaginary part is 0. If we plug in $\omega^* = \tan(\pi/4) = 1$, the complex part of the denominator vanishes and we recover the original bound:

$$\|S\|_\infty \geq |S(i)| = \frac{2}{2 - \frac{\alpha}{\gamma_p}} = \frac{1}{1 - \frac{\alpha}{2\gamma_p}}.$$

To set the real part to zero, it must be the case that

$$\frac{\alpha}{\gamma_p} - 2\omega^{*2} = 0 \implies \omega^* = \sqrt{\frac{\alpha}{2\gamma_p}}.$$

Plugging this in, we get that

$$\|S\|_\infty \geq \left|S\left(i\sqrt{\alpha/2\gamma_p}\right)\right| = \frac{1 + \frac{\alpha}{2\gamma_p}}{1 - \frac{\alpha}{2\gamma_p}} > \frac{1}{1 - \frac{\alpha}{2\gamma_p}}. \tag{3.30}$$

We see that this new bound is strictly greater than the one derived in inequality (3.29), and therefore is a better approximation of $\|S\|_\infty$. While inequality (3.29) generalizes to all value of n, the latter bound unfortunately requires us to find real roots of order n polynomials, which scales poorly for this problem.

Sequestration Feedback with Controller Species Degradation

Steady state analysis

Following the same notation as the previous sections, we can model the role of controller degradation as

$$\dot{x}_1 = \theta_1 z_1 - \gamma_p x_1 \tag{3.31a}$$
$$\dot{x}_2 = k_1 x_1 - \gamma_p x_2 \tag{3.31b}$$
$$\vdots$$
$$\dot{x}_n = k_{n-1} x_{n-1} - \gamma_p x_n \tag{3.31c}$$
$$\dot{z}_1 = \mu - \eta z_1 z_2 - \gamma_c z_1 \tag{3.31d}$$
$$\dot{z}_2 = \theta_2 x_n - \eta z_1 z_2 - \gamma_c z_2, \tag{3.31e}$$

where γ_p is the degradation of the process species x_i and γ_c is the degradation rate of the control species z_1 and z_2. At a high level we will proceed much in the same way as we did previously, however we will see that nonzero controller degradation leads to several technical challenges that do no appear when $\gamma_c = 0$. The first of

these arises from simply solving for the steady values around which we will linearize the model. Where previously we used the fact that $\dot{z}_1 - \dot{z}_2 = 0 \implies x_n^* = \mu/\theta_2$, where $*$ denotes a steady-state value. to subsequently solve for all other steady-state concentrations, we are now left with the messier relationship

$$\dot{z}_1 - \dot{z}_2 = 0 \implies x_n^* = \frac{\mu}{\theta_2} - \frac{\gamma_c}{\theta_2}(z_1^* - z_2^*).$$

This implies that, for $\gamma_c > 0$, we expect x_n to differ from the desired steady-state μ/θ by some error that depends on the values of z_1^* and z_2^*. Since this error is almost surely a function of many other parameters, we essentially lose the robust precise adaptation property where x_n^* is completely independent of the network's parameters. We will first calculate a general form for x_n^*, then derive a large η limit thats make further calculations tractable.

To begin, we use equations (3.31d) and (3.31e) to derive the relationships

$$\mu = z_1^*(\eta z_2^* + \gamma_c) \implies z_2^* = \frac{1}{\eta}\left(\frac{\mu}{z_1^*} - \gamma_c\right)$$
$$x_n^* = \frac{1}{\theta_2} z_2^*(\eta z_1^* + \gamma_c).$$

Combining these equations, we find that

$$x_n^* = \frac{\mu}{\theta_2} + \frac{\gamma_c \mu}{\eta\theta_2}\frac{1}{z_1^*} - \frac{\gamma_c}{\theta_2} z_1^* - \frac{\gamma_c^2}{\eta\theta_2}.$$

Finally, we observe that

$$z_1^* = \frac{\gamma_p^n}{\theta_1 \prod_i k_i} x_n^* = \frac{\theta_2}{\alpha} x_n^*,$$

which yields the relationship

$$x_n^* = \frac{\mu}{\theta_2} + \frac{\gamma_c \mu}{\eta\alpha}\frac{1}{x_n^*} - \frac{\gamma_c}{\alpha} x_n^* - \frac{\gamma_c^2}{\eta\theta_2},$$

$$\implies \left(1 + \frac{\gamma_c}{\alpha}\right) x_n^{*2} = \left(\frac{\mu}{\theta_2} - \frac{\gamma_c^2}{\eta\theta_2}\right) x_n^* + \frac{\gamma_c \mu}{\eta\alpha}. \tag{3.32}$$

While this quadratic can be solved explicitly, the result can be greatly simplified by again taking the limit of large η. Here the sense in which we take this limit is such that $\frac{\mu}{\theta_2} \gg \frac{\gamma_c^2}{\eta\theta_2}$ and $1 \gg \frac{\gamma_c \mu}{\eta\alpha}$. These reduce to the condition

$$\eta \gg \frac{\gamma_c^2}{\mu}, \frac{\gamma_c \mu}{\alpha}.$$

Combined with the previous assumption about the size of η we now have a large number of conditions to fulfill, however we find that in practice we rarely are in parameter regimes where a great deal of tuning needs to be done to satisfy everything. That being said, we can use this limit to reduce equation (3.32) to

$$\left(1 + \frac{\gamma_c}{\alpha}\right) x_n^{*2} = \frac{\mu}{\theta_2} x_n^* \implies x_n^* \approx \frac{\mu}{\theta_2} \frac{1}{1 + \frac{\gamma_c}{\alpha}}. \tag{3.33}$$

Using the same approximation, we can also compute

$$z_1^* = \frac{\theta_2}{\alpha} x_n^* \approx \frac{\mu}{\alpha + \gamma_c}, \tag{3.34}$$

$$z_2^* = \frac{\theta_2}{\eta z_1^* + \gamma_c} x_n^* \approx \frac{\alpha}{\eta}. \tag{3.35}$$

These will be useful for computing the linearized dynamics of the system in the next section.

As a sanity check, we can immediately see that $x_n^* = \mu/\theta_2$ when $\gamma_c = 0$, as expected. For $\gamma_c > 0$, equation (3.33) captures the steady-state error relative to the set point μ/θ induced by non-zero controller degradation. We see that, so long as the ratio $\gamma_c/\alpha \ll 1$, error will be negligible. What is unclear at this point is under what conditions this can be achieved while still ensuring stability of the overall system. To this end, we will now characterize stability and performance for $\gamma_c > 0$.

Linearized dynamics and characteristic equation

Here we present results analogous to those in section 3.4, omitting detailed proofs since the structure of the argument from this point on is essentially identical to what was show in the previous section. Because the only nonlinear terms in our system are in equations (3.31d) and (3.31e), the only matrix to change in our linearization from section 3.4 is

$$D = \begin{bmatrix} -\eta z_2^* - \gamma_c & -\eta z_1^* \\ -\eta z_2^* & -\eta z_1^* - \gamma_c \end{bmatrix} \approx \begin{bmatrix} -\alpha - \gamma_c & -\beta/(\alpha + \gamma_c) \\ -\alpha & -\beta/(\alpha + \gamma_c) - \gamma_c \end{bmatrix}.$$

Using this D matrix and proceeding with precisely the same calculation as before, we can derive the characteristic equation for the system:

$$(s + \gamma_p)^n (s + \gamma_c) \left[s + \gamma_c + \alpha + \frac{\beta}{\alpha + \gamma_c} \right] + \gamma_p^n \beta \frac{\alpha}{\alpha + \gamma_c} = 0. \tag{3.36}$$

We again take the appropriate limit of $\beta \gg (\gamma_c + \alpha)\gamma_p, (\gamma_c + \alpha)^2$ to follow the same argument as in section 3.4 to get the simplified expression in terms of $\sigma = s/\gamma_p$:

$$(1 + \sigma)^n \left(\frac{\gamma_c}{\gamma_p} + \sigma \right) = -\frac{\alpha}{\gamma_p}. \tag{3.37}$$

First we note that, when $\gamma_c = 0$, we recover equation (3.28) as expected. Proceeding as before, we can write the characteristic polynomial in terms of phase and magnitude constraints for $\sigma = i\omega^*$:

$$(1 + \omega^{*2})^{\frac{n}{2}} \sqrt{\frac{\gamma_c^2}{\gamma_p^2} + \omega^{*2}} = \frac{\alpha}{\gamma_p} \tag{3.38}$$

$$n \tan^{-1}(\omega^*) + \tan^{-1}\left(\frac{\gamma_p}{\gamma_c}\omega^*\right) = \pi. \tag{3.39}$$

Stability analysis.

Unfortunately, the additional complexity in equation (3.39) makes it challenging to write down the sort of explicit closed-form expressions for stability seen in theorem 3. While we can write out explicit stability conditions for $n = 2$, we will need to study particular parameter regimes for $n > 2$ as the summation relationship for $\tan^{-1}$ scales poorly.

To solve for ω^* in equation (3.39) we make use of the inverse trigonometric identity

$$\tan^{-1}(a) + \tan^{-1}(b) = \tan^{-1}\left(\frac{a+b}{1-ab}\right) \pmod{\pi}.$$

Applying this identity twice yields the relationship

$$\begin{aligned}
&2\tan^{-1}(\omega^*) + \tan^{-1}\left(\frac{\gamma_p}{\gamma_c}\omega^*\right) = \pi \\
\implies &\tan^{-1}\left(\frac{2\omega^*}{1-\omega^{*2}}\right) + \tan^{-1}\left(\frac{\gamma_p}{\gamma_c}\omega^*\right) = 0 \pmod{\pi} \\
\implies &\tan^{-1}\left(\frac{2\omega^* + \frac{\gamma_p}{\gamma_c}\omega^*(1-\omega^{*2})}{1-(1+\frac{\gamma_p}{\gamma_c})\omega^{*2}}\right) = 0 \pmod{\pi}.
\end{aligned}$$

Since the only value for which $\tan^{-1}(x) = 0$ is $x = 0$, the problem reduces to solving the equation

$$\begin{aligned}
&2\omega^* + \frac{\gamma_p}{\gamma_c}\omega^*(1-\omega^{*2}) = 0 \\
\implies &2 + \frac{\gamma_p}{\gamma_c}(1-\omega^{*2}) = 0 \\
\implies &\omega^* = \sqrt{2\frac{\gamma_c}{\gamma_p} + 1}.
\end{aligned}$$

Combining this with equation (3.38) yields the stability criterion

$$\frac{\theta_1\theta_2 k}{2} < \gamma_p(\gamma_c + \gamma_p)^2. \tag{3.40}$$

If we assume that we have full freedom to set control parameters, then inequality (3.40) that it is possible to make the production rates θ_1 and θ_2 large, so long as there is a compensatory increase in γ_c. This implies that we can, in a sense, sidestep the performance tradeoffs between speed and stability if we are willing pay a price in terms of *efficiency*, measured by the turnover rates of z_1 and z_2.

Next we will study what happens when $n > 2$. We note that there is an interesting topological distinction going from $n = 2$ to $n > 2$ which yields qualitatively different stability results. To see why this is the case, we return to equation (3.39):

$$n\tan^{-1}(\omega^*) + \tan^{-1}\left(\frac{\gamma_p}{\gamma_c}\omega^*\right) = \pi.$$

Recall that $\tan^{-1}(x) < \pi/2$ for all x. Because this is the case, when $n = 2$ it is always the case that $2\tan^{-1}(\omega^*) < \pi$, implying that satisfying the phase condition is strictly contingent of the value of the term $\tan^{-1}((\gamma_p/\gamma_c)\omega^*)$. On the other hand, for $n > 2$, there exist values of ω^* such that $n\tan^{-1}(\omega^*) \geq \pi$, so depending on the relative magnitude of the ratio γ_p/γ_c satisfying the phase condition may or may not depend strongly on γ_c.

If we look again at equation (3.37):

$$(1+\sigma)^n\left(\frac{\gamma_c}{\gamma_p} + \sigma\right) = -\frac{\alpha}{\gamma_p},$$

we notice that the only place in which γ_c appears is in the ratio γ_c/γ_p. One natural approach to studying the solutions to this equation is to examine what happens at various limits, namely $\gamma_c \ll \gamma_p$, $\gamma_c = \gamma_p$, and $\gamma_c \gg \gamma_p$. Here we will present results without going into formal detail, however the analysis can be made rigorous by analyzing equation (3.39).

Case I $\gamma_c \ll \gamma_p$**:** This case is fairly straightforward, as it is it reduces to the case of no controller degradation. We recover the characteristic polynomial

$$\sigma(1+\sigma)^n = -\frac{\alpha}{\gamma_p},$$

which has the same exact stability condition as in theorem 3.

Case II $\gamma_c = \gamma_p$: This case is representative of what happens when controller and process degradation have the same order of magnitude. We use $\gamma_p/\gamma_c = 1$ in equation (3.39) to find that the stability boundary is characterized by

$$\begin{aligned} n\tan^{-1}(\omega^*) + \tan^{-1}\left(\frac{\gamma_p}{\gamma_c}\omega^*\right) &= \pi \\ \overset{\gamma_c=\gamma_p}{\Longrightarrow} (n+1)\tan^{-1}(\omega^*) &= \pi \\ \Longrightarrow \omega^* &= \tan\left(\frac{\pi}{n+1}\right). \end{aligned}$$

Here it is useful to define the quantity

$$\tilde{\Omega}_n = \left(1 + \tan\left(\frac{\pi}{n}\right)^2\right)^{\frac{n}{2}},$$

where $\tilde{\Omega}_n$ differs from the previously defined Ω_n by a factor of $1/2$ in the argument of the tangent term. Using this expression, we can use equation (3.38) to derive the stability criterion

$$\frac{\alpha}{\gamma_p} < \tilde{\Omega}_{n+1} \implies \sqrt[n+1]{\frac{\theta_1\theta_2\prod_i k_i}{\tilde{\Omega}_{n+1}}} < \gamma_p.$$

This condition is qualitatively the same as the one in theorem 3 up to a constant difference accounted for by the $\tilde{\Omega}_{n+1}$ term.

Case III $\gamma_c \gg \gamma_p$: Following a similar line of reasoning as in the previous case, taking the limit $\gamma_p/\gamma_c \ll 1$ in equation (3.39) to show that

$$\begin{aligned} n\tan^{-1}(\omega^*) + \tan^{-1}\left(\frac{\gamma_p}{\gamma_c}\omega^*\right) &= \pi \\ \overset{\gamma_c\gg\gamma_p}{\Longrightarrow} n\tan^{-1}(\omega^*) &= \pi \\ \Longrightarrow \omega^* &= \tan\left(\frac{\pi}{n}\right). \end{aligned}$$

We again use equation (3.38) to find that the stability boundary is set by the following relationship:

$$\begin{aligned} (1+\omega^{*2})^{\frac{n}{2}}\sqrt{\frac{\gamma_c^2}{\gamma_p^2} + \omega^{*2}} &= \frac{\alpha}{\gamma_p} \\ \overset{\gamma_c\gg\gamma_p}{\Longrightarrow} \tilde{\Omega}_n\frac{\gamma_c}{\gamma_p} &= \frac{\alpha}{\gamma_p} \\ \Longrightarrow \tilde{\Omega}_n &= \frac{\alpha}{\gamma_c}. \end{aligned}$$

This implies that the stability criterion for this case is

$$\frac{\alpha}{\gamma_c} < \tilde{\Omega}_n \implies \sqrt[n]{\frac{\theta_1\theta_2\prod_i k_i}{\gamma_c\tilde{\Omega}_n}} < \gamma_p.$$

Notice that in the $n = 2$ case, ω^* is a function of γ_c and the subsequent stability criterion depends on the term $(\gamma_p + \gamma_c)^2$. This is quite different from the $n > 2$ cases where in each regime, the γ_c dependence in ω^* disappears. Similarly, in the stability criterion we see a linear (rather than quadratic) dependence on γ_c. This is a direct result of the previously mentioned topological difference between the $n = 2$ and $n > 2$ cases.

One interesting side effect of this results is that, when the system is purely oscillatory (on the stability boundary), the frequencies of oscillation may be dramatically different depending on n. Consider the case where $\gamma_c \gg \gamma_p$ If $n = 2$, this frequency will be

$$\omega = \gamma_p\omega^* = \gamma_p\sqrt{2\frac{\gamma_c}{\gamma_p} + 1} \approx \sqrt{2\gamma_p\gamma_c}.$$

If $n > 2$, we use the results from Case III above to find

$$\omega = \gamma_p\omega^* \approx \gamma_p \tan\left(\frac{\pi}{n}\right).$$

In the former case, ω scales with $\sqrt{\gamma_p}$, whereas in the latter case ω is independent of γ_c. This implies that for large controller degradation rates we would expect much faster oscillatory modes for $n = 2$ than for $n > 2$.

The effects of degradation on sensitivity and performance

Just as in section 3.4, we can write the generic sensitivity function for the linearized sequestration feedback system with degradation in terms of the variable $\sigma = \gamma_p s$ as

$$S(\sigma) = \frac{(1+\sigma)^n\left(\frac{\gamma_c}{\gamma_p} + \sigma\right)}{(1+\sigma)^n\left(\frac{\gamma_c}{\gamma_p} + \sigma\right) + \frac{\alpha}{\gamma_p}}. \tag{3.41}$$

For the case $n = 2$, we can again derive an explicit lower bound for $\|S(i\omega^*)\|_\infty$:

$$\begin{aligned} |S(i\omega^*)| &= \frac{\left|(1+i\omega^*)^2\left(\frac{\gamma_c}{\gamma_p} + i\omega^*\right)\right|}{\left|(1+i\omega^*)^2\left(\frac{\gamma_c}{\gamma_p} + i\omega^*\right) + \frac{\alpha}{\gamma_p}\right|}, \\ &= \frac{(1+\omega^{*2})\sqrt{\frac{\gamma_c^2}{\gamma_p^2} + \omega^{*2}}}{\left|\left(\frac{\gamma_c}{\gamma_p}(1-\omega^{*2}) - 2\omega^{*2}\right) + i\left(2\omega^*\frac{\gamma_c}{\gamma_p} + \omega^*(1-\omega^{*2})\right)\right|}. \end{aligned} \tag{3.42}$$

We can again solve for ω^* such that the real part of the denominator is zero:

$$\frac{\gamma_c}{\gamma_p}(1-\omega^{*2}) - 2\omega^{*2} = 0 \implies \omega^* = \sqrt{\frac{\alpha+\gamma_c}{2\gamma_p+\gamma_c}}.$$

If we evaluate equation (3.42) at ω^*, we can write the bound

$$\|S\|_\infty > |S(i\omega^*)| = \mathcal{F} = \frac{(1+\omega^{*2})\sqrt{1+\left(\frac{\gamma_c}{\omega^*\gamma_p}\right)^2}}{(1-\omega^{*2})+2\frac{\gamma_c}{\gamma_p}}. \tag{3.43}$$

It is easy to check that, for $\gamma_c = 0$, we recover the bound from inequality (3.30). As ω^* approaches $1 + 2\gamma_c/\gamma_p$, $\|S\|_\infty$ will asymptotically increase to ∞. Alternatively, increasing γ_c will decrease sensitivity, and consequently improve robustness. We can think of γ_c as capturing the inefficiency of our controller (higher degradation means the control species are degraded before being used in a sequestration reaction). In these terms, we see that increasing γ_c will reduce $\mathcal{F}$ at the cost of increased steady-state error (see Figure 3.3D-F). If we hold ε constant by varying both γ_c and θ_1, the we can decrease $\mathcal{F}$ at the cost of on decreasing efficiency of the controller (see Figure 3.3G-I). Finally, we can vary γ_c and θ_1 such that $\mathcal{F}$ is constant, which leads to a tradeoff between steady-state error and efficiency (see Figure 3.3J-L).

Controlling an Unstable Process

In all prior sections, we have assumed that the underlying process being controlled is open-loop stable. Here we will examine a simple model of an open-loop unstable process and describe which control architectures are capable of stabilizing the closed-loop system. To start, we will use a simple linear system as our process:

$$\dot{x}_1 = k_2 x_2 - \gamma_p x_1,$$
$$\dot{x}_2 = k_1 x_1 - \gamma_p x_2.$$

This system will be unstable when at least one eigenvalue of the matrix:

$$A = \begin{bmatrix} -\gamma_p & k_2 \\ k_1 & -\gamma_p \end{bmatrix}$$

has positive real part. With some straightforward linear algebra we can find that the eigenvalues of A are

$$\lambda_\pm = -\gamma_p \pm \sqrt{k_1 k_2}.$$

Because $k_1, k_2, \gamma_p > 0$, we know that $\lambda_- < 0$ for all parameters. λ_+, however, can be either positive or negative. In particular,

$$\sqrt{k_1 k_2} > \gamma_p \iff \lambda_+ > 0.$$

To facilitate our study of unstable processes, we will assume $\sqrt{k_1 k_2} > \gamma_p$ for the rest of the section. One immediate difference is that, due to the unstable process, any controller must now be repressive. To model this, we will first study the following architecture (described in equation (3.21) and the left panels of Figure 3.5):

$$\begin{aligned}
\dot{x}_1 &= \frac{k_2 x_2}{1 + \theta_1 z_1} - \gamma_p x_1, \\
\dot{x}_2 &= k_1 x_1 - \gamma_p x_2, \\
\dot{z}_1 &= \mu_1 - \eta z_1 z_2, \\
\dot{z}_2 &= \frac{\mu_2}{1 + \theta_2 x_2} - \eta z_1 z_2.
\end{aligned}$$

If $\theta_1 = \theta_2 = 0$, then this architecture reduces to the open-loop system described above. The controller topology is essentially the same as in the stable case, with the core difference that z_1 represses x_1 and x_2 represses z_2, where before these interactions were activating. Since now there is no reaction synthesizing z_2, we must add in some external production rate μ_2. We will again proceed by solving for the steady-state concentrations of each species and linearizing around these values. The steady-state concentrations are as follows:

$$\begin{bmatrix} x_1^* \\ x_2^* \\ z_1^* \\ z_2^* \end{bmatrix} = \left[\frac{\gamma_p}{k_1 \theta_2} \frac{\mu_2 - \mu_1}{\mu_1}, \frac{1}{\theta_2} \frac{\mu_2 - \mu_1}{\mu_1}, \frac{k_1 k_2 - \gamma_p^2}{\theta_1 \gamma_p^2}, \frac{\mu_1}{\eta} \frac{\theta_1 \gamma_p^2}{k_1 k_2 - \gamma_p^2} \right]^T.$$

If we now linearize around this fixed point, we can define a new set of parameters:

$$\begin{aligned}
\hat{k}_2 &= \frac{d}{dx_2} \left(\frac{k_2 x_2}{1 + \theta_1 z_1} \right)_{z_1^*} = \frac{\gamma_p^2}{k_1}, \\
\hat{\theta}_1 &= \left| \frac{d}{dz_1} \left(\frac{k_2 x_2}{1 + \theta_1 z_1} \right)_{x_2^*, z_1^*} \right| = \frac{\theta_1}{\theta_2} \frac{\gamma_p^4}{k_1^2 k_2} \frac{\mu_2 - \mu_1}{\mu_1}, \\
\hat{\theta}_2 &= \left| \frac{d}{dx_2} \left(\frac{\mu_2}{1 + \theta_2 x_2} \right)_{x_2^*} \right| = \theta_2 \frac{\mu_1^2}{\mu_2}, \\
\alpha &= \eta z_2^* = \frac{\mu_1 \theta_1 \gamma_p^2}{k_1 k_2 - \gamma_p^2}, \\
\beta &= \beta_1,
\end{aligned}$$

which characterize the linearized set of dynamics:

$$\dot{\mathbf{x}} = M\mathbf{x},$$

$$\mathbf{x} = \begin{bmatrix} x_1 \\ x_2 \\ z_1 \\ z_2 \end{bmatrix}, M = \begin{bmatrix} -\gamma_p & \hat{k}_2 & -\hat{\theta}_1 & 0 \\ k_1 & -\gamma_p & 0 & 0 \\ 0 & 0 & -\alpha & -\beta/\alpha \\ 0 & -\hat{\theta}_2 & -\alpha & -\beta/\alpha \end{bmatrix}.$$

Following the same methods in section 3.4, we can derive the characteristic polynomial for M,

$$p(s) = s(s-\lambda_+)(s-\lambda_-)\left(s+\alpha+\frac{\beta}{\alpha}\right) + \frac{\beta}{\alpha}\hat{\theta}_1\hat{\theta}_2 k_1,$$

where we now use $\lambda_\pm = -\gamma_p \pm \sqrt{k_1\hat{k}_2}$. If we plug in $\hat{k}_2$, we see that $\lambda_+ = 0$ and $\lambda_- = -2\gamma_p$. The fact that the process's eigenvalues change when comparing the open- and closed-loop systems is a byproduct of the fact that our original model was nonlinear, and is something that would not occur for a strictly linear system.

Again taking the limit of strong feedback, which here takes the form $\beta \gg \alpha^2, 2\alpha\gamma_p$, and setting $p(s) = 0$, we get the equation

$$s^2(s+2\gamma_p) = -\hat{\theta}_1\hat{\theta}_2 k_1.$$

The corresponding phase constraint for this equation when $s = i\omega$ is (after some algebra):

$$\tan^{-1}\left(\frac{\omega}{2\gamma_p}\right) = \frac{\pi}{2}.$$

Since $\tan^{-1}(x) < \pi/2$, there are no parameter values for which this phase constraint is achieved.

Next, we consider an alternative architecture, shown in Figure 3.5 and equation (3.22). This system is described by the same dynamics as before, except we now have z_1 directly repressing x_2 (rather than indirectly doing so via x_1):

$$\begin{aligned} \dot{x}_1 &= k_2 x_2 - \gamma_p x_1, \\ \dot{x}_2 &= \frac{k_1 x_1}{1+\theta_1 z_1} - \gamma_p x_2, \\ \dot{z}_1 &= \mu_1 - \eta z_1 z_2, \\ \dot{z}_2 &= \frac{\mu_2}{1+\theta_2 x_2} - \eta z_1 z_2. \end{aligned}$$

The steady-state values are almost identical to those of section 3.4, except we now have that

$$x_1^* = \frac{k_2}{\gamma_p\theta_2}\frac{\mu_2-\mu_1}{\mu_1}.$$

We can define another set of linearized parameters,

$$\hat{k}_1 = \frac{d}{dx_1}\left(\frac{k_1 x_1}{1+\theta_1 z_1}\right)_{z_1^*} = \frac{\gamma_p^2}{k_2},$$
$$\hat{\theta}_1 = \left|\frac{d}{dz_1}\left(\frac{k_1 x_1}{1+\theta_1 z_1}\right)_{x_1^*, z_1^*}\right| = \frac{\theta_1}{\theta_2}\frac{\gamma_p^3}{k_1 k_2}\frac{\mu_2-\mu_1}{\mu_1},$$

with $\hat{\theta}_2$, α, and β the same as before. Our linearized dynamics are now described by the matrix

$$M = \begin{bmatrix} -\gamma_p & k_2 & 0 & 0 \\ \hat{k}_1 & -\gamma_p & -\hat{\theta}_1 & 0 \\ 0 & 0 & -\alpha & -\beta/\alpha \\ 0 & -\hat{\theta}_2 & -\alpha & -\beta/\alpha \end{bmatrix},$$

with a corresponding characteristic polynomial

$$p(s) = s(s-\lambda_+)(s-\lambda_-)\left(s+\alpha+\frac{\beta}{\alpha}\right) + \frac{\beta}{\alpha}\hat{\theta}_1\hat{\theta}_2(s+\gamma_p),$$

with $\lambda_\pm = -\gamma_p \pm \sqrt{\hat{k}_1 k_2}$. The limiting form of the characteristic equation is now

$$s^2(s+2\gamma_p) = -\hat{\theta}_1\hat{\theta}_2(s+\gamma_p),$$

with the phase constraint

$$\tan^{-1}\left(\frac{\omega}{2\gamma_p}\right) = \tan^{-1}\left(\frac{\omega}{\gamma_p}\right).$$

Unlike in the previous architecture, this constraint *is* achievable for $\omega = 0$. This leads to a stability criterion of the form

$$0 < \frac{\hat{\theta}_1\hat{\theta}_2}{2},$$

which implies that the linear system is intrinsically stable so long as the parameters are set such that the system has a positive steady-state concentrations ($\mu_2 > \mu_1$, $k_1 k_2 > \gamma_p^2$). The in turn implies that the nonlinear system will be locally stable near the fixed point *independent* of the model's parameters.

Finally, we can find the sensitivity function for the stabilizing architecture. This is somewhat complicated by the fact that the process transfer function varies with control parameters, so it is difficult to separate the process and the controller transfer functions. However we can use a convenient form

$$S(s) = \frac{p_{ol}(s)}{p_{cl}(s)},$$

where $p_{cl}(s)$ is the characteristic equations for the closed-loop systems, and $p_o l(s) = \lim_{\theta_1 \to 0} p_{cl}(s)$ [48, 8]. Using

$$p_{cl}(s) = s^2(s + 2\gamma_p)\left(s + \alpha + \frac{\beta}{\alpha}\right) + \frac{\beta}{\alpha}\hat{\theta}_1\hat{\theta}_2(s + \gamma_p),$$

we get the sensitivity function (assuming large β):

$$S(s) = \frac{s(s + \gamma_p - \sqrt{k_1 k_2})(s + \gamma_p + \sqrt{k_1 k_2})}{s^2(s + 2\gamma_p) + \hat{\theta}_1\hat{\theta}_2(s + \gamma_p)}.$$

Note that it is important the we take care with the limits, as the roots of $p_{ol}(s)$ should reflect the eigenvalues of the unstable open-loop system. This is used to generate the right-hand plots in Figure 3.5A and B.

References

[1] Manfred Rizzi et al. "In vivo analysis of metabolic dynamics in Saccharomyces cerevisiae: II. mathematical model". In: *Biotechnology and bioengineering* 55.4 (1997), pp. 592–608.

[2] Ethan Lee et al. "The roles of APC and Axin derived from experimental and theoretical analysis of the Wnt pathway". In: *PLoS biology* 1.1 (2003), e10.

[3] Birgit Schoeberl et al. "Computational modeling of the dynamics of the MAP kinase cascade activated by surface and internalized EGF receptors". In: *Nature biotechnology* 20.4 (2002), p. 370.

[4] Lea Goentoro and Marc W Kirschner. "Evidence that fold-change, and not absolute level, of β-catenin dictates Wnt signaling". In: *Molecular cell* 36.5 (2009), pp. 872–884.

[5] Guy Shinar et al. "Input–output robustness in simple bacterial signaling systems". In: *Proceedings of the National Academy of Sciences* 104.50 (2007), pp. 19931–19935.

[6] H El-Samad et al. "Surviving heat shock: control strategies for robustness and performance". In: *Proceedings of the National Academy of Sciences of the United States of America* 102.8 (2005), pp. 2736–2741.

[7] Naama Barkai and Stan Leibler. "Robustness in simple biochemical networks". In: *Nature* 387.6636 (1997), p. 913.

[8] Fiona A Chandra, Gentian Buzi, and John C Doyle. "Glycolytic oscillations and limits on robust efficiency". In: *science* 333.6039 (2011), pp. 187–192.

[9] Tau-Mu Yi et al. "Robust perfect adaptation in bacterial chemotaxis through integral feedback control". In: *Proceedings of the National Academy of Sciences* 97.9 (2000), pp. 4649–4653.

[10] Thomas S Shimizu, Yuhai Tu, and Howard C Berg. “A modular gradient-sensing network for chemotaxis in Escherichia coli revealed by responses to time-varying stimuli”. In: *Molecular systems biology* 6.1 (2010), p. 382.

[11] Dale Muzzey et al. “A systems-level analysis of perfect adaptation in yeast osmoregulation”. In: *Cell* 138.1 (2009), pp. 160–171.

[12] Edward J Hancock et al. “The Interplay between Feedback and Buffering in Cellular Homeostasis”. In: *Cell systems* 5.5 (2017), pp. 498–508.

[13] Pablo Szekely et al. “Evolutionary tradeoffs between economy and effectiveness in biological homeostasis systems”. In: *PLoS computational biology* 9.8 (2013), e1003163.

[14] Jörg Stelling et al. “Robustness of cellular functions”. In: *Cell* 118.6 (2004), pp. 675–685.

[15] Miri Adler et al. “Optimal regulatory circuit topologies for fold-change detection”. In: *Cell systems* 4.2 (2017), pp. 171–181.

[16] James E Ferrell Jr. “Perfect And Near-perfect Adaptation In Cell Signaling”. In: *Cell Systems* 2.2 (2016), pp. 62–67.

[17] H El-Samad, JP Goff, and M Khammash. “Calcium Homeostasis And Parturient Hypocalcemia: An Integral Feedback Perspective”. In: *Journal of Theoretical Biology* 214.1 (2002), pp. 17–29.

[18] Karl Johan Aström and Richard M Murray. *Feedback Systems: An Introduction For Scientists And Engineers*. Princeton University Press, 2008.

[19] Wenzhe Ma et al. “Defining Network Topologies That Can Achieve Biochemical Adaptation”. In: *Cell* 138.4 (2009), pp. 760–773.

[20] Gunter Stein. “Respect the unstable”. In: *IEEE Control Systems* 23.4 (2003), pp. 12–25.

[21] Domitilla Del Vecchio and Richard M Murray. *Biomolecular feedback systems*. Princeton University Press, 2015.

[22] Jürgen Werner. “System Properties, Feedback Control And Effector Coordination Of Human Temperature Regulation”. In: *European Journal of Applied Physiology* 109.1 (2010), pp. 13–25.

[23] Michael J Rust et al. “Ordered Phosphorylation Governs Oscillation Of A Three-protein Circadian Clock”. In: *Science* 318.5851 (2007), pp. 809–812.

[24] Cellina Cohen-Saidon et al. “Dynamics and variability of ERK2 response to EGF in individual living cells”. In: *Molecular cell* 36.5 (2009), pp. 885–893.

[25] Victor Sourjik and Ned S Wingreen. “Responding to chemical gradients: bacterial chemotaxis”. In: *Current opinion in cell biology* 24.2 (2012), pp. 262–268.

[26] Corentin Briat, Ankit Gupta, and Mustafa Khammash. "Antithetic integral feedback ensures robust perfect adaptation in noisy biomolecular networks". In: *Cell systems* 2.1 (2016), pp. 15–26.

[27] Miki Jishage and Akira Ishihama. "Transcriptional Organization And In Vivo Role Of The Escherichia coli Rsd Gene, Encoding The Regulator Of RNA Polymerase Sigma D". In: *Journal of Bacteriology* 181.12 (1999), pp. 3768–3776.

[28] Victoria Hsiao et al. "Design and implementation of a biomolecular concentration tracker". In: *ACS synthetic biology* 4.2 (2014), pp. 150–161.

[29] Elisa Franco et al. "Negative autoregulation matches production and demand in synthetic transcriptional networks". In: *ACS synthetic biology* 3.8 (2014), pp. 589–599.

[30] Reed D McCardell et al. "Control of bacterial population density with population feedback and molecular sequestration". In: *bioRxiv* (2017). 10.1101/225045. eprint: https://www.biorxiv.org/content/early/2017/11/25/225045.full.pdf. URL: https://www.biorxiv.org/content/early/2017/11/25/225045.

[31] Fabio Annunziata et al. "An Orthogonal Multi-input Integration System To Control Gene Expression In Escherichia coli". In: *ACS Synthetic Biology* 6.10 (2017), pp. 1816–1824.

[32] Ioannis Lestas, Glenn Vinnicombe, and Johan Paulsson. "Fundamental limits on the suppression of molecular fluctuations". In: *Nature* 467.7312 (2010), pp. 174–178.

[33] Yili Qian and Domitilla Del Vecchio. "Realizing 'Integral Control' In Living Cells: How To Overcome Leaky Integration Due To Dilution?" In: *Journal of The Royal Society Interface* 15.139 (2018). ISSN: 1742-5689. DOI: 10.1098/rsif.2017.0902.

[34] Hendrik Wade Bode. *Network analysis and feedback amplifier design*. van Nostrand, 1945.

[35] Jordan Ang et al. "Considerations for using integral feedback control to construct a perfectly adapting synthetic gene network". In: *Journal of theoretical biology* 266.4 (2010), pp. 723–738.

[36] Yili Qian, Cameron McBride, and Domitilla Del Vecchio. "Programming Cells To Work For Us". In: *Annual Review of Control, Robotics, and Autonomous Systems* (2017).

[37] Noah Olsman et al. "Hard limits and performance tradeoffs in a class of sequestration feedback systems". In: *bioRxiv* (2018). **I am the primary author, and developed most results and all figures in the paper. Yoke Peng Leong proved results pertaining to the stability margin of the system with controller degradation.**, p. 222042.

[38] Lingchong You et al. “Programmed population control by cell-cell communication and regulated killing”. In: *Nature* 428.6985 (2004), p. 868.

[39] Frederick K Balagaddé et al. “Long-term monitoring of bacteria undergoing programmed population control in a microchemostat”. In: *Science* 309.5731 (2005), pp. 137–140.

[40] Corentin Briat, Ankit Gupta, and Mustafa Khammash. “Antithetic proportional-integral feedback for reduced variance and improved control performance of stochastic reaction networks”. In: *Journal of The Royal Society Interface* 15.143 (2018), p. 20180079.

[41] Yuval Hart et al. “Paradoxical signaling by a secreted molecule leads to homeostasis of cell levels”. In: *Cell* 158.5 (2014), pp. 1022–1032.

[42] Lauren Narcross et al. “Microbial Factories For The Production Of Benzylisoquinoline Alkaloids”. In: *Trends in Biotechnology* 34.3 (2016), pp. 228–241.

[43] Mary J Dunlop, Jay D Keasling, and Aindrila Mukhopadhyay. “A Model For Improving Microbial Biofuel Production Using A Synthetic Feedback Loop”. In: *Systems and Synthetic Biology* 4.2 (2010), pp. 95–104.

[44] Marie E Csete and John C Doyle. “Reverse engineering of biological complexity”. In: *science* 295.5560 (2002), pp. 1664–1669.

[45] Thomas Folliard. “A synthetic viral feedback loop results in robust expression”. In: *ACS Synthetic Biology* (2017).

[46] Gabriele Lillacci, Yaakov Benenson, and Mustafa Khammash. “Synthetic control systems for high performance gene expression in mammalian cells”. In: *Nucleic Acids Research* (2018).

[47] Gabriele Lillacci et al. “A synthetic integral feedback controller for robust tunable regulation in bacteria”. In: *bioRxiv* (2017), p. 170951.

[48] Fiona A Chandra, Gentian Buzi, and John C Doyle. “Linear control analysis of the autocatalytic glycolysis system”. In: *American Control Conference, 2009. ACC’09.* IEEE. 2009, pp. 319–324.

Chapter 4

ARCHITECTURE AND TRADEOFFS IN THE HEAT SHOCK RESPONSE SYSTEM

4.1 Introduction

Biological control systems, much like engineered ones, are faced with a variety of heterogeneous constraints that shape their design [1, 2]. Because of this, the selective pressures of evolution have likely not only selected for nominal performance, but also for robustness and efficiency [3]. While many different system architectures may be able to perform a given task, it is reasonable to assume that the ones that actually evolve reflect a balance between the myriad tradeoffs faced by the cell.

In this chapter, we examine such tradeoffs in the context of the Heat Shock Response (HSR) system of *E. coli*. When a cell encounters a rapid increase in temperature, there is a corresponding increase in the rate at which its proteins become misfolded. If too many of the cell's proteins are misfolded, the cell will likely die. To prevent this, cells will produce Heat Shock Proteins (HSPs) whose job is to rapidly refold proteins so that the organism can continue functioning normally.

From a systems perspective the HSR clearly must be an extremely fast and robust system, as it is vital to a cell's ability to respond to sudden and unexpected stress. On the other hand, if heat shock is a rare event then it would be wasteful for the cell to constantly produce HSPs at a high rate. Intuitively, we would expect that a strong architecture would be capable not only of refolding proteins, but would do so as quickly, efficiently, and robustly as possible.

We find that the natural HSR system in *E. coli* does an excellent job balancing these various tradeoffs. To demonstrate this, we examine several hypothetical alternative architectures for the system, and show that the complexity of the full system results in performance that none of the simpler systems can match. While it is possible for these reduced architecture to perform well on a given metric, e.g. efficiency or speed, they are limited in their ability to do well on many tasks simultaneously. We find that the strong performance of the natural HSR system is due to several elegant mechanisms, for example a layering of planning and control modules, that work together to make the system highly functional.

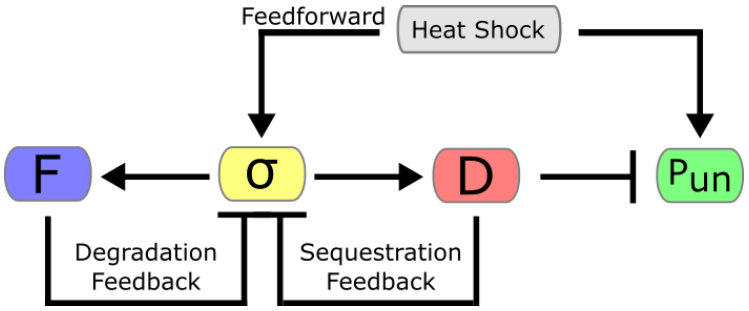

Figure 4.1: Abstract block diagram of the full HSR System. This shows a high-level representation of how the HSR system uses a combination of feedforward and feedback mechanisms to regulate the level of unfolded protein in a cell. Arrows signify effects which increase concentration, while flat-headed line signify repression of activity.

In section 4.2, we will present a new reduced-order model of the HSR system that faithfully captures the quantitative results of more complex models. In section 4.3 we will present hypothetical alternative architectures to the HSR system. In section 4.4 we analyze tradeoffs between several response metrics, and compare the relative performance of the architectures discussed in section 4.3. Because this chapter has a large number of parameters, their description is in the supplement at the end.

4.2 Reduced-Order Model

The core of the HSR system involves four classes of proteins: the unfolded proteins which the system is trying to refold, the chaperone whose job it is to refold proteins, the σ factor that regulates the expression of all proteins involved in heat shock response, and the proteases that degrades the σ factor. While the real HSR system has a variety of chaperones and proteases that are expressed during heat shock, we follow previous work [4, 5] and substitute a single chaperone (DnaK) denoted $[D]$ and a single protease (FtsH) denoted $[F]$ in our model. Each of these has a corresponding mRNA responsible for its translation ($[M_D]$ and $[M_F]$, respectively), and the system is controlled by a single σ factor (σ^{32}) denoted $[\sigma]$ that regulates RNA transcription and has a constant amount of mRNA ($[M_\sigma]$) at all times. This assumption comes from the fact that $[M_\sigma]$ transcription is regulated by a separate mechanism, independent of what we study in this model. We ignore the effects of temperature on the protein synthesis rates, which is admittedly a simplification but is consistent with prior modeling work by domain experts [4, 5].

Before heat shock occurs, much of the σ factor is inactivated by DnaK. This occurs because σ^{32} contains a region that closely resembles an unfolded protein, so any DnaK not in the process of refolding proteins will bind to σ^{32}, effectively

sequestering it. The protease FtsH will target sequestered σ factor for degradation, effectively giving it a high turnover rate (i.e. rapid production and degradation). Both provide feedback control.

Upon heat shock in the cell, two key events occur. The first is an increase in unfolding rate of proteins $k_{un}(T_{high}) = \delta \cdot k_{un}(T_{low})$, and the second is an increase in σ factor production represented by the parameter $\eta(T)$ in translation of σ, which ultimately leads to the increased production of DnaK and FtsH. This change in η is mediated by a temperature-dependent change to the structure of the σ^{32} mRNA, caused by a melting of certain bonds that result in the RNA being more accessible to ribosomes. This acts as a direct temperature sensor in the HSR system. Increases in unfolded protein cause an immediate increase in free σ factor, because the high concentration of unfolded protein displaces any sequestered σ factor bound to DnaK. This increase in free σ factor, along with the increased production rate, cause a fast spike in production of DnaK and FtsH. Because the σ factor is no longer sequestered it will no longer be degraded by FtsH, further boosting its net production. Once DnaK has reduced unfolded protein to pre-shock levels, excess chaperone will re-sequester σ factor and facilitate degradation via protease, reducing production of both DnaK and FtsH. These mechanisms act as two negative feedback loops between σ factor and the proteins it regulates.

In Figure 4.1 we present a block diagram of the full system containing a single feedforward mechanism and two feedback loops. A more detailed explanation of the biology of the HSR system can be found in [6]. Our deterministic model of the system consists of 6 ODEs:

$$[\dot{\hat{\sigma}}] = k_p \eta(T)[M_\sigma] - k_{pd}[\hat{\sigma}] - k_{pr}[\sigma : D : F] \tag{4.1}$$

$$[\dot{M}_D] = k_{mD}[\sigma] - k_{md}[M_D] \tag{4.2}$$

$$[\dot{M}_F] = k_{mF}[\sigma] - k_{md}[M_F] \tag{4.3}$$

$$[\dot{\hat{D}}] = k_p[M_D] - k_{pd}[\hat{D}] \tag{4.4}$$

$$[\dot{F}] = k_p[M_F] - k_{pd}[F] \tag{4.5}$$

$$[\dot{\hat{P}}_{un}] = k_{un}(T)([P_{tot}] - [\hat{P}_{un}]) - k_f[P : D], \tag{4.6}$$

and 6 algebraic relationships:

$$[\sigma : D] = K_{\sigma D}[\sigma][D] \tag{4.7}$$

$$[\sigma : D : F] = K_{\sigma F}[\sigma : D][F] \tag{4.8}$$

$$[P : D] = K_{PD}[P_{un}][D] \tag{4.9}$$

$$[\hat{\sigma}] = [\sigma] + [\sigma : D : F] + [\sigma : D] \tag{4.10}$$

$$[\hat{D}] = [D] + [P : D] + [\sigma : D] + [\sigma : D : F] \tag{4.11}$$

$$[\hat{P}_{un}] = [P_{un}] + [P : D]. \tag{4.12}$$

Note that $[\hat{\cdot}]$ denotes the total quantity of the protein, $[\cdot]$ represent the free (i.e. unbound) quantity of the protein, and $[\cdot : \cdot]$ represents complexed proteins. We provide tables describing all variables (table 4.1) and parameters (table 4.2) of the system in section 4.6 for reference. This model is based on a more complex one proposed by El-Samad *et al.* [4], which contains a mix of 31 algebraic and differential equations. One of the core assumptions that makes both our model and previous ones tractable is that fast dynamics (e.g. biochemical interactions) are assumed to be at quasi-steady state and that no delays are explicitly modeled. In section 4.5 we discuss how these assumptions make it difficult to study certain properties of the HSR, such as the relationship between feedforward response and delays in the system. While this likely plays an important role in biology, our model likely undersells the role of planning (here feedforward) in the HSR system.

Our model not only has fewer equations, but also has the property that the algebraic relationship can be explicitly approximated, whereas in the original work these constraints had to be implicitly solved. In section 4.6 we explain in more detail how we derive this model from the original and justify our approximations. The simplicity not only makes the model tractable for theoretical analysis, but also makes it possible to simulate the system using an explicit solver in MATLAB (as opposed to the implicit solver required for the original model).

We believe that this model is relatively simple while still accurately capturing the complexity of the natural HSR system. Our formulation manages to be simple enough to be analytically tractable, yet complicated enough to have interesting performance tradeoffs (which will be analyze in sections 4.3 and 4.4). Due to the model's relative simplicity, it is possible to analytically approximate the steady-state solutions of most quantities in the system. First we note that $[\sigma]_{ss}$ determines $[\hat{D}]_{ss}$

and $[F]_{ss}$:

$$[M_D]_{ss} = \frac{k_{mD}}{k_{md}}[\sigma]_{ss} \implies [\hat{D}]_{ss} = \frac{k_p}{k_{pd}}\frac{k_{mD}}{k_{md}}[\sigma]_{ss},$$
$$[M_F]_{ss} = \frac{k_{mF}}{k_{md}}[\sigma]_{ss} \implies [F]_{ss} = \frac{k_p}{k_{pd}}\frac{k_{mF}}{k_{md}}[\sigma]_{ss}.$$

Next, if we are in the regime where the system is capable of efficient refolding ($[P_{tot}] \gg [P_{un}]_{ss}$) and that feedback results in most DnaK being bound to unfolded protein ($[P : D] \approx [\hat{D}]$), then we get the relationship

$$[\hat{D}]_{ss} \approx \frac{k_{un}(T)}{k_f}[P_{tot}]. \tag{4.13}$$

This yields the relationship

$$[\sigma]_{ss} \approx \frac{k_{pd}}{k_p}\frac{k_{md}}{k_{mD}}\frac{k_{un}(T)}{k_f}[P_{tot}]. \tag{4.14}$$

We note that this independence of $[\sigma]_{ss}$ and the protease rate k_{pr} was observed experimentally in [6].

Next we can see from equation (4.1), with the assumption that the intrinsic protein degradation rate is much slower than active degradation via FtsH ($k_{pd} \ll k_{pr}$), that

$$[\sigma : D : F]_{ss} \approx \frac{k_p}{k_{pr}}\eta(T)[M_\sigma]. \tag{4.15}$$

Finally, if we assume that there is enough FtsH such that it will bind to most sequestered σ factor ($[\sigma : D] \ll [\sigma : D : F]$, or equivalently $K_{\sigma F}^{-1} \ll [F]$), we can combine these terms to see that $[\hat{\sigma}]_{ss} \approx [\sigma]_{ss} + [\sigma : D : F]_{ss}$.

The result of this design is a fast system that is able to quickly create new DnaK proteins when heat shock first occurs, and is then able to quickly adapt down once the system has been stabilized (see green curves in figure Figure 4.2). In the next section we will explore in more depth how and why this architecture performs so well.

4.3 Architecture

Here we can observe some interesting properties of equations (4.14) and (4.15). First we note that, when the assumptions of the previous section hold, the biochemical parameters $K_{\sigma F}$, $K_{\sigma D}$, and K_{PD} *do not* appear anywhere in the steady state equations. This tells us that the system in some sense abstracts away the particulars of the

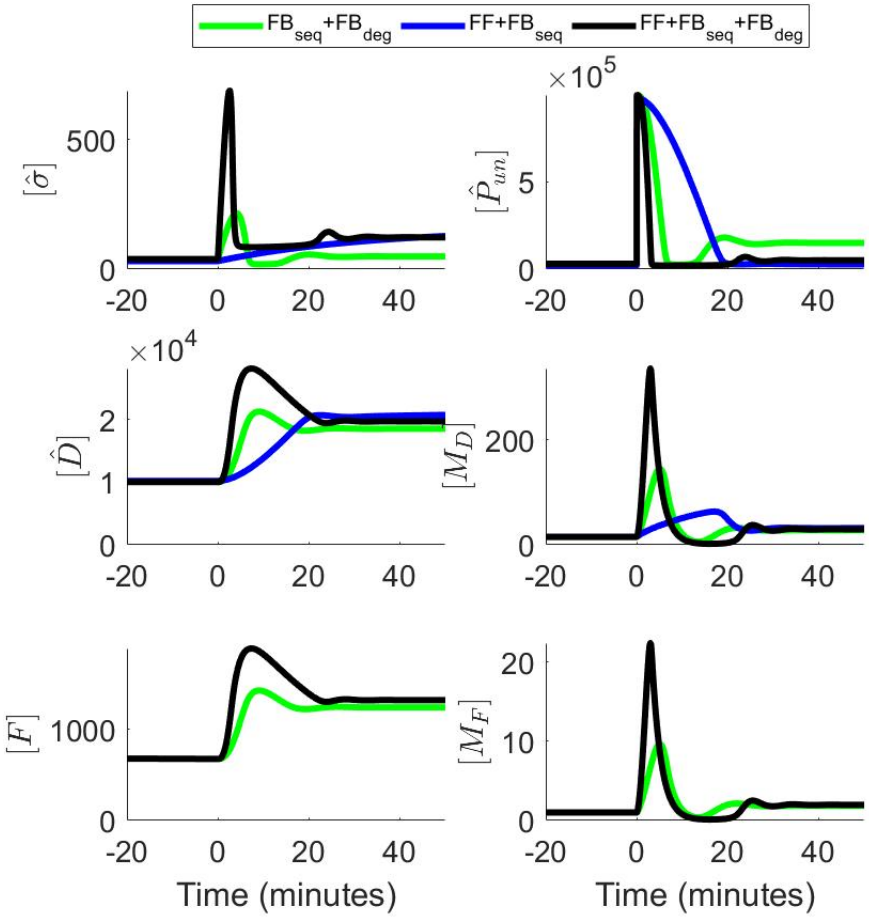

Figure 4.2: The dynamics of the architectures described in section 4.3. Here we see that, for a given set of parameters, the full HSR system architecture responds much more quickly than the simpler designs. We choose parameters to match pre-stimulus steady-state values of $[\hat{\sigma}]$ and $[\hat{D}]$ as closely as possible. For all architectures we use parameters as described in table 4.2. We note that the dynamics of $[F]$ match almost exactly to those of $[\hat{D}]$ up to scaling (the same is true of their respective mRNAs), this is because our simple model of protein synthesis leads to these species having the same dependence on $[\sigma]$, up to parameter scaling. We note that the bottom two panels do not have blue trajectories because $[F]$ does not appear in that architecture.

binding kinetics and makes the system purely dependent on the topology of the network at the biochemical level. This is largely a result of assumptions regarding time scales (i.e. that biochemistry is much faster than gene expression) and concentration scales (i.e. the inequalities that allowed us to derive equations (4.14) and (4.15)). While it is not obvious from the physics of the system that these assumptions all must hold simultaneously, it seems to be the case that the HSR system evolved to operate in a regime where they are correct.

Second we note that, since $[\sigma]_{ss}$ and $[\sigma : D : F]_{ss}$ reflect different aspects of the overall concentration of σ factor, we would intuitively expect them to be governed by many of the same parameters. In fact we see that, with the exception of the protein synthesis rate k_p, the parameters that *do* appear in both equations (4.14) and (4.15) are entirely non-overlapping. When we consider the temperature dependent parameters $\eta(T)$ and $k_{un}(T)$, we see that all of the feedforward architecture (i.e. direct measurement and response to changes in temperature caused by the parameter η) is encapsulated by $[\sigma : D : F]_{ss}$ in equation (4.14), and all of the feedback architecture (measurement of and response to changes in $[P_{un}]$, rather than T directly, mediated by k_{un}), is reflected by $[\sigma]_{ss}$ in equation (4.15).

If we now think about the dynamics of the system (see curves in Figure 4.2), this separation is a nice feature. We note that, to compare different architectures, we choose parameters such that the steady-state values of $[\hat{\sigma}]$ are the same across simulations. When heat shock first occurs, the fast increase in production via $\eta(T)$ and decrease in degradation via FtsH will cause a spike in σ factor, allowing for a fast initial refolding response. Because these terms do not appear in the steady-value of $[\hat{\sigma}]_{ss}$ in equation (4.14), it effectively allows for tuning of dynamics independently of steady-state response in the system. We note that the approximations presented here do not capture the precise value of $[P_{un}]_{ss}$ accurately, because equation (4.13) implies $[P_{un}]_{ss} = 0$. The simulations in Figure 4.2 show that $[P_{un}]_{ss}$ has a small but non-zero steady-state value.

To provide contrast to our analysis so far, we will now examine some alternative designs for the HSR system. We will describe first some qualitative features of the different designs, and then in the next section delve into more quantitative comparisons.

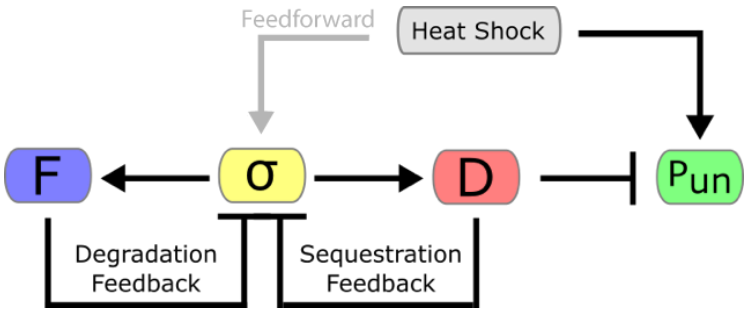

Figure 4.3: Block Diagram of the Sequestration and Degradation Feedback Architecture

Sequestration and Degradation Feedback Architecture

This architecture assumes that there are two feedback control mechanisms in response to heat shock that respectively sequester σ factor with DnaK, and then degrade it (see Figure 4.3):

$$\begin{aligned}
[\dot{\hat{\sigma}}] &= k_p \eta [M_\sigma] - k_{pd}[\hat{\sigma}] - k_{pr}[\sigma : D : F] \\
[\dot{M}_D] &= k_{mD}[\sigma] - k_{md}[M_D] \\
[\dot{M}_F] &= k_{mF}[\sigma] - k_{md}[M_F] \\
[\dot{\hat{D}}] &= k_p[M_D] - k_{pd}[\hat{D}] \\
[\dot{F}] &= k_p[M_F] - k_{pd}[F] \\
[\dot{\hat{P}}_{un}] &= k_{un}(T)([P_{tot}] - [\hat{P}_{un}]) - k_f[P : D].
\end{aligned}$$

This system incorporates dynamics analogous to those in equations (4.1), (4.2), (4.4), (4.6), (4.9), (4.11) and (4.12). The only difference is that in this case the translation rate of σ factor, η, does not increase with temperature. This architecture effectively has a lower σ^{32} translation rate than an architecture with the feedforward mechanism.

We see in Figure 4.2 that this system has a somewhat slower adaptation time to that of the system with full regulation, and the steady state concentration of $[\hat{P}_{un}]$ is higher, implying imprecise adaptation. When feedback is present there is more than enough total σ factor to produce the requisite amount of DnaK to refold proteins. In the absence of the feedforward response, it is the case that most of the σ factor is needed to produce as much DnaK as possible, so the small amount that is sequestered and degraded has a significant impact on the steady-state level of $[\hat{P}_{un}]$. In this sense, it seems that a significant role of the feedforward loop is to ensure that there is enough total σ factor to balance the effects of degradation feedback. Because $k_{pr} \gg k_{pd}$,

even small amounts of sequestered protein can lead to reduced levels of DnaK when the system is saturated, consequently increasing the final level of unfolded protein.

Feedforward and Sequestration Feedback Architecture

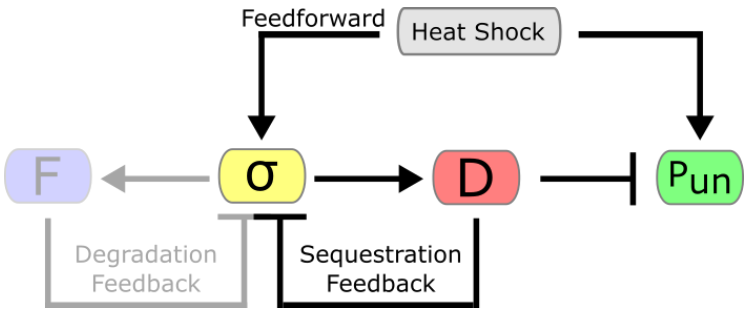

Figure 4.4: Block Diagram of the Sequestration Feedback Architecture

This architecture contains only a single feedback loop where DnaK binds to σ factor, sequestering it (see Figure 4.4). We also add in the effect of the feedforward mechanism, which essentially provides an immediate response to temperature changes via an increase to the translation rate of σ factor. In terms of the model, we simply modify the equation for $[\hat{\sigma}]$ so that η is temperature dependent and $k_{pr} = K_{\sigma F} = 0$,

$$[\dot{\hat{\sigma}}] = k_p \eta(T)[M_\sigma] - k_{pd}[\hat{\sigma}]. \tag{4.16}$$

This is almost identical to the full HSR system described in section 4.2, except that it lacks the degradation feedback loop mediated by the protease FtsH. This feedback serves to regulate the free amount of $[\sigma]$, but has no direct affect on the total amount $[\hat{\sigma}]$. We can use the same argument from section 4.2 to see that $[\sigma]_{ss}$ will be approximately the same as in equation (4.14):

$$[\sigma]_{ss} \approx \frac{k_{pd}}{k_p}\frac{k_{md}}{k_{mD}}\frac{k_{un}(T)}{k_f}[P_{tot}],$$

And the complex will have the form

$$\begin{aligned}[\sigma : D]_{ss} &= [\hat{\sigma}]_{ss} - [\sigma]_{ss} \\ &\approx \frac{k_p}{k_{pd}}\left(\eta(T)[M_\sigma] - \frac{k_{un}(T)}{\gamma}[P_{tot}]\right),\end{aligned} \tag{4.17}$$

where

$$\gamma = k_f \frac{k_p^2}{k_{pd}^2}\frac{k_{mD}}{k_{md}}.$$

We can think of this feedback system as serving two purposes. First, we see that it provides the benefit generally seen in feedback systems, namely that the signal

level (in this case $[\sigma]$) can be directly coupled to the disturbance that it is trying to compensate for, $k_{un}(T)$. This feedback mechanism can also serve to provide fast response for the system, in that a large amount of σ factor can be stored in the complex $[\sigma : D]$ and quickly released during heat shock (see the blue curves in Figure 4.2).

The downside to this architecture is that it is, in a sense, leaky. We see from equation (4.16) that the time scale for $[\hat{\sigma}]$ to reach steady state is determined by the protein degradation rate k_{pd}, which is typically quite slow (we use $k_{pd} = .03\text{min}^{-1}$, corresponding to a dilution-limited time scale of about 30 minutes). If the system has a low initial amount of σ factor, (corresponding to a small value of $[M_\sigma]$), then the time to refold proteins may be comparable to the scale of k_{pd} (as seen in the blue curves in Figure 4.2). Since the cell division time of *E. coli* is approximately 20-30 minutes, it would likely be dangerous (if not lethal) for the cell to respond on such a long time scale.

Alternatively, the cell could have a high initial amount of $[\hat{\sigma}]$ (large $[M_\sigma]$), and a correspondingly large amount of $[\sigma : D]$. This would allow for fast response, however $[\hat{\sigma}]$ would still reach steady state on time scale set by k_{pd}. This implies that after the cell has already adapted to heat shock, it would still be synthesizing σ factor unnecessarily and simply sequestering it into the complex $[\sigma : D]$, as can be seen by the fact that equation (4.17) is a function of both $\eta(T)$ and $k_{un}(T)$.

This is in contrast from the full model in section 4.2, where sequestered and free σ factor are governed by separate parameters (see equations (4.14) and (4.15)). Intuitively, this is a result of the protease providing much faster degradation than would intrinsically be seen in a cell (i.e. $k_{pr} \gg k_{pd}$).

Natural Architecture

The simpler architectures described in the previous sections serve to motivate the benefits of the natural HSR system (seen in Figure 4.1). We see that the structure of equations (4.1) to (4.12) allows for a layering of what we might consider planning (the terms in the feedforward loop $\eta(T)$ and $[M_\sigma]$, contained in the expression for $[\sigma : D : F]_{ss}$ in equation (4.15)) and control (the terms in the feedback loop k_{mD}, k_{md}, and k_f, contained in the expression for $[\sigma]_{ss}$ in equation (4.14)).

The independence of parameters in these layers allows for evolution to tune the system's dynamics independent of steady-state expression levels, a powerful feature that likely has been taken advantage of over the billions of years the system has

been in place. In the next section, we will explore parametric variations in these different architectures to gain a better understand of the tradeoffs that constrain their performance.

4.4 Tradeoff Analysis

In this section we will explore quantitative tradeoffs in performance for the HSR system. While the primary goal of the system is to refold proteins, we can see from Figure 4.2 that simply achieving a good steady state does not fully characterize the performance of the different architectures. We see that, while all of the architectures are capable of achieving a good steady state, they do so on different time scales and with different levels of efficiency. We define the response time to be the amount of time between when heat shock occurs, and when $[\hat{P}_{un}]$ first comes within 5% of $[\hat{P}_{un}]_{ss}$. We define the inefficiency of the response to be:

$$\text{Inefficiency} = 1 - \frac{[P:D]_{ss}}{[\hat{D}]_{ss}},$$

the fraction of $[\hat{D}]$ that is not being utilized for protein folding at steady state. Intuitively we might think of the most efficient response as the one that produces exactly as much $[\hat{D}]$ as there is $[\hat{P}_{un}]_{ss}$. Any excess $[\hat{D}]$ is not refolding proteins, and is thus considered to be in excess. An ideal architecture would not only be able to refold proteins efficiently, but would also minimize response time and inefficiency.

In Figure 4.5 we explore these tradeoffs by randomly varying the parameters $[M_\sigma]$ and $K_{\sigma D}$, and examining the performance of architectures that refold at least 85% of proteins within 100 minutes. The specifics of these thresholds are somewhat arbitrary, but the key idea is to only look at parameter sets where the HSR system is at least somewhat functional. Intuitively, it does not matter how fast or efficient a circuit is if it is not able to perform the primary task of refolding proteins. The reasoning behind our choice of $[M_\sigma]$ and $K_{\sigma D}$ as the varying parameters is that they directly affect σ factor dynamics and are not global parameters of the cell (like k_p and k_{pd}). We omit varying k_{pr} and $K_{\sigma F}$, the respective protease degradation and binding rates, because they are only present in the full architecture and would not affect the simpler architectures.

We see in Figure 4.5A that there is a clear separation between the architectures with degradation feedback (green and black points) and the one without it (blue points). This is due to the fact that much of the fast response time of the system is tied to

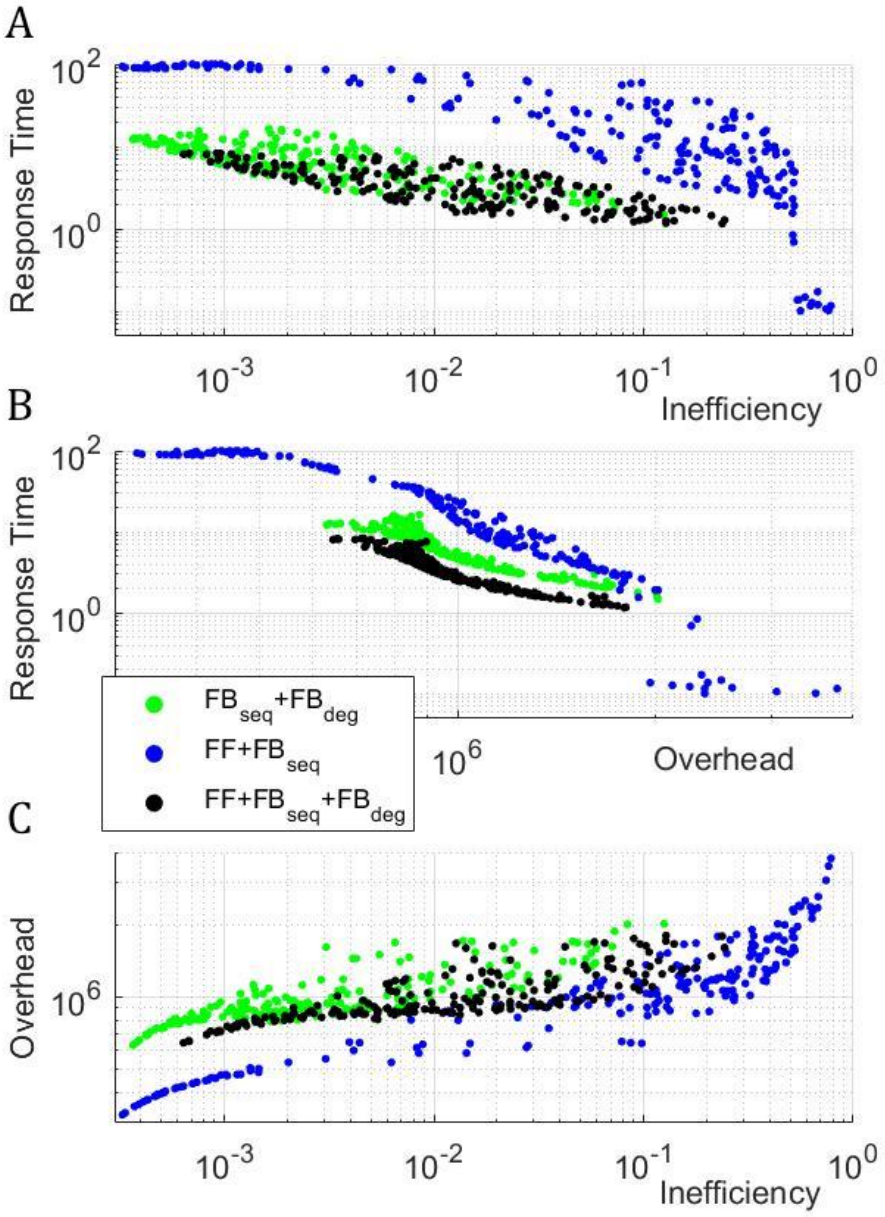

Figure 4.5: Tradeoffs across HSR architectures. Here we simulate the dynamics of each architecture for 1000 random parameter sets, where we sample values over $M_\sigma \in [1, 100]$ and $K_{\sigma D} \in \left[10^{-4}, 10^{-2}\right]$, with all other parameters kept as they are in Figure 4.2. These two parameters allow us to tune both the total amount of σ factor and the strength of the sequestration feedback loop (for the architectures with feedback). Each panel shows a different pairwise tradeoff between performance metrics, providing insight into the robustness of the qualitative features discussed in section 4.3.

the degradation mechanism, so in order for the architecture without it to respond quickly, it must greatly overproduce DnaK and consequently be highly inefficient.

One might also consider efficiency in terms of the rate at which a circuit incurs metabolic overhead. It is likely that cells face heat shock rarely, so it makes sense to think about how much ATP (the common unit of energy in the cell) per minute a given architecture uses in the absence of heat shock. While precise numbers for this may be difficult to come by, a reasonable proxy can be calculated easily in terms of how much ATP is spent on protein production, as this is likely the dominant metabolic expense to the cell. Using estimates of ATP use as a function of protein size, we estimate a cost of $\alpha = 2400 \frac{\text{ATP}}{\text{protein}}$ for large proteins (DnaK and FtsH) and $\beta = 1200 \frac{\text{ATP}}{\text{protein}}$ for small proteins (σ factor) [7]. The overhead rate is then computed from the steady-state production rates in the absence of heat shock,

$$\text{Overhead} = \beta k_p \eta(T_{low})[M_\sigma] + \alpha k_p [M_D]_{ss} + \alpha k_p [M_F]_{ss}.$$

We see in Figure 4.5B that the more complex architectures outperform the simpler ones. First we see again that the systems with degradation outperform the one without it. Because the feedforward mechanism allows for a very fast change to the translation rate of σ factor, it is the case that for a given protein overhead the feedforward system systematically responds more quickly to heat shock. The few cases that respond quickly but with high overhead also likely sacrifice a great deal of resources to overproduce DnaK and are effectively behaving as an open-loop response.

In Figure 4.5C we see that the full HSR system actually performs worse in terms of the tradeoff between overhead and inefficiency. This is because the simpler architecture that perform well in this tradeoff (i.e. those that are efficient and cheap), have the worst response time. This tells us that evolution may have selected strongly for architecture that optimizes response time, at the expense of some performance on the other two metrics.

4.5 Discussion

In this work, we presented a novel theoretical perspective on the architecture and design of the heat shock response system in *E. coli*. We showed that the HSR system seen in nature has many desirable properties, such as layering, speed, and efficiency. Further, we showed that simpler hypothetical architectures for the HSR system are not sufficient to match the response of the full architecture.

More generally, we believe that the HSR system serves as an ideal example of engineering tradeoffs in a biological setting. While several architectures are capable of performing the task of refolding proteins, there are many other performance metrics that may be subject to selective pressure. In engineered control systems stability is a primary goal, however properties such as speed, robustness, and cost are equally important for a system to be functional in the real world. Similar constraints are likely pervasive in biology, leading to the apparent complexity of many biological systems beyond what would naively be necessary.

Our analysis shows, through a combination of theory and simulation, that it is possible to systematically investigate the role of complexity in biology. In the future, we plan to expand our model to incorporate stochastic effects and a more nuanced model of heat shock. While our deterministic model was sufficient to ask many interesting questions, it is not able to tell us how noise in the system affects performance. Because σ factor is often at very low copy number, it is likely that stochastic effects play an important role and may present tradeoffs that are hidden in the deterministic setting.

While it is difficult to analytically study the role this sort of discrete delay in the dynamics, these simulations result yield insight into how biology might tune parameters to improve transient performance. It appears that when dynamics are slow (low k_p) there are moderate benefits to long advanced warning. For fast dynamics the benefits are larger and require less warning. Since we are essentially tuning the turnover rate of all proteins in the system, this implies that the systems which get the most out of this sort of warning are those that have high gains and thus are less efficient.

We find it encouraging that even a relatively simple model like that of the HSR system yields dynamics are quite complex and difficult to analyze in general. While we derived some approximate results, the nonlinearities in the system make it difficult to write down closed-form solutions to the various steady-states of the system in general. Further, these structural nonlinearities make it challenging to say anything precise about the dynamics of the system. Because the heat shock radically disturbs the system, linearizations that work well locally do a poor job of describing the global dynamics. We hope that future will yield deeper theoretical insights into the types of complex control systems that are pervasive in biology.

4.6 Supplemental Information

Description of Variables and Parameters

Variable	Description	Initial Condition
σ	The σ factor σ^{32}, regulates transcription of HSPs	30
D	The chaperone DnaK, responsible for refolding proteins	10,000
F	The protease FtsH, responsible for degrading σ factor	1,000
M_D	DnaK mRNA, responsible for translation of DnaK	10
M_F	FtsH mRNA, responsible for translation of FtsH	3
P_{un}	Unfolded protein in the cell	30,000

Table 4.1: Variable descriptions for Chapter 4.

Here we present tables describing the variables and parameters of the HSR system, along with descriptions and initial conditions/parameter values used in typical simulations. We followed parameters as much as was possible from [4], with the only difference being the translation rates k_{mD} and k_{mF} which had to be fit to typical steady-state values seen in their simulations. The reason for this is that these two parameters in our model reflect a large number of processes in their original model (mostly involving the binding of RNA polymerase), which we found could be simplified while still faithfully reproducing the dynamics seen in [4].

Model Reduction and Assumptions

In [4] and [5], detailed models of the HSR system are presented which aim to capture all relevant cellular processes at a mechanistic level. These models are quite complex (each containing on the order of 30 equations), and incorporate biochemistry, gene expression, and transcription/translation. Since these processes occur on vastly different time scales, the original models make a quasi-steady state assumption and treat fast processes as if they are algebraic (rather than differential) equations.

This makes simulations tractable, however the algebraic constraints were so complex that they could only reasonably be simulated with an implicit Differential-Algebraic Equation (DAE) solver. The shear number of equations makes it difficult to make an simplifications that would allow for analytic approximations to the algebraic constraints. To simplify the system, we observed that much of the complexity of the original model stems from the author's detailed description of transcriptional regulation. Because they explicitly σ factor binding to RNA polymerase and the consequent binding of polymerase to various sites on the genome, about 1/3 of the equations have little to do with the actual heat shock response and mostly govern

Parameter	Description	Value
k_p	Translation rate of proteins	20min^{-1}
k_{pd}	Intrinsic degradation rate of proteins	0.03min^{-1}
k_{pr}	Protease degradation rate of σ factor	5min^{-1}
k_{mD}	Transcription rate of DnaK mRNA	0.45min^{-1}
k_{mF}	Transcription rate of FtsH mRNA	0.03min^{-1}
k_{md}	Degradation rate of mRNA	0.5min^{-1}
$K_{\sigma D}$	Dissociation constant for $[\sigma : D]$ binding	$\frac{1}{400}M^{-1}$
$K_{\sigma F}$	Dissociation constant for $[\sigma : D : F]$ binding	$\frac{1}{400}M^{-1}$
K_{PD}	Dissociation constant for $[P : D]$ binding	$\frac{1}{400}M^{-1}$
$[P_{tot}]$	Total amount of protein in the cell	$2 \cdot 10^6$
$[M_\sigma]$	Amount of σ factor mRNA in the cell	10
$\eta(T_{low})$	Pre-shock translation rate of σ factor	0.35min^{-1}
$\eta(T_{high})$	Post-shock translation rate of σ factor	1.75min^{-1}
k_f	Protein refolding rate	15000min^{-1}
$k_{un}(T_{low})$	Pre-shock protein unfolding rate	75min^{-1}
$k_{un}(T_{high})$	Post-shock protein unfolding rate	$\delta \cdot 75\text{min}^{-1}$
δ	Heat shock magnitude	2

Table 4.2: Description of parameters in Chapter 4.

transcriptional regulation.

We observed that, so long as RNA polymerase and promoter regions are not saturated, all of these relationships could be captured simply by the level of free σ factor in the cell. Additionally we observe that, given the parameter values observed in biology, FtsH is generally far in excess of σ factor. This means that we can safely ignore conservation equations for FtsH, further simplifying the model. These assumptions yield the model described by equations (4.1) to (4.12). In our model, the only equations that have implicit dependences are equations (4.10) to (4.12). Combining these equations with equations (4.7) to (4.9), we can get the relationships:

$$[\sigma] = \frac{[\hat{\sigma}]}{1 + K_{\sigma D}[D](1 + K_{\sigma F}[F])},$$

$$[D] = \frac{[\hat{D}]}{1 + K_{PD}[P_{un}] + K_{\sigma D}[\sigma](1 + K_{\sigma F}[F])},$$

$$[P_{un}] = \frac{[\hat{P}_{un}]}{1 + K_{PD}[D]}.$$

These equations all depend on each other, so analytical expressions for $[\sigma]$, $[D]$, and $[\hat{P}_{un}]$ would require us to solve a system of three nonlinear equations. Fortunately,

we can simplify the system by making assumptions based on biological information. First we assume $[\sigma : D] \ll [P_{un} : D]$, or equivalently $K_{\sigma D}[\sigma] \ll K_{PD}[P_{un}]$. This gives us a simpler equation for free DnaK:

$$[D] = \frac{[\hat{D}]}{1 + K_{PD}[P_{un}]}.$$

Now we can solve for $[\sigma]$ if we know $[D]$, and $[D]$ if we know $[P_{un}]$. Using the equations for $[D]$ and $[P_{un}]$, we get a quadratic with the solution:

$$[P_{un}] = \frac{-\alpha + \sqrt{\alpha^2 + 4\beta}}{2},$$
$$\alpha = K_{PD}^{-1} - [\hat{P}_{un}] + [\hat{D}], \beta = \frac{[\hat{P}_{un}]}{K_{PD}}.$$

Since we can solve for $[P_{un}]$ independently of $[D]$ and $[\sigma]$, we can solve the entire system explicitly, give values of $[F]$, $[\hat{D}]$, $[\hat{\sigma}]$, and $[\hat{P}_{un}]$ determined by the ODES in equations (4.1) to (4.6). With this result, we were able to simulate the model with the MATLAB ode15s function, and have it match almost exactly to the results in [4].

References

[1] John C Doyle and Marie Csete. "Architecture, constraints, and behavior". In: *Proceedings of the National Academy of Sciences* 108.Supplement 3 (2011), pp. 15624–15630.

[2] Oren Shoval et al. "Evolutionary trade-offs, Pareto optimality, and the geometry of phenotype space". In: *Science* 336.6085 (2012), pp. 1157–1160.

[3] Fiona A Chandra, Gentian Buzi, and John C Doyle. "Glycolytic oscillations and limits on robust efficiency". In: *science* 333.6039 (2011), pp. 187–192.

[4] H. El-Samad et al. "Surviving heat shock: Control strategies for robustness and performance". In: 102.8 (2005), pp. 2736–2741. DOI: 10.1073/pnas.0403510102.

[5] Hiroyuki Kurata et al. "Module-based analysis of robustness tradeoffs in the heat shock response system". In: *PLoS Comput Biol* 2.7 (2006), e59.

[6] Eric Guisbert et al. "Convergence of molecular, modeling, and systems approaches for an understanding of the Escherichia coli heat shock response". In: *Microbiology and Molecular Biology Reviews* 72.3 (2008), pp. 545–554.

[7] B. Alberts. *Molecular Biology of the Cell: Reference edition*. Molecular Biology of the Cell: Reference Edition v. 1. Garland Science, 2008. ISBN: 9780815341116. URL: https://books.google.com/books?id=iepqmRfP3ZoC.

Chapter 5

CONCLUSION

The overarching theme of the work presented here is that the type of systems thinking that pervades engineering is not just a useful metaphor for understanding life, but in fact provides a wide variety of constructive tools to help us analyze the design and architecture of biological processes. It is worth noting that the set of tools used for each of the problems presented is diverse, combining theory and simulation, physics and engineering, and some techniques that are not neatly categorized.

As systems and synthetic biology mature, I hope that a cohesive theory will emerge that yields a unified perspective of biological control. Some of this will undoubtedly come directly from the classical theory of control systems, however biology is already starting to open up new avenues of research that require more than just re-purposing old techniques. For example, in Chapter 2 we sought to understand fold-change detection by combining the classical idea of integral feedback control with physical models of protein activation. To characterize the performance of these systems and understand their tradeoffs, we had to analyze notions of sensitivity which are quite particular to biology.

Similarly, in Chapter 3 we used a variety of standard results from control theory, but sought to use them to understand the sequestration feedback mechanism, which is quite distinct from any electrical or mechanical controller. To solve this problem, we had to develop new proof methods that took advantage of the particular structure of the system. Finally, Chapter 4 analyzes a system that has many properties analogous to classical control systems, yet is deeply constrained by the nonlinearities of biomolecular interactions. Because of this, standard linear analysis tools turned out to yield little insight. The key step to making progress came from understanding the biology of the system and reducing the mathematical model to something tractable enough for efficient simulation and analysis.

Going forward, there are several research frontiers that I believe will prove to be fertile ground for systems thinking in biology. Though a great deal of progress has been made towards understanding robustness at the level of circuits, there is still a large gap between the performance of natural and synthetic circuits. Where many natural circuits exhibit robust behavior over a wide range of environments

and conditions, synthetic circuits are often quite fragile. While the capacity to reliably implement feedback controllers (like the sequestration circuit in Chapter 3) is a promising development, most robust natural circuits contain a large number of feedback loops and are far more complex than what is currently feasible to implement in synthetic contexts. Given the evolutionary conservation of many circuits (e.g., in developmental signaling or metabolism), it is likely the case that the consistent appearance of complex feedback architecture is necessary for robust function. Until we can not only build complex circuits, but also develop reliable design guidelines for their implementation, it will likely be difficult for synthetic systems to match their natural counterparts.

While the origin of this performance gap is likely multifactorial, one likely culprit is our poor understanding of the constraints imposed by resources in the cell. Oftentimes when we write down a circuit diagram, we implicitly virtualize away many core biological processes so that we can describe a given system using a simple model. For example, it is common to describe the expression of proteins with the reaction kinetics

$$\begin{aligned}
&\text{gene}_{\text{off}} \underset{k_{off}}{\overset{k_{on}}{\rightleftharpoons}} \text{gene}_{\text{on}},\\
&\text{gene}_{\text{on}} \xrightarrow{k_m} \text{gene}_{\text{on}} + \text{mRNA} \xrightarrow{\gamma_m} \emptyset,\\
&\text{mRNA} \xrightarrow{k_p} \text{mRNA} + \text{protein} \xrightarrow{\gamma_p} \emptyset.
\end{aligned}$$

This model captures the general features of the central dogma of molecular biology, but puts a layer of abstraction between complex biological processes and the rate parameters of the model. Take the translation rate k_p as an example. The parameter k_p encapsulates the entire complex process of a ribosome binding to an mRNA, recruiting tRNA which must in turn bind the correct amino acids, the ribosome moving along the mRNA and elongating a new protein, and the subsequent folding of the protein into its functional conformation. All of this, wrapped up in a single rate!

The reason this model is useful is that, in nominal physiological conditions, the actual kinetic process of transcription and translation is well approximated by these equations. An important and understudied question is what happens when the assumptions of the model break down? One consequence of our simplified model is that the expression of different proteins from different mRNAs is independent, i.e. the rate of translation $k_{p,1}$ of a protein p_1 is not affected by whether or not another

protein p_2 is being translated at a rate $k_{p,2}$. If we imagine a situation in which so much mRNA is present that ribosomes are in relatively scarce supply, then there must be some implicit coupling between translation rates as mRNA will effectively be competing for ribosomes.

Following through with this logic, we would predict that the rates have some functional form $k_{p,i}(R, M)$ where R is the number of ribosomes in the cell and M is the total number of mRNA. Qualitatively we can predict that $\lim_{R\to\infty} k_{p,i}(R, M) = k_{p,i}$ should be true, in other words the rate is asymptotically independent of M as R becomes large. This captures the effect of what is sometimes referred to as ribosomal loading. This effect is believed to sometimes cause synthetic circuits to not behave as expected, for example when the circuit contains a reporter that produces so many fluorescent proteins that the production of other proteins in the circuit is indirectly repressed [1]. If we are ever to develop a predictive design framework for synthetic circuits, it will likely be essential to quantitatively understand what the resource requirements for a given circuit are [2]. In the ribosomal loading case, this may look like some total mRNA budget for a circuit that is based on the expected number of spare ribosomes in a given cell. This type of analysis would need to be repeated for each constraining resource that factors into the synthesis of biological parts.

This is a potential way to frame the notion of layering and abstraction in biological circuits [3]. We can say that there exists a good layering when it is possible to abstract away many underlying physical processes into simple, independent parameters. By understanding how this layering breaks down, we will both gain insight into the fundamental constraints of biological processes and develop theory-driven design guidelines for synthetic circuits. It is likely the case that the design of evolved pathways we see in natural contexts all fall inside these guidelines, whatever they may be. If this is true, it will likely be possible to test the hypothesis that there really are fundamental constraints on circuit design by comparing many different pathways, quantified in the appropriate way, to see if they all follow some universal laws of biological circuit design. By understanding in a rigorous way the connection between the detailed physical and chemical reality of the most basic biological processes and coarse-grained phenomenological representations of functional behavior of a cell, it may become possible to understand the architecture of life.

Biology is undoubtedly complex, but I see no fundamental barriers to developing a theoretical framework for understanding the structure of living systems. With each

technological development, from single-cell imaging to gene editing, it becomes easier and easier to understand the inner workings of the cell. We often like to think of theory as driving technology and experiments, but a theory can only be as predictive as experiments are precise. The results I presented here would have been impossible to develop even 30 years ago, when quantitative information about biomolecular processes was extremely hard to come by. If all goes well, the rapid development of new technology will results in a comparable expansion of theoretical and computational tools. To quote Craig Venter and Daniel Cohen, "If the 20th century was the century of physics, then the 21st century will be the century of biology" [4].

BIBLIOGRAPHY

[1] Laurent Potvin-Trottier et al. “Synchronous long-term oscillations in a synthetic gene circuit”. In: *Nature* 538.7626 (2016), p. 514.

[2] Domitilla Del Vecchio et al. “Future systems and control research in synthetic biology”. In: *Annual Reviews in Control* (2018).

[3] Thomas P Prescott and Antonis Papachristodoulou. “Layered decomposition for the model order reduction of timescale separated biochemical reaction networks”. In: *Journal of theoretical biology* 356 (2014), pp. 113–122.

[4] Craig Venter and Daniel Cohen. “The century of biology”. In: *New Perspectives Quarterly* 21.4 (2004), pp. 73–77.